ENHANCE ENERGY CLIVE MMV PLAN

APPENDICES C:

Geochemical Effects on Deep Strata in Case of CO_2 Leakage from the Leduc D3-A and Nisku D2 Oil Reservoirs in the Clive Oil Field in Alberta

July, 2019

APPENDIX C

Geochemical Effects on Deep Strata in Case of CO_2 Leakage from the Leduc D3-A and Nisku D2 Oil Reservoirs in the Clive Oil Field in Alberta

Confidential Client Report to Enhance Energy Inc.

by

Alberta Innovates – Technology Futures

March 2012

Disclaimer

1. This Report was prepared as an account of work conducted at the ALBERTA INNOVATES - TECHNOLOGY FUTURES ("AITF") on behalf of Enhance Energy Inc. All reasonable efforts were made to ensure that the work conforms to accepted scientific, engineering and environmental practices, but AITF makes no other representation and gives no other warranty with respect to the reliability, accuracy, validity or fitness of the information, analysis and conclusions contained in this Report. Any and all implied or statutory warranties of merchantability or fitness for any purpose are expressly excluded. Enhance Energy Inc. acknowledges that any use or interpretation of the information, analysis or conclusions contained in this Report is at its own risk. Reference herein to any specified commercial product, process or service by trade-name, trademark, manufacturer or otherwise does not constitute or imply an endorsement or recommendation by AITF.

2. The information contained in this Report is confidential and may not be distributed, referenced or quoted without the prior written approval of Enhance Energy Inc.

3. Any authorized copy of this Report distributed to a third party shall include an acknowledgement that the Report was prepared by AITF and shall give appropriate credit to AITF and the authors of the Report.

4.

Authors

This report was prepared by a team of AITF staff comprising:

Stephen Talman, Ph.D.

Stefan Bachu, Ph.D., P.Eng.,

Alberta Innovates Technology Futures

Executive Summary

The objective of the Alberta Carbon Trunk Line project being implemented by Enhance Energy Inc. is to collect CO_2 from large-scale industrial CO_2 emitters in and around Alberta's Industrial Heartland for use in CO_2-assisted enhanced oil recovery in aging oil reservoirs in central Alberta. Alberta Innovates – Technology Futures has performed several studies to assess the effects of injecting CO_2 in the Leduc D3-A and Nisku D2 oil reservoirs in the Clive oil field. The objective of the study reported here is to assess the likely geochemical interactions between the injected CO_2 and the rocks and water contained in these two oil reservoirs and in overlying saline aquifers assuming that leakage of CO_2 or CO_2-rich water from the reservoir may occur. These geochemical reactions were modelled using the geochemical code PHREEQC. The results presented here are restricted to equilibrium calculations; these results represent upper limits on the extent of geochemical reactions. Specifically, the extent of chemical trapping of CO_2 and acid neutralization reported here represent upper limits for the scenarios modelled.

Within the oil reservoirs, in both of which the host rock is relatively pure dolomite, the interaction between the injected CO_2 and reservoir minerals will lead to the breakdown of feldspars, present in minor amounts, to form clays. There is also some transformation of the carbonate minerals within the reservoir, however, this will be minor. Overall, the predicted geochemical reactions will lead to a trivial decrease in porosity in the oil reservoirs; with no expected impact on reservoir characteristics, particularly permeability, and hence on oil recovery.

This thick seal overlying the Leduc D3-A and Nisku D2 oil reservoirs constitutes a barrier to upward migration and leakage of CO_2 from these oil reservoirs. The greatest risk of leakage of fluids (CO_2 or acidified brines) from the oil reservoirs will be associated with well bores that penetrate these reservoirs. Leaking fluids will interact with formation water and minerals in a succession of saline aquifers. These are, in ascending order: Lower Mannville, Viking, Basal Belly River and Upper Belly River. These overlying aquifers, being of siliciclastic nature, are mineralogical more complex than the carbonate oil reservoirs, hence the resultant geochemical reactions are accordingly more complex. In the case of pure CO_2 leakage into these aquifers, the general tendency will be for the pre-existing feldspars and complex clays to breakdown, forming the simpler, more acidic clay mineral kaolinite and a pure silica phase. As well, significant quantities of the magnesium carbonate, magnesite, are predicted to form within the Basal and Upper Belly River aquifers. As with the oil reservoirs, the predicted changes in the porosity of the lower two aquifers (Lower Mannville and Viking) are inconsequential; however, this is not the case for the upper two aquifers; an increase in porosity is expected within the Basal Belly River aquifer, while a significant porosity reduction is expected within the Upper Belly River aquifer. Permeability is not expected to change, at least not in the two lower aquifers (Lower Mannville and Viking), and maybe only locally in the two upper ones (Basal and Upper Belly River).

The capacity of the aquifers overlying the oil reservoirs to trap CO_2, either within mineral phases or as bicarbonate in the water, is also greater in the upper two aquifers (Basal and Upper Belly River) than in the lower ones (Lower Mannville and Viking). One reason for this is the markedly lower salinity in the former than in the latter. Calculations suggest that, following equilibration with a free-phase CO_2, free CO_2 will continue to exist within the Mannville and Viking aquifers but not in the Basal and Upper Belly River aquifers. Leakage through any of these aquifers will also result in some dispersion and dilution of any vertical flux of CO_2 into each of these aquifers.

Leakage of acidified brines into these aquifers will result in a more complex set of reactions. In contrast to the case of pure CO_2 leakage where the rock acts to buffer pH changes associated with the acidification of aquifer water, the flow of cation-laden brines can induce acid forming reactions. As such, the pH of waters resulting from the mixing of CO_2-enriched reservoir-derived water with that from the overlying aquifers will generally be lower (the water will be more acidic) than in the case of pure CO_2 flow. This has implications when considering trace metal mobility within affected aquifers – generally the mobility of trace elements, such as lead and arsenic, increases as pH decreases.

The results presented here represent the state towards which reservoir and aquifer mineralogy and water chemistry will ultimately tend when interacting with fluids in and leaking from the oil-reservoirs into which CO_2 is injected. Nevertheless, these geochemical calculations provide insights into mechanisms which may be responsible for reducing leakage rates and related effects, while also providing an insight into potential compositional changes induced by CO_2 leakage that may influence future monitoring approaches.

Alberta Innovates Technology Futures

Table of Contents

List of Figures

Alberta Innovates Technology Futures

List of Tables

List of Tables (Concluded)

1. Introduction

1.1 Background

Interpretation of the temperature record on a scale of centuries to millennia indicates a slight increase in global annual temperatures in the last 150 years, in the order of 0.76ºC (IPCC, 2007). It is very likely (>90% likelihood) and generally accepted that the main cause of the observed global warming is the increase in atmospheric concentrations of greenhouse gases, mainly carbon dioxide (CO_2), but also methane (CH_4) and nitrous oxide (N_2O) (IPCC, 2007). Although a direct causal link between the carbon cycle, including CO_2 and CH_4, and global warming has not been demonstrated, circumstantial evidence points toward this link, which has generally been accepted by a broad segment of the scientific community, the general public and policy makers.

A major challenge in mitigating climate change effects is the reduction of anthropogenic CO_2 emissions through a broad portfolio of measures which includes increasing energy efficiency and conservation, and switching from fossil-based energy production to other forms of energy such as nuclear, solar, wind and other renewables. Capture of CO_2 from large stationary sources prior to potential release into the atmosphere, and utilization or storage in various geological media (this process is known as Carbon Capture, Utilization and Storage, or CCUS) has been recognized also as one of the main technologies available today for reducing anthropogenic emissions of CO_2 in the atmosphere. The “utilization” in CCUS consists mainly in using CO_2 captured from large stationary sources for CO_2 enhanced oil recovery (CO_2-EOR). Currently there are more than a hundred CO_2-EOR operations in the world, the great majority of them being in the U.S. However, they predate CCUS, most of them use CO_2 from natural CO_2 reservoirs rather than anthropogenic sources, and, for various reasons, they are not considered as CO_2 storage operations. Only the Weyburn-Midale project in southeastern Saskatchewan, which uses CO_2 from a coal-gasification plant in North Dakota, is considered as a CO_2 storage operation.

Aware of the potential of CCUS to reduce anthropogenic CO_2 emissions, the federal, Alberta and Saskatchewan governments have provided significant financial support for the implementation of large-scale CCUS demonstration projects in western Canada. Among the projects that have been initiated in western Canada is Enhance Energy Inc. project “Alberta Carbon Trunk Line”, known also as ACTL.

1.2 The ACTL Project

Enhance Energy Inc. will construct and operate the Alberta Carbon Trunk Line, which is a 240 km pipeline that will collect CO_2 from industrial emitters in and around Alberta’s Industrial Heartland and transport it to aging oil reservoirs in central Alberta, more specifically to the Clive oil field first and beyond it as the project progresses, for secure storage in CO_2-EOR projects (Figure 1). The Clive oil field is located east to northeast of Joffre and immediately north of the Red Deer River. At full capacity the ACTL route will

provide access to oil reservoirs capable of producing an additional billion barrels of high-quality light-crude oil while storing 14.6 Mt CO_2.

Figure 1: Location of the Alberta Carbon Trunk Line (ACTL). Reproduced from Enhance Energy Inc.'s fact sheet at http://www.enhanceenergy.com.

All CCUS projects require the study of the fate and effects of the stored CO_2, and the development of an active monitoring program to ensure that there is no CO_2 leakage from the storage unit. In the case of CO_2-EOR operations, CO_2 is stored in the respective oil reservoir(s), and monitoring of the fate and effects of CO_2 in the reservoir(s) is part of the engineering practice. However, monitoring for CO_2 leakage and for effects of CO_2 injection outside the reservoir requires knowledge of the sedimentary succession above the oil reservoir(s) into which CO_2 is injected. Conceptually, the sedimentary succession in a CCUS operation can be divided into:

1) The storage complex comprising the injection unit (reservoir) and primary caprock (seal) above the injection unit, which in this case comprise the Leduc D3-A and Nisku D2 oil reservoirs and the Calmar Formation (caprock);
2) The succession of aquifers and aquitards between the primary seal and the base of protected groundwater, which in this case comprise the succession from the Devonian Stettler Formation to the Upper Cretaceous Belly River Group; and

3) The sedimentary succession from the base of shallow protected groundwater, defined in Alberta as groundwater with salinity (Total Dissolved Solids, or TDS) less than 4000 mg/L, to the ground surface, which in this case is the sedimentary succession overlying the Belly River Group.

Effects of CO_2 injection are generally of two types:

- Geomechanical, as a result of pressure increase during CO_2 injection; and
- Geochemical as a result of CO_2 coming in contact with formation water and rocks. These effects are particularly important if CO_2 leaks into protected groundwater that is used for human consumption and for agricultural and industrial purposes (hence the division of the sedimentary succession presented previously).

In the case of the Alberta Carbon Trunk Line project, Enhance Energy Inc. has retained Alberta Innovates – Technology Futures (AITF) to study these effects in a staged approach that consists of several phases. In Phase 1 of the study, AITF in collaboration with University of Saskatchewan studied the geology, hydrogeology, rock mineralogy and geomechanical properties of the sedimentary succession from the top of the Leduc D3-A and Nisku D2 oil reservoirs, whose primary seal (caprock) is the combined interval of the anhydritic upper portion of the Nisku Formation and the shaley Calmar Formation, to the ground surface (Bachu et al., 2011; Oar et al., 2011).

The study area was defined as illustrated in Figure 2 covering 171 sections of land. A total of 1715 wells were drilled within the study area, of which 660 wells reach the top of the Nisku Formation; most of those are located within the D2 pools. Elevations for the ground surface in the study area range from 790 to 910 mASL (Figure 3). The land surface elevation is generally higher in the west and lower in the east, with the Red Deer River in the southeast and associated tributaries in the northeast portions of the study area. Topographical highs are found in the southwest and west-central portions of the study area. In Phase 2 of the study, the leakage potential of the wells penetrating the Leduc D3-A and Nisku D2 oil reservoirs was examined (Faltinson et al., 2011), and geomechanical effects of CO_2 injection were assessed based on numerical modelling (Soltanzadeh et al., 2012).

This report presents the results of geochemical modelling of effects of CO_2 on the Leduc D3-A and Nisku (2-D) oil reservoirs, and on the strata in the sedimentary succession overlying these reservoirs up to the Belly River Group below the protected groundwater in the Clive area. This work was performed also as part of Phase 2 of the study.

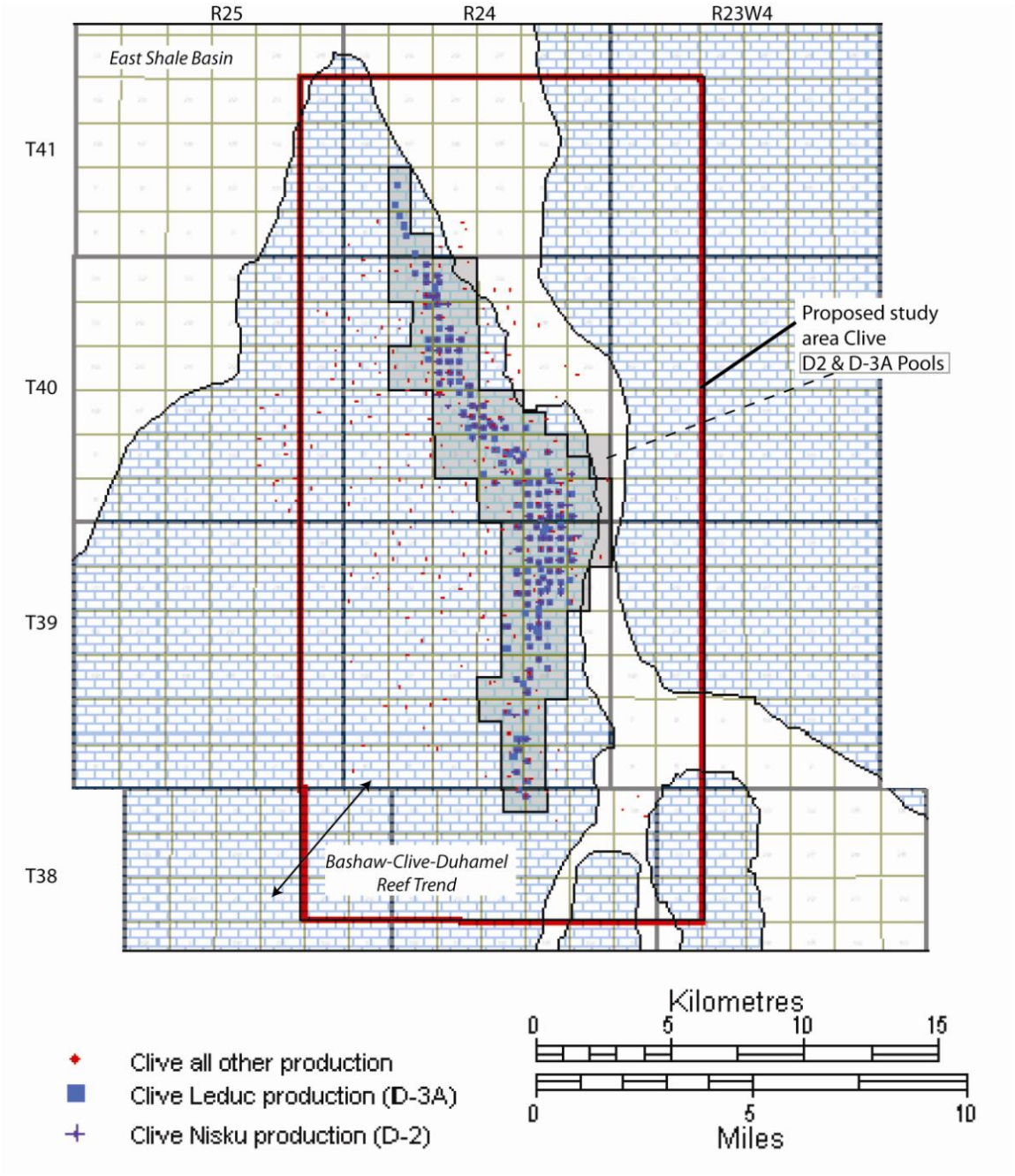

Figure 2: Clive study area, delineated by the red line, for the assessment of the sedimentary succession above the Leduc D3-A and Nisku D2 oil reservoirs in the Clive oil field.

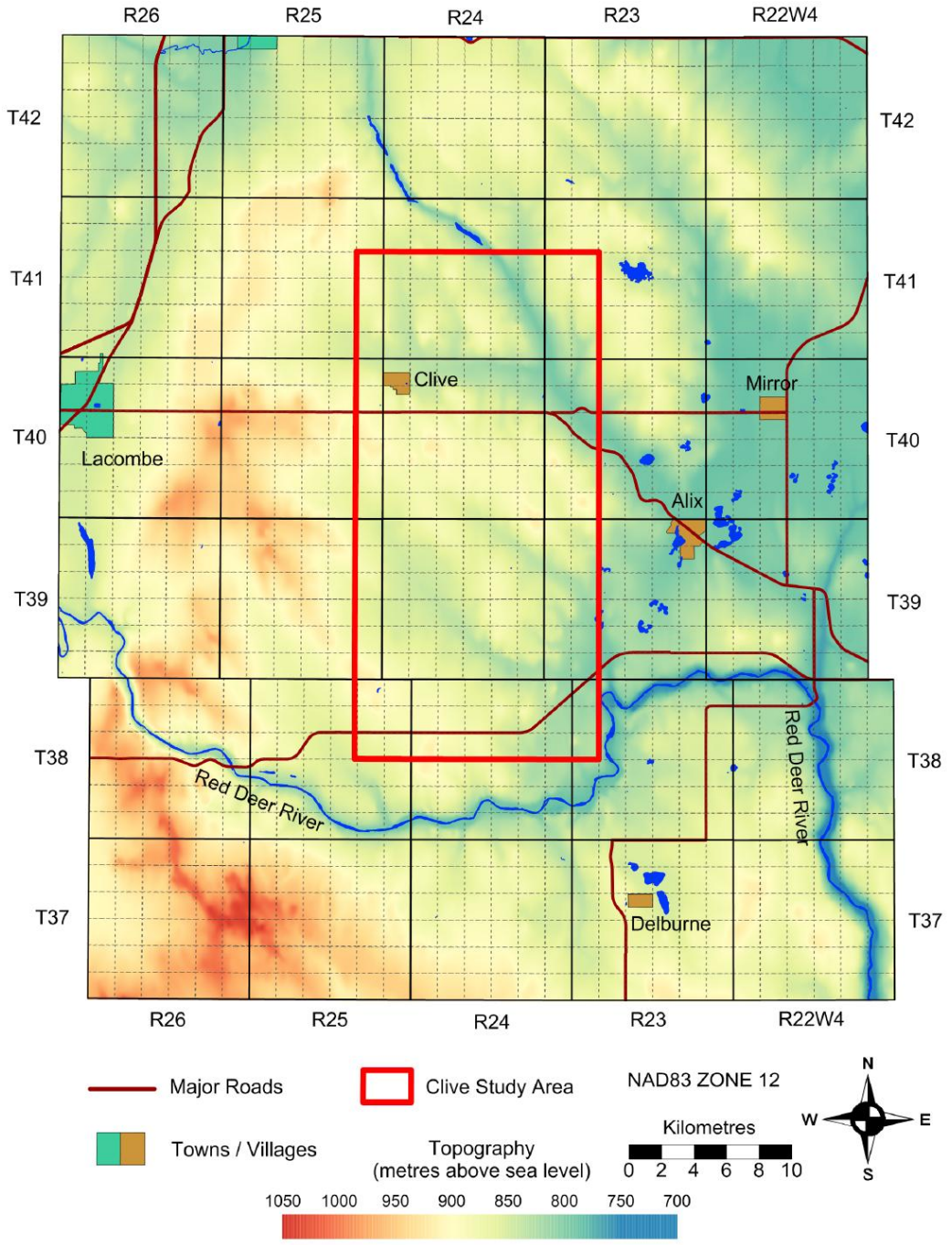

Figure 3: Regional topographic map of the region around the Clive study area (Topography DEM from GeoBASE; roads and DLS grid from GeoScout).

1.3 Modelling of geochemical interactions

Interactions between injected gases and the host reservoir, its caprock, and overlying strata, are dictated by the chemical properties of the phases which exist prior to, and

following gas injection (in this case CO_2). Aspects of these phase properties which are relevant to this study have been previously presented in Bachu et al. (2011). Carbon dioxide and CO_2-charged waters contact the mineral and cement phases in rocks and wells, respectively, whose characteristics are also reported in Bachu et al. (2011) and Faltinson et al. (2011).

Through the extensive period of contact between the formation water and the solid rock phases, the water composition evolves towards equilibrium with the minerals found in the respective aquifers and reservoirs. This equilibrium will be disturbed by the presence of CO_2 either as a dense, supercritical fluid, or in gaseous phase in the case of leakage into shallow strata. The fluid and rock properties required to define the chemical interactions between these phases are documented in this report. This begins with compositional aspects of the various phases (Chapter 2), followed in Chapters 3 and 4 by more detailed analysis of their chemical properties, including equilibrium relationships. The most probable geochemical interactions between these disparate phases (reservoir and aquifer minerals, water and the injected CO_2) are presented in Chapter 5. The report ends with a brief summary and conclusions regarding the geochemical effects of injecting and storing CO_2 in the Nisku D2 and Leduc D3-A reservoirs in the Clive oil field and their importance.

Any injected CO_2 will be relatively pure (e.g., Wigston and Ryan, 2011). However, depending on the in-situ temperature, pressure and fluid(s) composition, the injected gas has the potential to strip volatile components from existing fluid phase(s). This effect is responsible for the generation of a methane-rich bank at the leading edge of the plume of injected CO_2 injected into a saline aquifer that contains a significant amount of dissolved methane (Doughty and Freifeld, 2012). As well, modelling results suggest a similar effect can arise in H_2S-rich formation waters (Ghaderi et al., 2011). The presence of H_2S can greatly modify the geochemical behaviour of CO_2/water/rock systems. While H_2S is noted as present in waters recovered from the oil reservoirs, there is no indication of its concentration; it is simply noted as being present in the samples. Ghaderi et al. (2011) cite Hutcheon (1999) as reporting high H_2S contents in brines recovered from the Nisku Formation in deeper regions closer to the Rocky Mountain Thrust and Fold Belt as a result of thermosulphate reduction. However, in the absence of specific knowledge about the concentrations of H_2S in the local waters and oils within the study area, modelling such interactions are outside the scope of this current work. There is no indication about the presence of H_2S in the Cretaceous aquifers overlying the Devonian Leduc 3D-A and Nisku 2D oil reservoirs in the Clive oil field (Bachu et al., 2011), and its presence is not expected based on the characteristics of these aquifers and generally of the Cretaceous strata.

2. Relevant Prior Work

This chapter presents a review of previously-reported results (see Bachu et al. 2011) regarding the characteristics of the rocks and waters in the Leduc D3-A and Nisku D2 oil reservoirs and overlying formations in the Clive oil field that are required to define the possible geochemical interactions analyzed in this report. These geochemical interactions involve mineral phases which are generally referred to herein by their mineral names. These are defined in terms of their chemical composition in Appendix A.

2.1 Geology

Sedimentary strata in the Clive area are the result of deposition predominantly within two distinct stages of tectonic evolution of the Alberta Basin. The first stage involves an early Phanerozoic (Cambrian) to Late Jurassic deposition on the western passive cratonic margin of the proto North American continent. During this stage, deposition of sedimentary strata was dominated by the growth of carbonates (Figure 4), especially during the Devonian, including the Leduc (D3) reef complex and the overlying Nisku Formation D2 which form the Clive oil field.

The second major phase of basin evolution involves orogenic cycles affecting the western cratonic margin of North America. Two major cycles are represented in the Alberta Basin by the Jurassic-Early Cretaceous Columbian and Late Cretaceous-Tertiary Laramide orogenies. The accretion of terranes on the western cratonic margin caused dislocation of a supracrustal wedge that was stacked and thickened north-eastward onto the cratonic margin, the weight of which produced the foreland trough east of the Cordillera. As a result of tectonic loading at the western margin of the basin during the Columbian orogeny, Paleozoic strata were tilted south-westward with a slope in the Clive area of approximately 13 m/km (0.74º). Major erosional events prior to Cretaceous deposition resulted in significant removal of Mississippian strata, and complete erosional removal of Triassic and Jurassic sediments in the area. Consequently, in the Clive area the Devonian Big Valley and the Mississippian Exshaw and Banff formations are successively exposed west to east beneath Cretaceous strata at the sub-Cretaceous unconformity (Figure 4).

The second stage of basin evolution saw a cessation of carbonate growth due to a major influx of siliciclastics. Throughout Mesozoic time the foreland basin, created as a result of the Columbian and Laramide orogenies and paralleling the Rocky Mountain chain, was the locus of much of the sedimentation derived from erosion of the newly formed Cordillera. The majority of sedimentary units filling this foreland trough are continuous across the study area, except for those strata in proximity to the base of the Tertiary and Quaternary deposits, which were truncated as a result of Cenozoic erosional events (Scollard and Paskapoo formations). Only the Bearpaw Formation is limited in extent in the study area due to non-deposition. Coal zones are found within the Upper Mannville, and the Belly River and Edmonton groups (Figure 4).

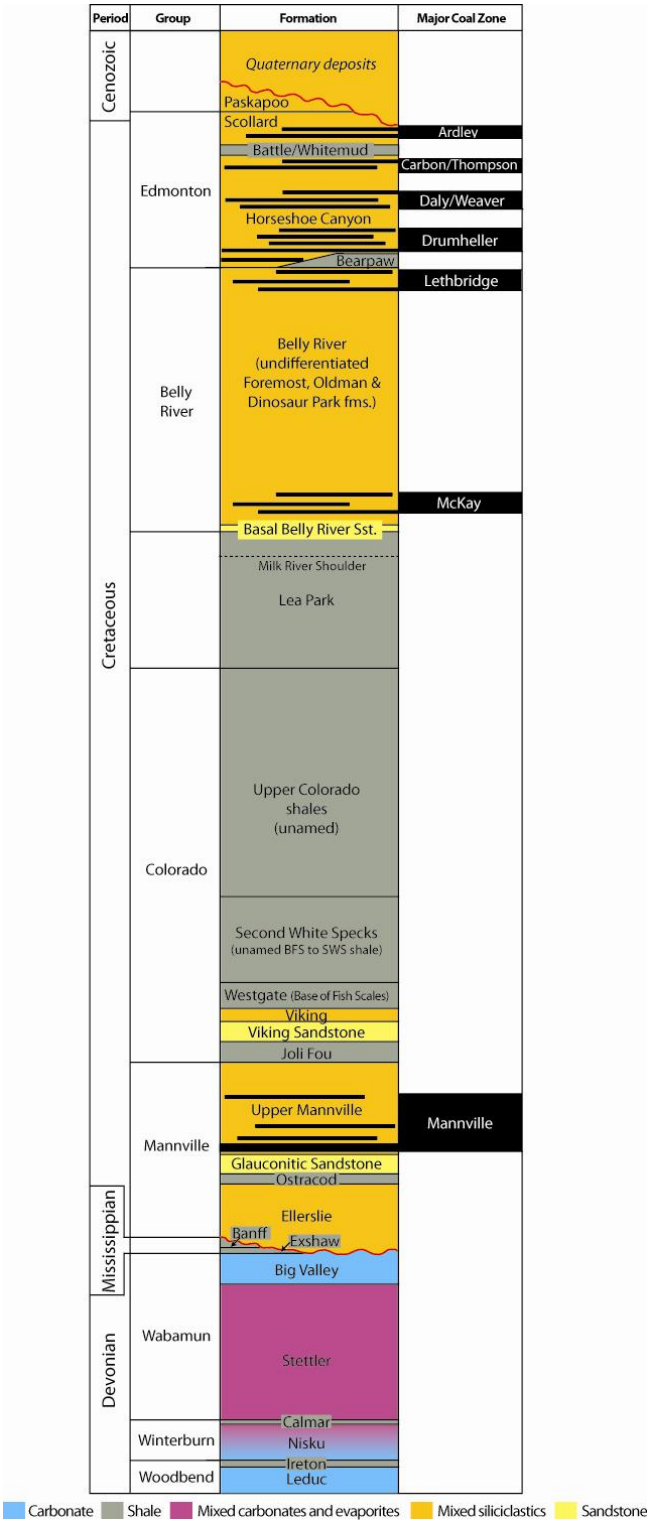

Figure 4: Lithostratigraphic column, including major coal zones, in the Clive study area.

The Quaternary unconsolidated surficial sediments generally consist of lacustrine deposits underlying glacially derived tills. Incised within these deposits are buried bedrock valleys and meltwater channels filled with fluvially-derived sand and gravel. Meltwater channels trending northwest to southeast transect the Clive area.

2.2 Hydrostratigraphy and Flow of Formation Waters

The sedimentary succession consists of four geological packages (in ascending stratigraphic order): 1) Upper Devonian carbonates, evaporites and shales; 2) Carboniferous shales present in the west and south; 3) a thick package of Mesozoic mixed siliciclastics and shales; all overlain by 4) Cenozoic till, glacio-fluvial and lacustrine sediments (Figure 4). The hydrostratigraphic column (Figure 5) has been constructed based on the geological framework, data quality and availability, and previous larger-scale hydrogeological studies of the Clive and adjacent areas (Bachu et al., 2011).

The Nisku D2 oil reservoir is overlain by the Calmar Formation (both are part of the Winterburn Group), which constitutes the primary caprock. A total of four deep aquifers and five aquitards have been identified in the sedimentary succession overlying the reservoirs targeted for CO_2-EOR, listed in ascending order: Calmar-Wabamun Aquitard, Lower Mannville Aquifer (including the Ellerslie, Ostrocod and Glauconitic Sandstone), Upper Mannville–Joli Fou Aquitard, Viking Aquifer, Colorado–Lea Park Aquitard, Basal Belly River Aquifer, McKay Aquitard, Upper Belly River Aquifer, and Bearpaw Aquitard. Shallower strata contain three aquifers and one aquitard: Horseshoe Canyon Aquifer, Whitemud-Battle Aquitard, Paskapoo Aquifer, and Surficial Aquifer, the last two being in contact at the top of the bedrock.

Fluid flow in the Lower Mannville Aquifer is complex and directed primarily towards the center of the Clive area from the southeast and northwest, and out of the Clive area toward the northeast. A composite pressure-elevation plot indicates a vertical component of fluid flow based on a measured super-hydrostatic gradient of 12.7 kPa/m, which is higher than the corresponding hydrostatic gradient, thus indicating a vertical upward flow component. The hydraulic evidence based on a pressure-elevation plot (Figure 6) indicates that there is no hydraulic communication between the Nisku Formation and the Lower Mannville Aquifer in the Clive area. Therefore, the Calmar-Wabamun Aquitard is a strong barrier to cross-formational flow in this area.

Fluid flow in the Viking Aquifer is directed towards the southwest. A vertical gradient of 10.4 kPa/m (Figure 6) indicates that flow in the Viking Aquifer is mainly lateral, with no indication of a vertical flow component. Hydraulic heads in the Viking Aquifer are much lower than those in the Lower Mannville Aquifer, indicating underpressuring. The differences in both flow patterns and hydraulic gradients in these two aquifers indicate that they are not in hydraulic communication and that the intervening Upper Mannville-Joli Fou Aquitard is strong.

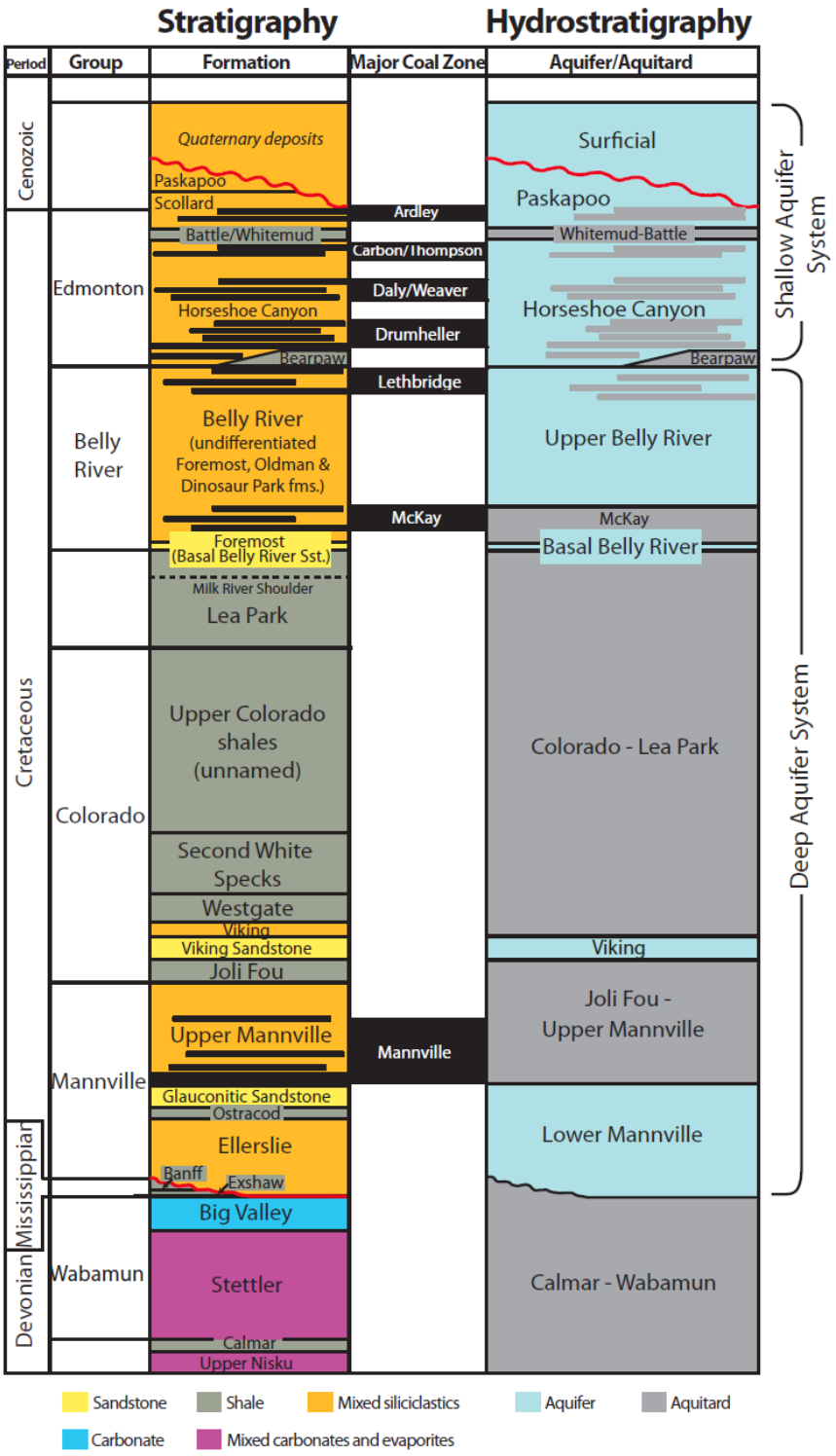

Figure 5: Lithostratigraphic and hydrostratigraphic charts in the Clive study area.

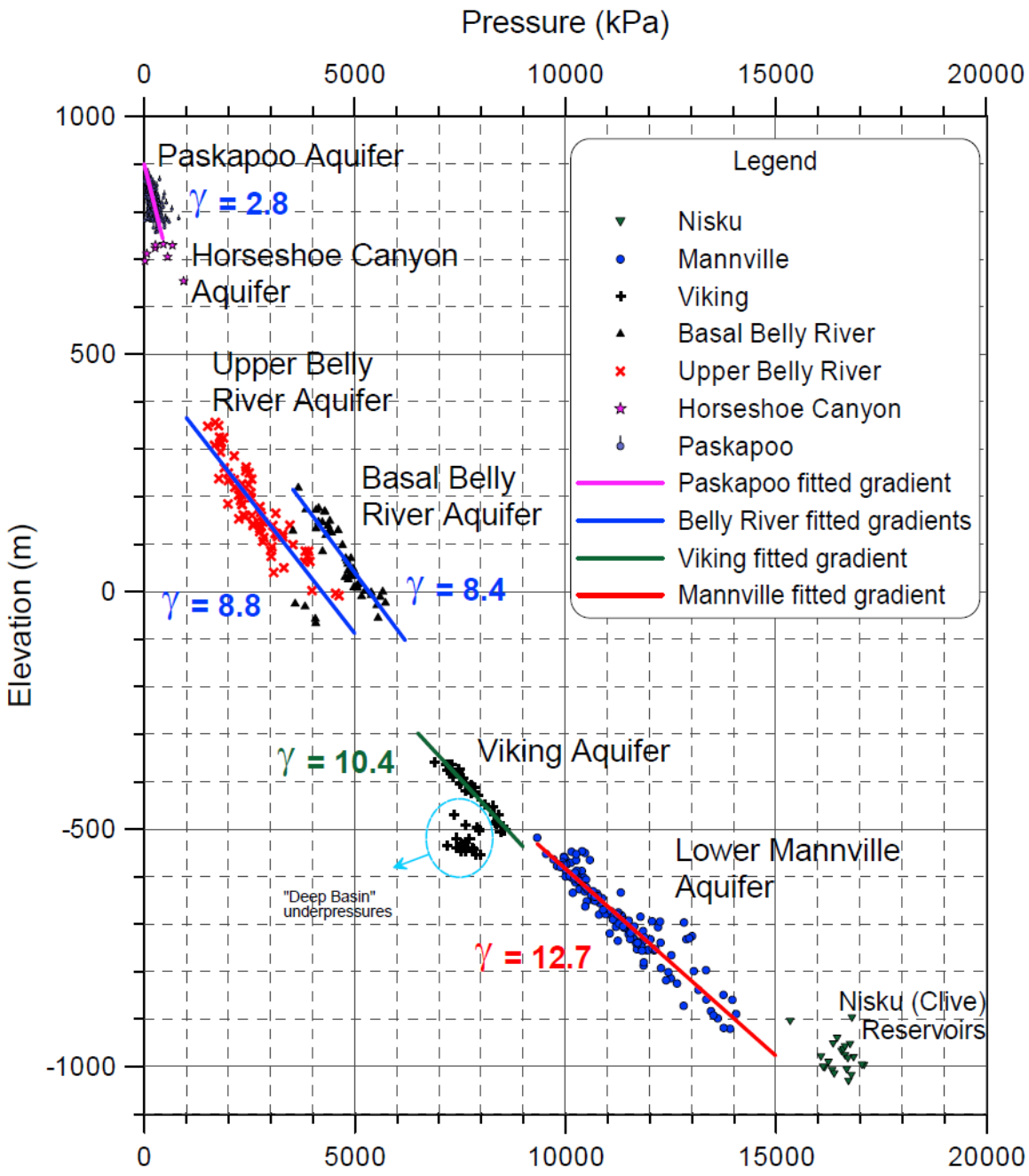

Figure 6: Pressure-elevation (p-z) plot for the aquifers overlying the Leduc D3-A and Nisku D2 reservoirs in the Clive area shown in Figure 3.

Fluid flow in the Basal and Upper Belly River aquifers is directed towards the southwest, with hydraulic heads in the 350 m to 550 m range, indicating under-pressuring. Vertical pressure analysis shows that the Basal and Upper Belly River aquifers have a downward, downdip component of flow, based on vertical gradients of 8.4 and 8.8 kPa/m, respectively (Figure 6). These gradients are significantly lower than in the underlying Viking Aquifer, and, together with hydraulic heads that are much higher than in the Viking Aquifer, indicate that the intervening Colorado-Lea Park Aquitard is strong.

The Upper Belly River Aquifer appears to be underpressured relative to the Basal Belly River Aquifer (Figure 6) and hydraulic head isolines are shifted, indicating that the McKay Coal Zone separating the Basal and Upper Belly River Aquifers seems to be a strong aquitard.

The flow in the shallow Horseshoe Canyon, Paskapoo, and Surficial aquifers is controlled by surface topography (see Figure 3) and is different from that in the deep aquifers. The hydraulic heads are much higher than in the Upper and Basal Belly River aquifer and range between 718 – 798 m in the Horseshoe Canyon and 800 – 880 m in the Paskapoo aquifer. These aquifers (Horseshoe Canyon and Paskapoo) have a subhydrostatic vertical gradient of 2.8 kPa/m (Figure 6). This hydraulic gradient is significantly different from those in the deeper aquifers and indicates the presence of strong downward flow component, likely of meteoric origin (rain and snowmelt water) flowing downwards through these aquifers.

The differences in flow pattern, hydraulic heads and hydraulic gradients (see Figure 6) indicate the presence of a barrier or multiple barriers (mudstones and coal beds), between the shallow Horseshoe Canyon, Paskapoo and Surficial aquifers themselves, and also between the shallow and deep aquifers in the Clive area. Furthermore, all the aquifers in the sedimentary succession between the caprock of the Leduc D3-A and Nisku D2 oil reservoirs and the potable groundwater aquifers (Horseshoe Canyon, Paskapoo and Surficial), namely Lower Mannville, Viking, and Basal and Upper Belly River, are underpressured with respect to hydrostatic conditions (Figure 6, and also Bachu et al., 2011).

2.3 Salinity and Composition of Formation Waters

The distribution of total dissolved solids (TDS) in the Lower Mannville Aquifer is quite variable. Salinity increases northward in the Clive area from less than 80 g/L in the south to more than 120 g/L in the northeast. The TDS distribution in the Viking Aquifer is distinctly different from that in the underlying Lower Mannville Aquifer, varying from roughly 30 g/L in the south of the Clive area to 40 g/L in the northeast. Formation waters are significantly fresher in the Basal Belly River Aquifer compared to the underlying Viking and Lower Mannville aquifers, with TDS values in the 12 to 14 g/L range. Salinity of formation water in the Upper Belly River Aquifer is less than 10 g/L in the Clive area. Salinity in the overlying Horseshoe Canyon Aquifer is even lower, in the 5 g/L range, while TDS in the Paskapoo Aquifer varies between 0.5 g/L and 2 g/L. Finally, TDS values in the Surficial Aquifer range from ~400 mg/L to ~700 mg/L. The salinity variation within and between the various aquifers overlying the Leduc (D3-A) and Nisku D2 oil reservoirs in the Clive area confirms the conclusions reached through the hydrodynamic analysis that these aquifers are separated by the intervening aquitards (i.e., they are not in hydraulic communication).

Cross-plots of Na, percent cationic Ca and Mg, and the anionic percent of SO_4 and HCO_3 versus TDS for the Lower Mannville, Viking, Basal and Upper Belly River aquifers

are shown in Figures 7 and 8. There are two distinct clusters in the formation water chemistry data. The Basal and Upper Belly River aquifers have much lower TDS, and therefore, plot separately from the two deeper aquifers (Lower Mannville and Viking). Cross-plots for the shallower aquifers (Horseshoe Canyon and Paskapoo) are shown on Figure 8 combined with the underlying Basal and Upper Belly River aquifers for comparison purposes.

The relationship between Na and TDS for all the aquifers forms a strong positive linear trend throughout the entire range of TDS (Figures 7a and 8a). A slight relative decrease in sodium concentration, hence deviation in the linear trend, is observed in the high salinity range (> 100 g/L) in samples from the Lower Mannville Aquifer (Figure 7a). This is the result of slightly higher calcium concentration in these samples.

Percent cationic calcium versus TDS forms a rather scattered plot with a slight exponential trend, also increasing with TDS (Figures 7b and 8b). Higher calcium percentages (above 5%) and concentrations are observed in the Lower Mannville Aquifer and coincide with the high salinity plume in the central and northeastern parts of the Clive area. In contrast, the Basal and Upper Belly River aquifers have similar but low percentages of calcium. The Paskapoo Aquifer contains relatively high proportions of calcium (up to 10%) (Figure 8b), which is much higher than the deep aquifers.

Magnesium concentrations are relatively low for all the aquifers, generally below 2% Mg, with a slight increase in concentration with increasing TDS (Figure 7c). The Paskapoo Aquifer has the highest proportions of magnesium of up to 5% (Figure 8c).

Bicarbonate concentrations (Figure 7d) for the Lower Mannville and Viking aquifers decrease with increasing TDS. Bicarbonate ranges from almost 3% to 20% for TDS below 40 g/L. For higher salinity waters (TDS > 40 g/L), bicarbonate drops to less than 2%. A plot of bicarbonate versus TDS can also be used to distinguish the Basal Belly River Aquifer from the overlying Upper Belly River Aquifer. Groundwater in the Upper Belly River Aquifer has bicarbonate up to 15%. In contrast, the Basal Belly River Aquifer has generally less than 6% bicarbonate. Higher bicarbonate concentrations in the Upper Belly River Aquifer indicate the presence of fresh meteoric recharge waters, whereas low bicarbonate concentrations in the Basal Belly River Aquifer are indicative of more evolved waters, still of a meteoric origin but more saline and of a slightly different composition (e.g., Chebotarev, 1955; Hanor, 1994). The bicarbonate fraction in the Horseshoe Canyon and Paskapoo aquifers (Figure 8d) is much higher than in deep aquifers and ranges from 20% to 70%, indicating the presence of fresh meteoric waters.

Sulphate concentrations generally tend to decrease with increasing TDS. Sulphate concentrations in the Lower Mannville and Viking aquifers are negligible. Percent sulphate in the Basal and Upper Belly River aquifers are highly variable, ranging from less than 1 to over 30% (Figure 7e). The Upper Belly River Aquifer generally has more dissolved sulphate than does the Basal Belly River Aquifer. The Paskapoo aquifer has the highest fraction of sulphate, ranging between 10% and 40% (Figure 8e).

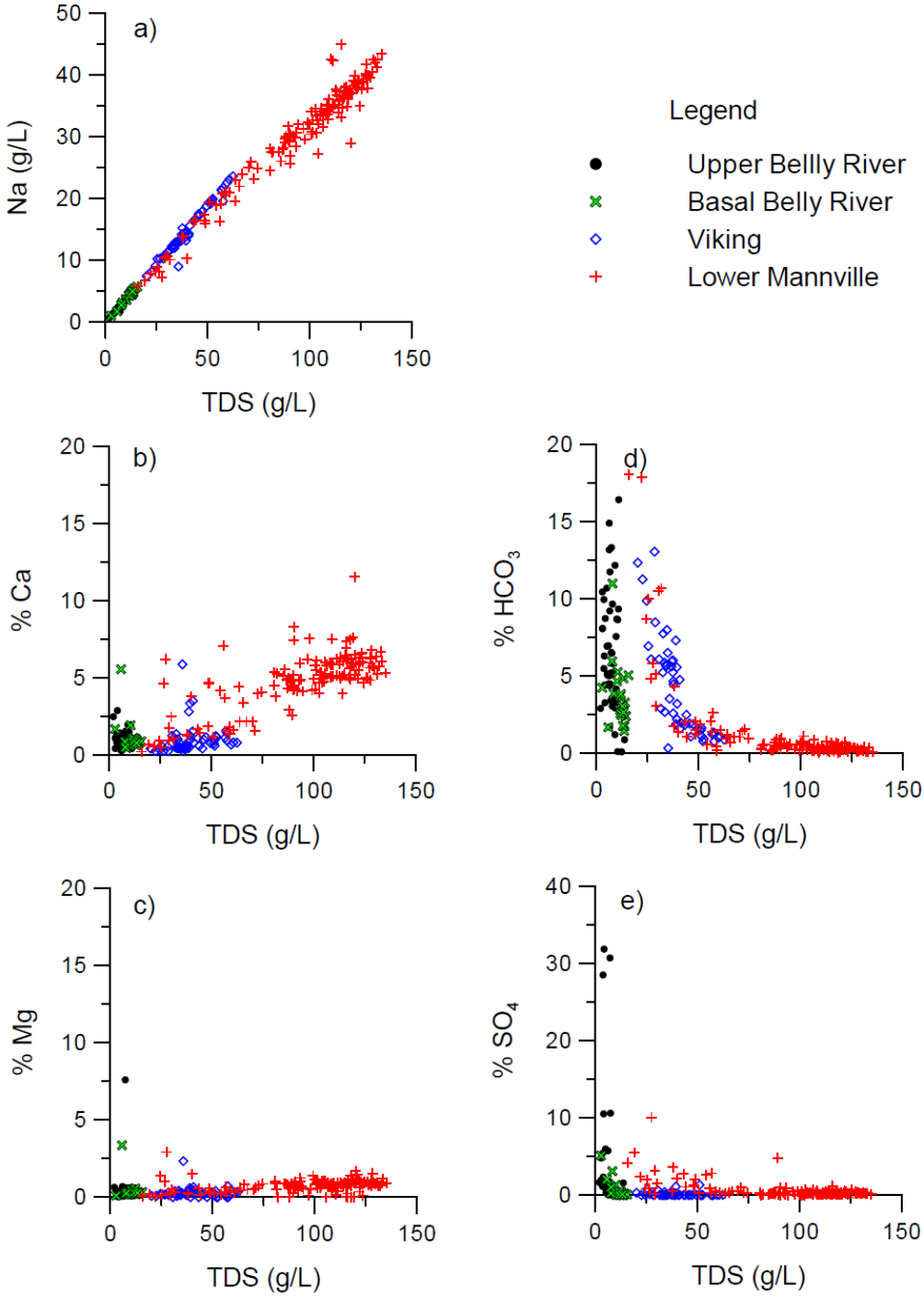

Figure 7: Cross-plots of: (a) sodium (Na), (b) percent calcium (%Ca), (c) percent magnesium (%Mg), (d) percent bicarbonate (%HCO_3), and (e) percent sulphate (%SO_4), versus Total Dissolved Solids (TDS) in the Lower Mannville, Viking, Basal and Upper Belly River aquifers.

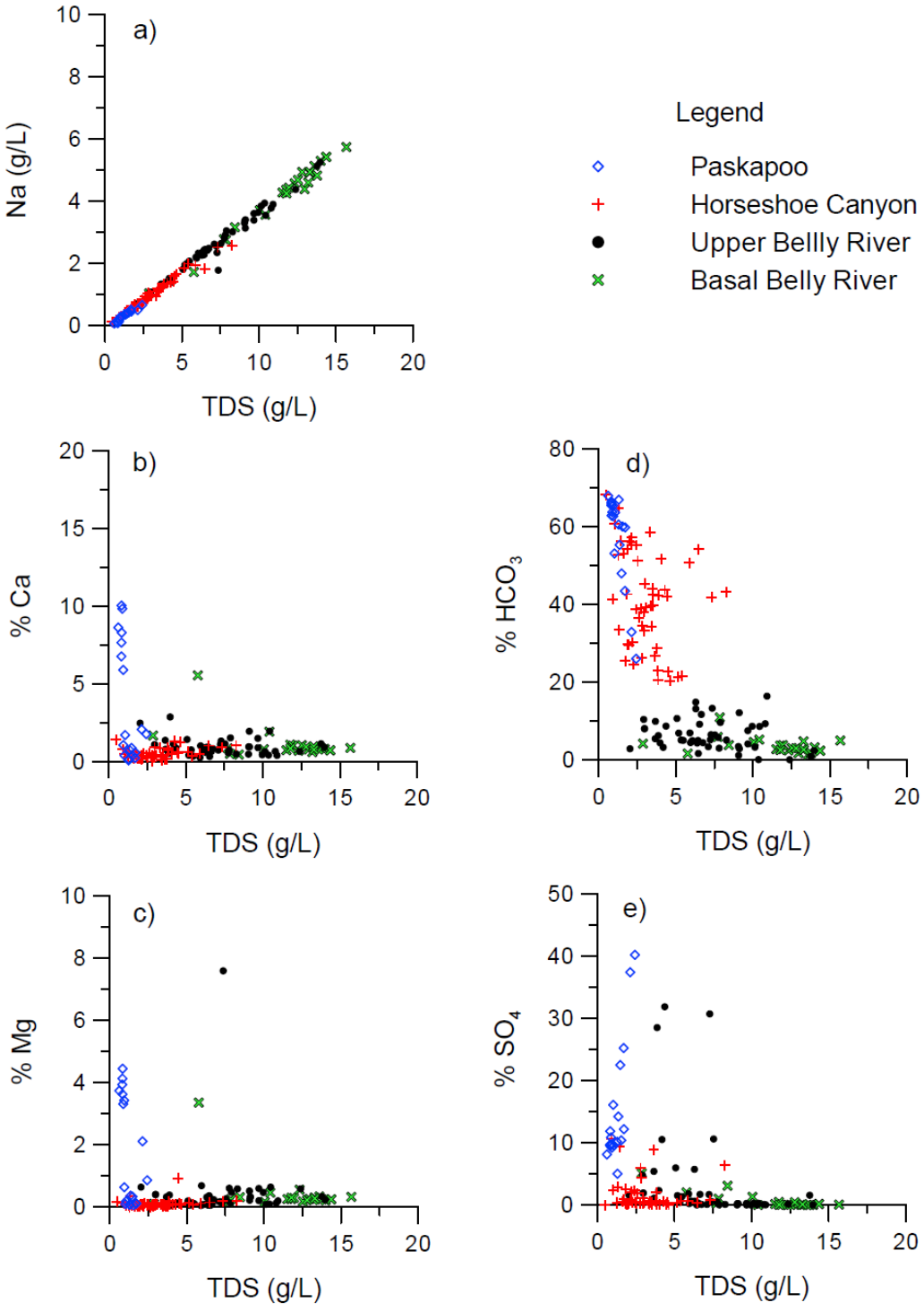

Figure 8: Cross-plots of: (a) sodium (Na), (b) percent calcium (%Ca), (c) percent magnesium (%Mg), (d) percent bicarbonate (%HCO_3), and (e) percent sulphate (%SO_4), versus Total Dissolved Solids (TDS) in the Basal and Upper Belly River, Horseshoe Canyon and Paskapoo aquifers.

Higher SO_4 concentrations are associated with formation waters of meteoric origin that have somewhat evolved in a local-scale flow system (Chebotarev, 1955). With increasing residence time and water-rock interaction, sulphate concentrations decrease and chloride concentrations increase until chloride becomes the dominant ion (Hanor, 1994).

There is only one dominant water type, Na-Cl, observed in all the deep aquifers (from Lower Mannville to Upper Belly River), i.e., more than 50% of all cations and anions in all waters in all of the aquifers are represented by sodium (Na^+) and chloride (Cl^-), respectively. Groundwater in the shallow aquifers, on the other hand, consists of several different water types. The results of the water chemistry analysis indicate that four groundwater types are found in the shallow aquifers (Horseshoe Canyon to Surficial). Generally wells in the study area have Na-HCO_3 based groundwater with varying amounts of calcium and magnesium. Those wells associated with the expected recharge area are dominated by Na-Ca-Mg-HCO_3 based groundwater. It appears that wells located adjacent to the ancient buried river valley and meltwater channel have a Na-HCO_3 based groundwater with hardness ranging from approximately 10 to 53 mg/L.

Seven representative water samples have been selected for use in modelling the geochemical effects of CO_2 in the oil reservoirs and overlying strata in case of leakage. Table 1 presents the location of these samples and corresponding in-situ pressures and temperatures, estimated from direct measurements at nearby wells (Melnik, personal communication), and Table 2 presents the composition of these water samples. The water samples are listed in ascending stratigraphic order. Two samples are provided for the Lower Mannville aquifer due to the significant differences in water salinity.

Table 1: Location and in-situ characteristics of representative water samples from reservoirs and aquifers in the Clive study area. Samples are listed in ascending stratigraphic order

No.	Aquifer or Reservoir	Well Location	Depth (m)	Pressure (kPa)	Temperature (ºC)	Density (kg/m^3)
1	Leduc	100/03-21-40-24W4/00	1920	17,250	65	1,145
2	Nisku	100/04-12-40-24W4/00	1890	16,900	60	1,145
3	Lower Mannville-1	102/16-20-40-24W4/00	1615	11,500	55	1,074
4	Lower Mannville-2	100/06-34-38-24W4/00	1610	11,850	57	1,046
5	Viking	100/11-08-40-24W4/00	1420	7,000	50	1,025
6	Basal Belly River	100/10/36/40/23W4/00	720	7,100	35	1,010
7	Upper Belly River	102/03-02-40-24W4/03	600	3,150	30	1,005

Table 2: Composition of representative water samples from reservoirs and aquifers in the Clive study area (all values are given in mg/L except for pH; TDS is calculated). The pH is assumed to be measured at 23ºC.

No.	Cations			Anions			TDS	pH
	Na	Ca	Mg	Cl	HCO_3	SO_4		
1	56,522	20,567	3,071	131,464	456	425	213,522	6.7
2	50,065	19,139	3,815	121,400	730	530	195,679	6.4
3	32,724	5,542	1,107	63,000	488	374	103,728	6.5
4	25,070	1,522	345	41,800	737	387	70,055	6.8
5	12,758	260	49	18,667	2,760	15	34,509	7.8
6	4,825	120	34	8,350	244	2	13,775	8.3
7	2,484	56	16	3,770	303	6	6,750	8.4

2.4 Rock Porosity

Core data for the Cretaceous aquifers have been assembled and analysed (Table 3). Plug-scale porosity values vary between 1% and 27%, with median values varying between 10.0% and 10.8% (Table 3). Well-scale porosity values vary between 5.3% and 26.5%, with median values ranging between 9.4% and 12.2%. Field-scale porosity values are around 10% (Table 3). As a general observation, it appears that, overall, porosity decreases with increasing depth, which is expected for siliciclastic sediments. The lowest average porosity at both core- and well-scales is observed in the Lower Mannville Aquifer, the deepest aquifer described. The Viking Aquifer has higher average porosity than the Lower Mannville Aquifer, with core-scale median of 10.0% and well-scale median of 10.2%. The Basal Belly River Aquifer is the shallowest has the highest median core- and well-scale porosity at 10.8% and 12.2%, respectively. The field-scale values show similar trends for the Lower Mannville and Viking aquifers.

Table 3: Core porosity processed in Cretaceous aquifers within the Clive study area and in the Nisku 2D and Leduc 3D-A oil reservoirs.

Aquifer	No. Wells	No. Plugs	Porosity (%)						
			Core Scale			Well Scale			Field Scale
			Min	Median	Max	Min	Median	Max	
Upper Belly River	2	0	-	-	-	-			-
Basal Belly River	1	12	1.6	10.8	22.5	12.2			-
Viking	14	263	1.0	10.0	27.0	5.3	10.2	26.5	10.6
Lower Mannville	22	853	1.0	10.1	25.9	5.7	9.4	15.2	9.7
Nisku 2D	77	3402	0.1	4.9	29.9	1.4	6.1	9.0	5.2
Leduc D3-A	78	3496	0.1	5.8	36.0	3.3	5.4	9.3	5.9

2.5 Mineralogy

A detailed mineralogical characterization of samples recovered from core taken in and above the the Leduc D3-A and Nisku D2 oil reservoirs of the Clive field is given in Bachu et al. (2011, Appendix D). The data presented therein are restricted to bulk chemical analysis of the samples, X-ray diffractograms (XRD), SEM photomicrographs and X-ray dispersive elemental analysis to assist in mineral phase identification. These data are summarized and expanded with further interpretation in Chapter 4 in this report.

2.6 Analysis of the Potential for CO_2 Leakage through Wells

Currently, 252 wells within the Clive oil field penetrate the Leduc D3-A and Nisku D2 oil reservoirs that are the target for CO_2 enhanced oil recovery. These wells were evaluated for the potential of CO_2 leakage into adjacent permeable reservoirs, shallow aquifers and to surface (Faltinson et al., 2011). Well data were compiled from data warehouse vendor GeoScout, the Energy Resources Conservation Board (ERCB) and Alberta Environment and used in the evaluation. Leakage potential software was used to process the data and assign semi-quantitative leakage potential scores, together with a manual process of validating and adjusting the scores (Faltinson et al., 2011). Operating data from the ERCB relating to reported cases of surface casing vent flow (SCVF), gas migration (GM) and casing leaks or failures (CF) were then retrieved and incorporated into the overall assessment of leakage potential for all of the 252 wells of interest. While the leakage potential scores do not quantify absolute probability of leakage, they do suggest an ordinal ranking of wells that may be more likely to be problematic based on experience with Alberta wells that have, in the past, demonstrated a higher likelihood of leaking.

All wells assessed as having high shallow, deep, or shallow and deep leakage potential scores, and, in particular, wells with high leakage potential scores in combination with reported SCVF and/or CF were identified. Six wells with high leak potential scores in combination with casing failure were flagged for special attention when developing the Leduc D3-A and Nisku 2D reservoirs for CO_2 enhanced oil recovery and CO_2 storage: 00/02-10-040-24W4, 00/04-08-041-24W4, 00/09-20-040-24W4, 00/10-02-040-24W4, 00/11-21-040-24W4 and 00/14-03-040-24W4.

It is important here to draw a distinction between the various fluids that theoretically may leak from the Leduc D3-A and Nisku D2 reservoirs. If reservoir water or oil leak into any of the intervening aquifers (secondary traps) between the oil reservoirs and shallow potable groundwater (i.e., Lower Mannville, Viking, and Basal and Upper Belly River), they will not leak higher up in the succession because all these aquifers are underpressured, some of them significantly, such that the leaked reservoir water or oil will be trapped in these pressure sinks. Only CO_2, which is driven by buoyancy, may leak in aquifers higher up in the succession if it finds a pathway. Thus, oil and reservoir water may leak into shallow aquifers only through wells that penetrate these reservoirs, while CO_2 may leak directly though any of these wells or through a combination of reservoir wells and offset wells that do not penetrate the oil reservoirs per se.

2.7 Summary

All the geological, hydrogeological and mineralogical evidence collected and interpreted in Phase 1 of this work indicates that the Leduc D3-A and Nisku D2 oil reservoirs in the Clive area are capped by a strong and thick primary seal (caprock), the Calmar-Wabamun Aquitard (which includes in places remnants of the Carboniferous shales of the Exshaw and Lower Banff formations). This primary seal constitutes a barrier to upward migration and leakage of CO_2 from the oil reservoirs targeted for CO_2 enhanced oil recovery in the area. The primary caprock is overlain in turn in by a succession of aquifers, listed in ascending order: Lower Mannville, Viking, Basal Belly River and Upper Belly River, separated by strong intervening aquitards: Joli Fou, Colorado, McKay and Bearpaw, which constitute secondary traps and secondary barriers, respectively, for any CO_2 that may leak from the oil reservoirs through wells that penetrate the oil reservoirs. The strength of the aquitards in the sedimentary succession indicates that no CO_2 leakage is possible through the natural geological and hydrogeological system in the Clive area. The only possible leakage pathway for CO_2 injected in the Leduc D3-A and Nisku D2 reservoirs is through one or more of the 252 wells that penetrate the oil-producing horizons in these reservoirs. The deep aquifers and aquitards in the study area are overlain by a succession of shallow aquifers which are within the depth of protected groundwater in the area: Horseshoe Canyon, Scollard-Paskapoo and Surficial.

Equilibrium relationships between the minerals and formation water in the sedimentary succession from the Leduc D3-A oil reservoir to the Upper Belly River aquifer, as well as the geochemical reactions that are expected to be induced in the these strata by injected CO_2, or by leakage CO_2 or associated brines into them, are presented in the following chapters.

3. Chemical Equilibrium Relationships of Water Samples Associated with the Clive Field

Potential reactions which can occur between the fluid and mineral phases within a rock system are determined by thermodynamic considerations. These include: the in-situ temperature and pressure, the composition of the waters within the rock, the mineral phases present, and, when present, the composition of any free gas. From this description the changes to these phases required to bring the system into equilibrium can be calculated. Estimates of the aquifer mineralogy will be given in the next chapter. The inputs and calculations required to define the aqueous phase are presented below. These calculations, while well defined, are complex and require the use of specialized chemical codes (or geochemical models) to perform. For this work, the geochemical model PHREEQC was used, primarily as it has the best developed treatment of the thermodynamics of very saline brines.

3.1 PHREEQC Description

PHREEQC is a free software developed by the United States Geological Survey (Parkhurst and Appelo, 1999). Its primary use is to determine equilibria in mineral/water systems at near surface conditions. It has been used extensively in this capacity and is consistently updated. In its most basic configuration the code will calculate the aqueous speciation (and aqueous activities) as well as the saturation state of minerals in an aqueous solution of known composition at a specified temperature using model parameters obtained from an assigned thermodynamic database. The equilibrium fugacity of gas components is also calculated; this is produced at output as the logarithm of the component's fugacity expressed in bars (1 bar = 100 kPa).

The program PHREEQC supports a number of options which can be used to further investigate the equilibrium behaviour of chemical systems. These include changing the temperature of the system, imposing further equilibrium constraints on the solution, and tracking the evolution associated with adding discrete amounts of individual components to the solution. Currently, PHREEQC does not correct for pressure variations. Brief descriptions of keywords used in the input files discussed here are given below.

The keyword **EQUILIBRIUM_PHASES** is used to add further equilibrium constraints. Examples of such calculations would be determining how much CO_2 must be re-introduced in order to bring a water into equilibrium with calcite, or how much halite may have precipitated during sampling (and associated cooling) from a water which was recovered from a hot, halite bearing, sedimentary rock. The parameters associated with this keyword are: the name of the component for which the equilibrium constraint is imposed, the equilibrium constraint, the component which is used to induce change in the system, and the total amount of this component in the system. For instance the string:

Calcite 0 CO2(g) 10

would be used to determine the amount of gaseous CO_2 (component name **CO2(g)**) which must be added into a water to bring the water into equilibrium (saturation index SI = **0**) with the component **Calcite**. The total amount of **CO2(g)** to be titrated is restricted to be less than **10** moles. If the change-inducing component is not specified, the equilibrium constraining mineral is taken to be the component added.

The evolution of the solution composition associated with the dissolution of one or more minerals (keyword **REACTION**) can be used to track the sequence of minerals which may precipitate from a reactive mineral/water system. The sequence of input data and information is more complex than for the **EQUILIBRIUM_PHASES** case as both the reactive phases and equilibrium phases must be defined. The sequence:

```
EQUILIBRIUM_PHASES 1
     Kaolinite      0.0    0.0
     Gibbsite       0.0    0.0
     K-mica         0.0    0.0
     K-feldspar     0.0    0.0
REACTION 1
     K-feldspar     1.0
     0.04 0.16 0.64 2.0 8.0 32.0 100 200 µmol
```

will simulate the dissolution of the component **K-feldspar** into a previously defined aqueous solution. Eight reaction steps are defined with the total number of moles (not the incremental amount) defined by the product of the stoichiometric factor **1.0** with the reaction total (e.g. **0.64**). In this example the system initially contains no other minerals; however, in the event that the dissolution of K-feldspar results in any of the four named minerals becoming supersaturated, the program will calculate the water composition, and amounts of the potential (although initially absent) co-existing minerals defined in the **EQUILIBRIUM_PHASES** section. The system could be initialized to be in equilibrium with, for example kaolinite, by replacing the expression

```
     Kaolinite      0.0    0.0
```

with

```
     Kaolinite      0.0    1.0
```

as this would introduce **1.0** moles of kaolinite into the system as a second, rapidly reacting, reactant. The expression

```
     Kaolinite      1.0    0.0
```

would be used to define a simulation in which kaolinite is initially absent, and is hindered from forming is solutions unless the saturation index is **1.0.**

Simultaneous reactions can be simulated by specifying more than one mineral associated with the **REACTION** keyword; the relative rates of addition of the minerals can be defined by using different stoichiometric factors. For instance, if one mineral, e.g. anorthite, is expected to react about 10 times faster than K-feldspar, then the input:

REACTION 1

Anorthite 10.0
K-feldspar 1.0
0.04 0.16 0.64 2.0 8.0 32.0 100 200 µmol

would, initially, simulate the simultaneous addition of 0.04 moles of anorthite and 0.004 moles of K-feldspar to the aqueous phase.

Another feature of PHREEQC allows users to generate subroutines to specify more complex reaction kinetics; however, this feature is not utilized in this study.

Databases and Activity Relations: Strictly speaking, thermodynamic databases are not software but they are an enabling component of the software. They consist of thermodynamic parameterizations of the phases required to define the physical system which is to be modelled. This typically involves an activity model for components dissolved in the aqueous phase and equilibrium constants for reactions defining the dissolution of solid and gaseous phases.

Mineral solubility is defined by an equilibrium constant; this is expressed as a product involving the activities of the reactants and reaction products. The activity of components dissolved in water is described by the relationship:

$$a_i = \gamma_i c_i \quad (1)$$

where a_i represents the activity of the solute i (mineral component), γ_i is the activity coefficient of component i, and c_i is the concentration of that component in water. The activity coefficients are functions of temperature, pressure and solution composition. Expressions relating the activity of specific ions to the concentration of aqueous components are generally referred to as solution models; traditionally geochemical studies have used an extended Debye-Hückel model with ion pairing to calculate solute activities (Appelo and Postma, 1993). This model is accurate for many natural waters; however, some of the waters in the sedimentary succession in the Clive oil field are very saline, and are well outside the concentration range of validity of the extended Debye-Hückel model. Special solution models are required to accurately model such saline solutions. These models are not yet fully developed although several theoretical treatments exist (e.g., Nesbitt 1982, Pitzer 1991). The best known and most fully developed such model is due to Pitzer (see Pitzer, 1991 for a review). Within Pitzer's (1991) framework, the activity coefficients arise, in part, because of pairwise and higher order interactions of the solutes.

The standard Pitzer approach treats electrolytes as being completely dissociated; ion pairing is generally considered less important in defining the behaviour of the ions. Instead, random, multi-body interactions between the individual ions dominate non-ideal behaviour of the ions. Briefly stated, the deviations between the experimental measurements on mean molal activity coefficients and those predicted using the Debye-Hückel theory are attributed to short-range interactions between ions. A suite of ion

interaction parameters are used to represent these interactions. These parameters can be extracted from experimental data, but their extraction is complex and time consuming and in many cases relevant experimental data are lacking.

The thermodynamic database PITZER.dat is included as part of the standard PHREEQC distribution package. It is primarily on a solution activity model reported in Harvie et al. (1984). This database, originally developed for the separate program, PHRQPITZ, includes Pitzer interaction parameters evaluated at 25°C for the system Na-K-Mg-Ca-H-Cl-SO_4-OH-HCO_3-CO_3-CO_2-H_2O (Plummer et al., 1988). A more extensive database (data0.ypf.R2), developed as part of the Yucca Mountain Project (YMP) for use with the geochemical code EQ3/6, was chosen in this study because it is better suited for studying the interaction between the rock and the highly-saline waters. Hereafter, this will be referred to as the YPF database. The YPF database was developed to predict the post-closure within the engineered barrier system of the YMP (Sandia National Laboratories, 2007). The original EQ3/6 was subsequently converted to a PHREEQC compatible format (Benbow et al., 2008). There are 40 elements, 236 aqueous species, and 450 solids in the YPF database. The system Na-K-H-Mg-Ca-Al-Cl-F-NO_3-SO_4-Br-CO_3-SiO_2-CO_2-O_2-H_2O is the core of the database development, with the applicable temperature ranging from 0°C to 200°C. Relative to the PITZER.dat, the YPF database involves a more comprehensive compilation of Pitzer parameters, and a more extensive set of mineral phases, especially aluminosilicates. More importantly, the temperature range over which the database is applicable is much greater than in the PITZER.dat database. It is noted that two versions of the Yucca Mountain Project database for dilute systems (data0.ymp.R2 and data0.ymp.R4) are the primary sources for silicate mineral log K data (Sandia National Laboratories, 2007) and the equilibrium constants describing gas dissolution into the aqueous phase.

It is important to recognize the limitations associated with the YPF database. The compiled selection of Pitzer parameters, equilibrium constants for aqueous species and solubility products for solids were obtained from various sources. Model validations have been performed for some binary (salt solutions with only two components such as $CaCl_2$) and mixed systems. However, for most of the binary systems, only a limited concentration range was examined. In the development of the YPF database, no guidelines were followed for data selection; as mentioned before, the database is essentially a compilation of data from various sources. Therefore, internal consistency was not necessarily maintained. A large number of aqueous species are included in the YPF database. Incorporation of aqueous species, if not bridged with the Pitzer model, could potentially lead to erroneous predictions. Finally, the database does not cover some of the compounds of interest to the geochemical modelling undertaken here. There are relatively few redox active species considered; this is because the database was primarily developed for use in oxidizing environments. Consequently, the description of sulphide minerals and the activity model for the sulphide species is restricted, this can be a significant limitation when dealing with many formation waters.

Finally, the PHREEQC default database for the Pitzer model does not contain any redox active species. Consequently, on encountering keywords that are required for the use of the Pitzer activity model, the default configuration of PHREEQC prevents the assigned oxidation potential from changing with imposed reactions. In contrast, when a database built around the Debye-Hückel activity model is used, the default behaviour is that the oxidation state varies with reactions. In order to model the evolution of solution compositions due to redox reactions, the keywords

-redox TRUE

must be added to the PHREEQC database following the keyword

PITZER.

This fact is not well described in the PHREEQC documentation but it is essential to ensure that redox systems are properly modelled. The dominant redox reactions in the systems considered here will involve iron and sulphur bearing minerals such as pyrite (FeS_2), siderite ($FeCO_3$), and anhydrite ($CaSO_4$) identified in some rock samples.

Results generated from the aqueous activity calculations are required to define equilibrium relationships between the aqueous phase and other phases. For instance, a separate gas phase will exist in equilibrium with an aqueous solution if the fugacity of each component in the gas phase is equal to the activity of these components in the aqueous phase multiplied by the Henry's law constant at the local temperature and pressure. Similarly, a mineral phase will be in equilibrium with an aqueous solution if the activity of that phase (generally equal to unity) is equal to the activity of this component in the aqueous phase multiplied by an equilibrium constant. The activity of the mineral component in the aqueous solution is expressed as a product of the aqueous activity of its constituent components in solution. As such, an accurate representation of the activity relations in each of the phases within a chemical system is of fundamental importance in the modelling of chemical systems, including geochemical modelling of CO_2 interactions with aquifer water and rocks. These activity models and the thermodynamic constants needed to determine phase stabilities are all included in the thermodynamic database, together with relevant temperature variations.

3.2 Composition of Formation Water

Analyses of waters recovered from the reservoirs of interest and several aquifers overlying them are reported in Table 2. These water analyses are incomplete; the reported components are commonly restricted to Ca, Mg, Na, Cl, SO_4, as well as alkalinity and pH, although selected samples also report K concentrations. As well, some of the reported Na values are likely derived from charge balance considerations rather than from an independent analytical determination, and as such the values include contributions from other ions, with K being the most important, in the solution.

As noted in previously, most waters, except the freshest waters in the study area (Figures 5 and 6) and all of the above waters listed in Table 2, are dominated by Na and

Cl. As well, with the exception of the waters recovered from the Belly River Group, the waters are relatively saline; and outside the recommended range of Debye-Hückel treatment of aqueous activities. However, given an appropriate activity model, this restricted water composition can be analysed with PHREEQC or other geochemical modelling codes to calculate the saturation state of some simple, commonly occurring, minerals both at surface and subsurface (in situ) conditions. Furthermore, it is generally possible to draw additional inferences based on the equilibrium relationships between these waters and common geological materials.

3.2.1 Equilibrium calculations with formation waters at surface conditions

The water compositions presented in Table 2 were used as input to the program PHREEQC. As discussed above, this software has been used extensively in the analysis and modelling of near surface waters. The database of thermodynamic constants used in this analysis is a temperature dependent, Pitzer-based model developed for saline solutions associated with evaporation of oxidizing ground waters (Sandia National Laboratories, 2007).

The results of PHREEQC calculations at near surface conditions are summarized in Table 4. This table gives the calculated saturation indices (SI) of commonly occurring minerals which contain only Na, Ca, Mg, Cl, CO_3, and/or SO_4. If a mineral is in equilibrium with a solution (water) the SI is 0. Practical sampling difficulties can lead to uncertainties in the water composition. These include sample contamination during recovery, poor sample preservation and analytical error. Typically saturation indices with a magnitude of less than 0.1 indicate that the water composition may be controlled by the solubility of the mineral phase. Table 4 demonstrates that, at surface conditions, all of the samples are clearly undersaturated with anhydrite and halite, but are in equilibrium or supersaturated with respect to calcite, as well as dolomite (not reported). Supersaturation with respect to a carbonate mineral is a common indication that CO_2 has been lost from the recovered water during sampling.

Table 4: Ionic strength (μ), calculated charge imbalance (CIB) and saturation indices (SI) of selected minerals, and the logarithm of the equilibrium CO_2 partial pressure (in bars) calculated at surface conditions for the formation water samples listed in Table 2.

Location	T (°C)	μ	CIB %	SI Anhydrite	SI Halite	SI Calcite	Log(PCO_2)
1	23	4.68	0.01	-0.30	-0.70	1.48	-1.90
2	23	4.28	0.00	-0.27	-0.84	1.26	-1.39
3	23	2.04	0.00	-1.31	-1.80	0.61	-1.29
4	23	1.28	0.33	-0.90	-1.48	0.63	-1.31
5	23	0.58	-0.01	-3.27	-2.44	1.48	-1.59
6	23	0.23	-3.44	-4.13	-3.15	0.76	-3.08
7	23	0.11	0.17	-3.75	-3.73	0.74	-3.04

That CO_2 may be lost during sampling is clearly shown by the calculated equilibrium CO_2 partial pressure (last column in Table 4). All of the samples have the potential to lose CO_2 to the atmosphere since the equilibrium with CO_2 partial pressure is greater than the atmospheric value of $\log(pCO_2) = -3.5$. Loss of CO_2 from the water samples will change the solution pH, and this can result in calcite supersaturation and, potentially, precipitation. As such, the possibility also exists that some Ca may have precipitated from these waters as calcite prior to analysis. However, at least in the samples from the deepest units, the potential loss is small as the concentration of Ca in these aqueous solutions is considerably greater than the total carbonate in solution; this condition restricts the amount of Ca which can precipitate.

Finally, the charge balance (reported in Table 4 as CIB%) for samples 1, 2, 3 and 5 is essentially perfect. This means that the total reported concentration of cations balances exactly with the reported anions, a condition which is generally an indication that the analysis is incomplete. Rather than analysing a full suite of dissolved constituents, one value is obtained by taking an incomplete analysis and adding enough of the missing constituent (generally Na) to achieve charge balance. (Samples 1, 2, and 5 are also lacking a K determination). Consequently, the results for these three samples listed in Table 2 likely represent independent (measured) analyses of Ca, Mg, Cl, and SO_4 as well as pH and alkalinity. Sample 3 is similar, although with an independent K determination.

3.2.2 Equilibrium calculations with formation waters at in-situ conditions and inferred water compositions

The results of the PHREEQC calculations at subsurface conditions are summarized in Table 5.

Table 5: Ionic strength (μ) and saturation indices of selected minerals, and the logarithm of the equilibrium fugacity of CO_2 (bars), calculated with PHREEQC at in situ temperatures for the formation water samples listed in Table 2 whose locations are listed in Table 1. The formation porosity (Table 3) is listed in the second column. Based on porosity of the Basal Belly River Group and on the upward increase of porosity with decreasing depth, an arbitrary value of 12.5% is applied for Upper Belly River Group for which there are no data.

Location	ϕ%	T (ºC)	μ	Anhydrite	Gypsum	Halite	Calcite	pCO_2(g)
1	5.9	65	4.68	-0.14	-0.39	-0.75	1.65	-1.33
2	5.2	60	4.27	-0.12	-0.32	-0.89	1.52	-0.99
3	9.7	55	2.04	-0.66	-0.76	-1.52	0.93	-1.00
4	9.7	57	1.28	-1.01	-1.10	-1.85	0.94	-0.96
5	10.6	50	0.58	-3.03	-3.05	-2.48	1.65	-1.23
6	12.2	35	0.24	-4.02	-3.93	-3.17	0.80	-2.88
7	12.5	30	0.11	-4.69	-3.56	-3.75	0.77	-2.93

Note again that only temperature corrections are applied to these calculations; corrections for in-situ pressures are neglected. The results presented here are essentially the same as those in Table 4; the samples are supersaturated with respect to calcite, and, with the exception of anhydrite in samples 1 and 2, they are significantly undersaturated with respect to the other minerals of interest for this restricted chemical composition.

The analyses in Table 2 can be supplemented with estimated values based on assumptions of water/mineral equilibrium. Components which are not analysed but are of importance to CO_2-mineral reactions are Si, Al and K. As well, analysed values of the bicarbonate content generally are not representative of in-situ conditions, as CO_2 commonly volatilizes during sample recovery.

Calcite is a very common mineral; it is generally safe to assume that the formation fluids are in equilibrium with calcite when it is present in the rocks. Although calcite does not appear as present in all the normative mineral calculations (see next chapter), there are indications of at least trace quantities of carbonate minerals in almost all of the rock samples. It is common practice to fix pCO_2 on the assumption that if a sample is supersaturated with respect to calcite it is because of the loss of CO_2 on sampling. Dolomite is also a very common constituent in sedimentary rocks; however, it is less reactive than calcite, and will generally not precipitate from formation water under ambient conditions (Warren, 2000). At elevated temperatures energetic barriers to its formation decrease and it may also exert an equilibrium control on the fluid composition.

There are potential problems with estimating CO_2 partial pressures in the formation waters using such corrections. Produced fluids may be mixtures of fluids, and mixtures of solutions do not necessarily demonstrate the same equilibrium relations as the source waters for the mixture. Alternatively, due to the absence of the mineral in the aquifer, the water may not have, in fact, been in equilibrium with a specific carbonate mineral. However, given the imperfections of in-situ water sampling, such assumptions are generally necessary to correct water analyses to better represent in-situ compositions. Given that some corrections must be made to the composition of these water samples, it is important to ensure that the eventual estimates for the composition of the water samples at in-situ conditions are stable (in equilibrium) with the in-situ mineralogy.

In a similar vein, the dissolved silica can also be fixed by assuming that the aqueous solution is in equilibrium with a specific silica-bearing mineral. Generally the upper bound for silica is fixed by equilibrium with metastable SiO_2 phases, such as cristobalite. These forms crystalize easily from supersaturated solutions, although the less reactive phase quartz, can be assumed (Rimstidt, 1997). It is assumed, for the calculations presented below, that the phase cristobalite is controlling the SiO_2 solubility. However, in the presence of Al and base cations, a number of clay minerals may be more stable than pure SiO_2 phases (Nesbitt, 1977, Garrels 1984).

As with SiO_2, the concentration of Al in solution can be estimated by assuming equilibrium with an aluminosilicate; here kaolinite was used. Aluminum hydroxides can control Al solubility in acidic, near-surface aqueous solutions, where more complex Al-bearing phases can be kinetically hindered. However, in the presence of quartz, many aluminosilicate phases will be more stable than the hydroxide. These should control Al solubility given an extensive time to reach equilibrium.

The water analyses listed in Table 2 are supplemented with values for the important constituents K (when absent from the analysis), Si, and Al to obtain compositions which are suitable for further modelling of the geochemical reactions. Furthermore, CO_2 which is assumed lost during sampling must be added back to the solution. These components are added by dissolving CO_2, kaolinite, SiO_2, and KCl into the aqueous solution up to the point where the solution is in equilibrium with the phases calcite, kaolinite, cristobalite and potassium feldspar. The additions of CO_2 will drive the system to be more acidic than the sampled solution; this is simulating the natural process which presumably led to the calcite supersaturation in the first place. Ideally, the other additions should not appreciably affect any of the other measured concentrations. Addition of SiO_2 has virtually no impact, and while kaolinite dissolution does consume acid, because of its low solubility, the effect on pH is minimal. Addition of KCl will increase the chloride concentration in the solution, but, as long as the amount of potassium remains small in comparison with the total chloride, no further corrections are needed. Ideally, an identical amount of NaCl should be removed from the solution; however, the analytical error on the original Cl measurement is expected to be about ±5%, so increases of this order are acceptable. The supplemental water compositions that satisfy the equilibrium relations described above are listed in Table 6

Table 6: Calculated composition (in moles/kg H_2O) of formation water samples of Table 2 equilibrated with calcite, K-feldspar (when no K analysis), cristobalite and kaolinite. The sample locations are listed in Table 1

Location	Al (moles/kg)	K (moles/kg)	Si (moles/kg)	log (pCO_2(g))	pH @T	SI (K-feldspar)
1	2.4×10^{-9}	2.68×10^{-2}	8.07×10^{-4}	0.42	4.73	0.00
2	4.4×10^{-9}	2.98×10^{-2}	7.47×10^{-4}	0.59	4.71	0.00
3	1.3×10^{-10}	1.3×10^{-2}	9.30×10^{-4}	-0.04	5.45	0.28
4	2.5×10^{-11}	5.08×10^{-3}	1.08×10^{-3}	0.01	5.73	0.15
5	2.0×10^{-11}	2.47×10^{-3}	1.03×10^{-3}	0.49	5.91	0.00
6	1.84×10^{-10}	5.134×10^{-3}	7.64×10^{-4}	-2.01	7.34	1.72
7	4.74×10^{-10}	3.07×10^{-4}	6.91×10^{-4}	-2.10	7.53	0.70

With these compositions, the formation water samples 1, 2 and 5 at in-situ conditions are constrained to be in equilibrium with calcite, cristobalite, kaolinite and K-feldspar. Cristobalite is a crystalline form of SiO_2, which is more soluble, and more readily

precipitated from solution, than quartz. Either cristobalite or chalcedony (another silica polymorph with solubility intermediate between quartz and cristobalite) is more likely to control aqueous silica content than quartz in low temperature sedimentary rocks (Kharaka et al., 1988). Calculated mineral saturation indices for several key minerals are listed in Table 7 for each of the formation water samples listed in Table 2.

Table 7: Saturation indices of key mineral phases in the formation water samples recorded in Table 2 with locations listed in Table 1. Two cases are presented for the water samples 6 and 7. Cristobalite equilibrium is assumed for the samples 6 and 7, while equilibrium with sodium montmorillonite is assumed for the samples 6A and 7A. Absent values represent saturation indices less than -2.5.

Mineral \ Site	1	2	3	4	5	6	6A	7	7A
Albite	-0.31	-0.5	-0.18	-0.02	-0.28	0.47	-0.54	0.3	-0.64
Anhydrite	-0.13	-0.11	-0.66	-1.48					
Aragonite	-0.16	-0.15	-0.14	-0.14	-0.13	-0.11	-0.11	-0.11	-0.11
Calcite	0	0	0	0	0	0	0	0	0
Chabazite	4.54	4.21	5.5	5.49	4.53	9.09	6.85	8.42	6.34
CO_2(g)	0.42	0.59	-0.04	0.00	0.49	-2.01	-1.99	-2.1	-2.08
Cristobalite(alpha)	0	0	0	0	0	0	-0.5	0	-0.46
Dawsonite	-2.02	-1.69	-1.63	-1.56	-0.82	-1.44	-0.93	-1.3	-0.82
Dolomite	0.84	0.96	0.9	0.93	0.78	0.98	0.99	0.95	0.98
Gypsum	-0.38	-0.31	-0.76	-1.10					
H_2O(g)	-0.67	-0.76	-0.83	-0.78	-0.92	-1.25	-1.25	-1.37	-1.37
Illite	-0.59	-0.68	-0.46	-0.53	-0.88	0.61	0.01	-0.05	-0.62
Kaolinite	0	0	0	0	0	0	0	0	0
K-feldspar	0	0	0.28	0.15	0	1.72	0.72	0.7	-0.24
Magnesite	-0.56	-0.47	-0.57	-0.53	-0.72	-0.63	-0.62	-0.68	-0.66
Montmo-Ca	0.36	0.23	0.41	0.42	0	1.03	-0.14	0.97	-0.12
Montmo-K	-0.07	-0.15	0.05	0.02	-0.32	0.94	-0.23	0.57	-0.52
Montmo-Mg	0.38	0.26	0.42	0.45	-0.01	1.03	-0.14	0.96	-0.12
Montmo-Na	0.4	0.27	0.49	0.56	0.19	1.17	0	1.08	0
Phillipsite	5.06	4.88	6.37	6.41	5.76	10.38	5.95	9.67	5.55
Pyrophyllite	-0.26	-0.29	-0.35	-0.35	-0.39	-0.47	-1.47	-0.5	-1.43
Quartz	0.48	0.49	0.5	0.49	0.51	0.54	0.04	0.55	0.08
SiO_2(am)	-0.46	-0.46	-0.46	-0.46	-0.47	-0.47	-0.97	-0.47	-0.93
Talc						0.47	-1.56	0.11	-1.74

With the exception of dolomite, quartz and several zeolites (e.g. phillipsite and chabazite) for which the thermodynamic data may be incorrect, the minerals saturation indices are small positive numbers (less than about 0.5) which indicates that the minerals may potentially precipitate from the solution, at equilibrium, or undersaturated in the modified solution.

Samples 3, 4, 6 and 7 have potassium included in the water analysis. The first two of these waters are slightly supersaturated with K-feldspar (saturation indices 0.14 and 0.28 respectively) which suggests that the water composition and the equilibrium assumptions are consistent. Samples 6 and 7 are significantly more supersaturated with respect to potassium feldspar. This suggest that the assumptions behind the calculations are inaccurate. Other observations also suggest that the corrected solution analysis is inaccurate; the saturation indices of the montmorillonite-type minerals and talc are also positive. Although slight supersaturation of the montmorillonites is also the case for other samples, the saturation index is considerably greater for samples 6 and 7. The situation can be mostly rectified if the aqueous silica concentration is determined by assigning the sodium form of montmorillonite as a stable phase. In essence, this suggests that the phase controlling the aqueous silica concentration is a clay, rather than a pure, metastable, form of silica.

Most of the other samples (i.e., not samples 6 or 7) are slightly supersaturated with respect to several clay minerals, generally a sodium (and other cationic forms) montmorillonite. This may also suggest that the choice of cristobalite as the silica controlling phase is incorrect. In subsequent calculations the slightly less soluble phase chalcedony is used (see Section 4.2.1) when deemed appropriate.

Interestingly, with the exception of the sulphate minerals anhydrite and gypsum (both of which are undersaturated and consequently likely absent from the host rock), the saturation indices of many mineral phases for water samples #3 and #4 are quite similar. These waters, while quite different in total dissolved solids content, are both recovered from the Lower Mannville Group. The fact that the same mineral suite is apparently in equilibrium with these waters is expected from the similarity of their origin.

4. Quantitative Mineralogy

The mineralogical characterization of core samples recovered in, and around the Clive oil field is reported in Bachu et al. (2011, Appendix D), although further interpretation of that data is required for numerical simulations of geochemical reactions between CO_2 and formation water and minerals. This interpretation involves estimating the mineral content of a rock by integrating various, independently determined physical and chemical properties of the rock. This involves determining a mineralogical composition that is consistent with results obtained from two (or more) analytical techniques. Semi-quantitative XRD can be used to detect which minerals are present in a rock sample, while not necessarily providing an accurate estimate of the proportions. X-ray fluorescence spectroscopy (XRF) gives an accurate representation of the chemical composition of the whole rock, while providing no information about the constituent minerals. Other techniques are available to determine the amount of carbon and sulphur in a rock specimen. Additionally, the chemical composition of individual mineral grains can be determined with an electron microprobe (EPMA). These data can be integrated using techniques described in Slaughter (1989), de Caritat et al. (1994) and Paktunc (1998) to provide a good estimate of the mineralogical composition, or mineral norm of a rock sample.

4.1 Laboratory Analyses

Samples were selected for mineralogical analysis from the Leduc D3-A and Nisku D2 oil reservoirs in the Clive oil field and from the aquifers and aquitards in the sedimentary succession above them. The sample identification, well location, sample depth and formation name are given in Table 8 (samples are numbered in order of sampling). The first nine rock samples are listed in ascending stratigraphic order starting with the Calmar Fm. and are from the caprock overlying the oil reservoirs of interest (Calmar Fm. and Wabamun Gp.) and aquifers higher up in the sedimentary succession except for the Ostracod zone which is a thin aquitard within the Lower Mannville Group. Note that the Ellerslie Fm, Ostracod Zone and Glauconitic Sandstone are all strata in the Lower Mannville Group. The next two samples (EN-10 and EN-11) are from the Nisku D2 and Leduc D3-A oil reservoirs. Samples EN-30 through EN-34 were collected and analyzed in a second sampling round to complete sampling of all lithostratigraphic units in the sedimentary succession above the oil reservoirs up to the Bearpaw Formation for which, being too shallow, no core samples exist. These are also listed in ascending stratigraphic order. Multiple samples were taken from the Calmar, Ostracod and Belly River formations. At the time of sampling, significant differences in lithology were recognized and two samples were taken from each to represent the observed heterogeneous formation mineralogy.

A number of different analytical techniques were used to evaluate the mineralogy of each sample. These include XRF (X-Ray Fluorescence), LECO[1] (Carbon and Sulphur

[1] The term LECO is the name of the original manufacturer for this specific type of instrument, and it is commonly used to indicate the apparatus from all manufacturers.

loss by ignition), ICP-MS (Inductively Coupled Plasma Mass Spectrometry analysis), XRD (X-Ray Diffraction), SEM (Scanning Electron Microscopy) and EDX (Energy Dispersive X-Ray analysis, on the SEM). The first three analytical results give a direct measurement of the elemental composition of the entire sample. SEM provides an image of a section of the core sample and allows portions to be analyzed by EDX. The SEM does allow identification of phases which are present in trace (or less amounts), and provides a means to evaluate the dimensions of a mineral and the relative relationship of the minerals. XRD provides the identity of the major minerals and gives an estimate of the relative percentage of each. It does not give the composition of the phase. If the phase is non-stoichiometric, it may not be easy to identify via XRD.

Table 8: Mineralogical sample identification, well location, depth, formation and type of mineralogical samples from the Clive study area analyzed in this study.

Sample	Well Location	Depth (m)	Formation	Type
EN-1	6-13-41-25W4	~ 1864.00	Calmar	Caprock
EN-2	6-13-41-25W4	~ 1860.50	Calmar	Caprock
EN-3	6-13-41-25W4	~1855.00	Wabamun	Aquitard
EN-4	11-5-41-23W4	~ 1492.00	Ellerslie (Lower Mannville)	Aquifer
EN-5	11-5-41-23W4	~ 1478.00	Ostracod Zone (Lower Mannv.)	Aquitard
EN-6	11-5-41-23W4	~1474.00	Ostracod Zone (Lower Mannv.)	Aquitard
EN-7	11-5-41-23W4	~ 1463.30	Glauconitic Ss (Lower Mannv.)	Aquifer
EN-8	11-12-41-25W4	~ 1388.00	Viking Ss	Aquifer
EN-9	9-35-41-23W4	~695.25	Basal Belly River Sandstone	Aquifer
EN-10	9-35-39-24W4	~1847.00	Nisku	Reservoir
EN-11	9-35-39-24W4	~1876.50	Leduc	Reservoir
EN-30	6-7-40-24W4	~1570.50	Lowermost Upper Mannville	Aquifer
EN-31	8-6-40-25W4	~1448.00	Colorado shales	Aquitard
EN-32	12-17-39-24W4	~1401.90	Viking Shale	Aquitard
EN-33	7-14-41-23W4	~548.00	Upper Belly River Sandstone.	Aquifer
EN-34	12-5-39-23W4	~748.50	Lowermost Upper Belly River	Aquifer

Estimates of the mineralogical composition of these core samples based on XRD peak heights are summarized in Table 9. The Calmar, Wabamun, Nisku and Leduc formations are primarily carbonate and/or sulphate mineral containing formations. The remaining are all siliceous, with the XRD analysis identifying quartz as the predominant mineral phase. The Leduc D3-A was found to be 100% dolomite. The Nisku D2 is predominately composed of anhydrite (calcium sulphate) and dolomite. However, the high amount of anhydrite observed is most likely due to the presence of an anhydrite vein in the core sample. The XRD results indicate that the Calmar Formation is dolomitic with 20 to 30% quartz and significant amounts of pyrite present. The Wabamun Group is predominately composed of anhydrite (calcium sulphate) and dolomite.

Table 9: Mineralogical composition of the analyzed samples (see Table 8) estimated from XRD analysis.

Mineral	Sample and Formation							
	EN-1 Calmar	EN-2 Calmar	EN-3 Wab.	EN-4 Eller.	EN-5 Ostr.	EN-6 Ostr.	EN-7 Glauc.	EN-8 Viking SS
Anatase						**< 1**	**< 1**	
Anhydrite			65					
Calcite		5				20	< 1	
Dolomite	70	50	35			5		
Halite								
Illite	5	5		< 1	5	5	5	< 1
Kaolinite		< 1		5	5	5	5	< 1
K-feldspar		5		5			< 1	
Plagioclase				< 1	< 1	< 1	< 1	5
Pyrite	5	5		< 1				< 1
Quartz	20	30	< 1	90	75	65	90	95
Siderite					15			

Table 9 continued.

Mineral	Sample and Formation							
	EN 9 Basal Belly River	EN-10 Nisku	EN-11 Leduc	EN-30 Upper Mannv.	EN-31 Colo.	EN-32 Viking Shale	EN-33 Upper Belly River	EN-34 Upper Belly River
Anatase						<1	<1	5
Anhydrite		70						
Calcite					20			
Dolomite		30	100		5		15	
Halite						5	<1	<1
Illite	5			5	5		5	5
Kaolinite	10			5	<1	5	5	5
K-feldspar				5			5	5
Muscovite						5		
Plagioclase	20			10		5	5	10
Pyrite				<1	5			<1
Quartz	65		<1	75	65	70	65	70
Siderite				<1		10		

The Ellerslie Fm. is almost entirely quartz with small amounts (approximately 5%) of kaolinite and potassium feldspar. Both samples from the Ostracod Zone are also quartz rich; however, the deeper Ostracod sample contains in addition siderite, kaolinite and illite, whereas the shallower sample contains calcite, dolomite, kaolinite and illite in addition to the quartz. The Glauconitic Sandstone is predominately quartz with 5% each of illite and kaolinite, and the lowermost Upper Mannville has about 75% quartz, 10% plagioclase and 5% of each of illite, kaolinite and potassium feldspar. The Viking

Sandstone sample has a higher proportion of quartz, and 5% calcium plagioclase. The Viking Formation shale has about 70% quartz and 5% of each kaolinite, muscovite, plagioclase and siderite. Halite was identified (5%) but is probably due to drilling fluid contamination. The Colorado shale is about 65% quartz, 20% calcite and 5% of each dolomite, illite and pyrite and the Basal Belly River Sandstone is 65% quartz, 20% plagioclase, 10% kaolinite and 5% illite. The lowermost Upper Belly River has about 70% quartz, 10% plagioclase and 5% each of illite, kaolinite and potassium feldspar. The Upper Belly River Fm. has about 65% quartz, 15% dolomite and 5% each of illite, kaolinite, potassium feldspar and plagioclase. Stratigraphic units above the Upper Belly River were not analyzed for mineralogical composition because of the lack of core in the study area. These results are also considered in detail together with the water compositions recovered from the same formation in the following section.

The concentration of major oxides of these samples, as determined by XRF analysis, is given in Table 10. As well, the concentration of inorganic carbon (as CO_2) and elemental sulphur (S) determined by LECO is also reported.

Table 10: Major oxide composition of rock samples as determined by XRF and LECO ($InCO_2$ and S). The $InCO_2$ values marked with an asterisk were estimated from the sample loss on ignition; ND represents composition below detection levels.

#	SiO_2	Al_2O_3	Fe_2O_3	Mg	Na_2O	CaO	K_2O	TiO_2	P_2O_5	MnO	$InCO_2$	S
1	24.1	5.24	2.05	14.48	0.24	19.61	2.01	0.28	0.05	0.02	29.63	0.79
2	33.9	8.94	2.72	12.02	0.34	13.92	3.78	0.41	0.09	0.03	22.11	0.25
3	0.8	0.21	0.09	8.76	0.00	36.83	0.02	0.00	0.00	0.00	20.13	13.93
4	90.8	1.32	1.25	0.29	0.04	0.91	0.27	0.23	0.01	0.02	6.53	0.79
5	49.7	13.00	12.49	2.81	0.41	2.64	2.94	0.55	1.07	0.13	13.75	0.09
6	53.4	9.08	2.11	1.87	0.39	12.88	1.75	0.48	0.28	0.08	18.74	0.58
7	82.8	7.74	1.14	0.41	0.53	0.49	1.49	0.81	0.13	0.01	1.87	0.22
8	92.2	2.02	1.54	0.28	0.31	0.41	0.39	0.09	0.10	0.01	2.16	0.35
9	79.3	8.94	2.10	0.65	1.92	0.49	1.98	0.39	0.09	0.03	1.21	0.04
10	0.49	0.12	0.12	20.40	nd	31.78	0.02	0.01	0.01	0.02	44.93*	1.70
11	0.78	0.24	0.14	20.63	nd	29.94	0.02	0.01	0.01	0.01	47.10*	0.11
30	69.9	16.15	2.05	0.52	2.03	0.16	3.41	0.77	0.03	0.01	1.58	0.56
31	47.7	11.22	5.64	1.89	0.54	10.42	2.23	0.54	0.19	0.02	25.19	3.47
32	60.4	13.82	8.7	1.65	1.02	0.63	2.33	0.72	0.27	0.11	9.68	0.27
33	63.3	10.47	4.6	3.27	1.35	3.87	2.53	0.45	0.17	0.08	10.96	0.2
34	59.4	16.97	5.8	2.07	1.8	0.45	2.12	0.76	0.11	0.03	5.39	0.43

There is a great deal of compositional variability seen in Table 10, with two samples containing greater than 90% silica (SiO_2) and three samples containing less than 1% SiO_2. Six samples contain in excess of 20% CO_2 (see column "$InCO_2$" in Table 10) indicating the presence of a significant proportion of carbonate minerals, and a single

sample contains greater than 10% S. Each of these chemical signatures gives an indication of the mineral within the core sample; however, integrating these data with the minerals identified as present in the sample by XRD gives a better indication of the relative mass of each mineral present in the samples. Results of such calculations are present in the following section.

4.2 Rock Mineralogy – Normative Calculations

The program LPNORM (de Caritat et al., 1994), and the data presented in Tables 8 and 9 were used to obtain accurate estimates of the proportion of each mineral within the rock (expressed as weight percentage). These proportions are also referred to as mineral norms; these are necessary input for the geochemical simulations presented in the Chapter 5. The normative calculation program, LPNORM (de Caritat et al., 1994) requires as input the chemical composition of the rock, (expressed as weight percent of the constituent oxides), as well as the total inorganic carbon of the sample, and the sulphur content. The composition of the constituent minerals is also a required input; commonly these are assumed to be the idealized mineral compositions. Compositional data obtained from an electron microprobe can also be incorporated into LPNORM data files to better constrain the mineralogical fit, although such data were not available for this study.

The user of LPNORM is allowed to indicate a specific objective function, as well as a series of constraints, on the calculated mineral norms. The most commonly imposed constraints are to maximize, or minimize, the amount of a particular mineral in the calculated norms. These can be particularly useful if the program is finding solutions which are incompatible with known properties, such as those determined from the XRD spectra. Other linear constraints, such as limiting the total amount of quartz in a sample to be less than or equal to a specified value based on independent determinations can also be imposed.

It was noted above that the composition of each mineral is required as input for LPNORM. Many mineral compositions are poorly constrained; this is particularly true for clay minerals. Since the outputs from the program LPNORM are used to define rock compositions for use in geochemical simulations, the minerals included in the LPNORM calculations are restricted to those for which thermodynamic data are available. If the composition of water in contact with the minerals is known this composition can also be used to constrain the mineral norm. For example, if the partial pressure of CO_2 at in-situ conditions is estimated by imposing the requirement of calcite equilibrium, then the presence of calcite should be required in the normative solution. Ideally, mineral phases should be restricted to those which are at, or nearly at, equilibrium with the formation water following corrections to in-situ conditions. Minerals which are significantly out of equilibrium with the co-existing water composition should be excluded from normative calculations unless there is unequivocal evidence of their presence in the rock.

4.2.1 Silica solubility

The stability of many minerals in the formation waters cannot be determined directly from the water compositional data presented in Table 2, as many key solute concentrations are absent from the available water analyses. This difficulty was overcome in constructing Table 7 by assuming that locally the waters are in equilibrium with the clay mineral, kaolinite, and the pure silica mineral, cristobalite. Since cristobalite is one of the more soluble polymorphs of silica, its choice will result in silica bearing minerals being more stable in these solutions (waters) than had a less soluble form been chosen.

The geochemical software package SOLMINEQ.88 (Kharaka et al., 1988) uses chalcedony, a slightly less soluble silica mineral, as an indicator mineral for estimating the *in-situ* temperatures of aquifers from which waters are produced when an aqueous silica analysis is available. This geo-thermometer is recommended for waters produced from reservoirs which are cooler than about 70ºC. This is above the assumed temperature of each of the formations considered here. Unfortunately, the thermodynamic database used for the calculations presented here (data0.ypf.r2) is not distributed with chalcedony in the solids database, so its thermodynamic properties must be added to the data base before it can be designated as an equilibrium phase. As well, the thermodynamic description of the silica (and silicate) minerals is quite different between data0.ypf.r2 and the database used by SOLMINEQ.88, due to the adoption of Rimstidt's (1997) estimates of low-temperature quartz solubility. Here the thermodynamic properties of chalcedony are estimated from the solubility of quartz and cristobalite listed in data0.ypf.r2, and the solubility of these minerals and chalcedony given in the SOLMINEQ.88 data base. Each of these solubility values are plotted as a function of temperature in Figure 9, together with the interpolated value used here to estimate the solubility product of chalcedony within the thermodynamic description of silica minerals used in data0.ypf.r2. Subsequent calculations presented here are based on the assumption that the aqueous solution is in equilibrium with one of these three silica phases. The specific phase chosen is based on equilibrium constraints imposed by other silicate phases; the phases chosen will noted in the accompanying text. Changes in the stable silica phase will result in minor changes in the equilibrium water compositions listed in Table 6.

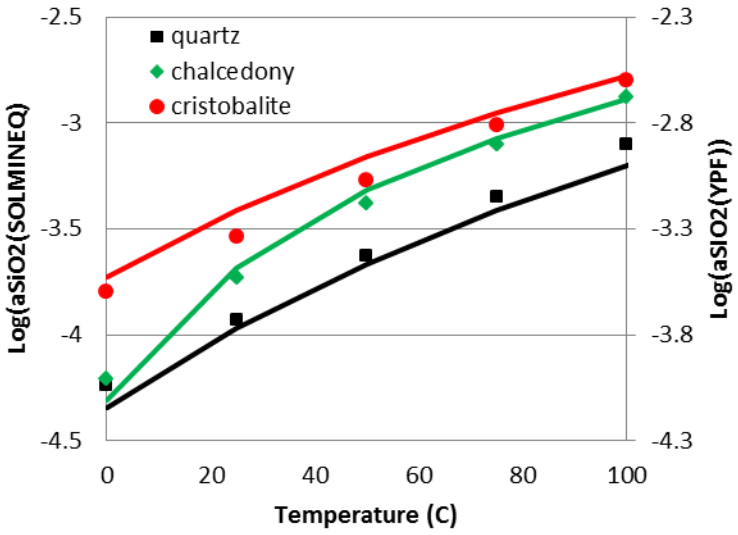

Figure 9: Solubility of the silica polymorphs quartz, α-cristobalite, and chalcedony as given in data0.ypf.r2 (lines, right Y axis) and the thermodynamic database accompanying SOLMINEQ88 (symbols, left Y axis). There is a roughly 0.2 log unit difference between the data sets. The green line representing chalcedony saturation is estimated from quartz and cristobalite solubilities and the relative differences established from the SOLMINEQ88 database.

4.2.2 Normative calculations of rock samples from the oil reservoirs and aquifers

Nine samples (Table 8) obtained from cores taken from the oil reservoirs (samples 10 and 11) and overlying aquifers (samples 4, 7, 8, 9, 30, 33, 34) were analyzed for mineralogical and chemical composition. Similarly, Table 2 presents the major ion composition of five waters recovered from the high permeability Mesozoic formations overlying the Leduc D3-A and Nisku D2 oil reservoirs in the area of the Clive field with a further two water analyses from the two reservoirs. These seven water analyses consist of one analysis from each of the Leduc, Nisku, Viking, Belly River, and Basal Belly River, and two from the Lower Mannville (Table 1). They may, ideally, be used to determine which minerals are stable, and hence likely to be present, within each formation. In the instance where there are two rock samples from a given formation, the rock sample for which the mineralogical analysis was most readily equilibrated with the recovered water was used for further geochemical modelling. These rock samples (En-4, and En-33) are discussed in some detail below along with the single samples from the remaining formations; the remaining two aquifer samples (samples En-7 and En-34) are also discussed briefly. The pairings between rock and water analyses are tabulated in Table 11.

Table 11: Correspondence between water and rock samples. The underlined rock samples were used in the PHREEQC modelling.

Water Sample	Formation	Ionic Strength	Mineralogy samples
1	Leduc	4.68	En-11
2	Nisku	4.27	En-10
3	Lower Mannville-1	1.28	En-4, En-7
4	Lower Mannville-2	2.04	En-4, En-7
5	Viking Sandstone	0.58	En-8
6	Basal Belly River	0.24	En-9
7	Upper Belly River	0.11	En-33, En-34

Reservoir Rocks (Leduc 3D-A and Nisku D2): XRD results from the reservoir samples (samples 10 and 11) indicate that the rocks are comprised almost entirely of dolomite and anhydrite (Table 8). This is in good agreement with the compositional data for the rock (Table 10) which show that the components present in these minerals (CaO, MgO, CO_2 or S) comprise greater than 98 wgt % of the samples. Following the corrections made to the composition of the aqueous solution (Tables 5 and 6) the recovered waters are at, or near equilibrium with calcite (equilibrium with calcite is a constraint), and anhydrite (SI(anhydrite) = -0.11 and -0.13 for samples 10 and 11). These SI values for anhydrite are within commonly encountered values in waters recovered from anhydrite bearing rock; the slight undersaturation may be due to analytical errors, errors in the solution activity model, and/or failure to make corrections for subsurface pressures[2]. The solutions are both significantly supersaturated with respect to the most stable magnesium/calcium carbonate (ordered dolomite), and marginally undersaturated with respect to its least stable form (disordered dolomite). This is a common occurrence, and can be treated in modelling by maintaining a constant degree of saturation with respect to either of these phases (SI(dolomite) = 0.96 and 0.84 respectively for samples 10 and 11). Thus, the recovered waters are compatible with the dominant minerals found in the reservoir, although only if the stability of the dolomitic mineral is intermediate between the ordered and disordered dolomite. The composition of the aqueous solution was further constrained to be in equilibrium with K-feldspar, kaolinite (Section 3.2.2) and chalcedony (Section 4.2.1). Following this set of corrections, the clay minerals Na-montmorillonite and Mg-montmorillonite are also in equilibrium with the fluid (SI <0.1), so these phases are also incorporated into the suite of minerals included in the LPNORM calculation.

[2] Anhydrite solubility increases with increasing pressure (Monnin, 1990); including pressure corrections to the existing solution model would lead to a greater departure (more negative SI) on the order of a further 0.1, from equilibrium.

There are also analyses for Fe_2O_3, TiO_2, P_2O_5 and MnO listed in Table 10. These components are not represented in either any of the identified mineral phases, or in the solution analyses. Typically TiO_2 is found in sediments as the chemically inert mineral anatase (TiO_2). Phosphate is typically found either in phosphate minerals such as apatite or vivianite. Iron and manganese may reside in a number of mineral phases, either as integral to the phase (e.g. pyrite, siderite, rhodochrosite or vivianite), or as trace impurities in clays and carbonates. In the absence of any guidance from other analysis, these oxides are generally assigned to specific phases. Ideally, the fluid/rock interactions should not be greatly impacted by this choice; however, in instances where these oxides are present in significant quantities this condition will not be satisfied, and further mineralogical work must be undertaken to further constrain the siting of iron and manganese within the rock. However, in the two reservoir samples, these oxides are present at only trace levels. The LPNORM results for each of the samples discussed here are given in Table 12.

Clearly, samples 10 and 11 are dominated by dolomite, with anhydrite as the only other significant phase (present at about 7% in sample 10; the content of anhydrite in the larger hand specimen shown in Section 11.10 of Bachu et al., 2011 is clearly greater than this). The presence of other minerals, such as quartz, calcite, and K-feldspar, within these samples is inferred solely from the bulk chemical analysis and equilibrium considerations.

Table 12: Mineralogical composition (weight %) of aquifer samples based on LPNORM analysis. The entry for illite corresponds to the contributions from illite and montmorillonite.

Formation	Leduc	Nisku	Lower Mannville	Upper Mannville	Viking	Basal Belly River	Upper Belly River
Water sample	**1**	**2**	**3**	**4**	**5**	**6**	**7**
Rock sample	**EN-11**	**EN-10**	**EN-4**	**EN-30**	**EN-8**	**EN-9**	**EN-33**
Albite			0.34	14.54	2.20	14.31	11.42
Anatase	0.01	0.01	0.23	0.77	0.09	0.39	0.45
Anhydrite		7.07					
Calcite	2.20	0.76	0.90		0.23		
Dolomite	94.40	91.34	1.33	0.53	0.97	1.61	12.73
Iron (hydr)oxide						1.13	
Illite *		0.19		11.18	2.05	8.22	17.43
Kaolinite	0.55	0.13	2.44	17.82	1.85	5.00	4.35
K-feldspar	0.12	0.12	1.60	20.15		11.30	8.00
Pyrite	0.21		1.48	1.05	0.67	0.07	0.37
Muscovite						0.52	
Quartz	0.45	0.22	88.41	31.24	89.15	54.18	38.37
Rhodochrosite	0.02		0.03	0.02	0.02	0.05	0.13
Siderite		0.15	0.36	1.89	1.39	1.11	5.90
Vivianite		0.02	0.02	0.08	0.25	0.23	0.43

Lower Mannville Group: As noted in Section 2.3, there are two water samples (3 and 4) recovered from within the Lower Mannville Group. Although the salinity of these samples differs greatly, the minerals which are stable in both waters (at cristobalite saturation) are similar (Table 7). Dolomite and the montmorillonites are all clearly supersaturated in both water samples (although at levels comparable to those seen in other water samples used in this study). Additionally, the saturation index of the alkali feldspars (albite and K-feldspar) in both water samples are within a range of +/-0.3 of equilibrium. This is a greater deviation than might be expected based on ideally sampled waters and perhaps this indicates there was some minor contamination of the recovered water with drilling fluids.

The core samples, EN-4 and EN-7 are recovered from the Lower Mannville Group. Sample EN-4 clearly contains significant quantities of kaolinite, quartz and K-feldspar, with minor amounts of pyrite and albite. XRD results from Sample EN-7 identify the clay minerals illite and kaolinite, and quartz, although the chemistry suggests that it also contains minor amounts of the alkali feldspars, calcite, and anatase.

LPNORM calculations utilizing the minerals at or near equilibrium with the inferred local water composition did not unequivocally satisfy the constraints provided by the XRD results. The best agreement was with the sample EN-4 which was calculated to be predominantly quartz (just less than 90%), with kaolinite, dolomite, pyrite and K-feldspar present at levels of 1 - 2.5%, and with traces of calcite and albite. This is in good agreement with the XRD results.

For sample EN-7 there was less agreement between the LPNORM and XRD results; the normative calculation gave a quartz content of less that 50%, as well as significant volumes of dolomite and siderite (meaning that these minerals would be expected to show a signal with XRD). XRD peaks from both of these minerals were not noted (Table 9). Similarly, the calculated alkali feldspar content was considerably higher than that suggested by the XRD results. It was possible to add constraints so that the normative quartz content is increased to 75%, but to do so required including several minerals which are very reactive in the recovered Lower Mannville waters, but this was not performed. Specifically, significant volumes of halite (NaCl) are required; its presence in the rock is incompatible with the recovered water composition. The inability to integrate the water analyses with the LPNORM and XRD results suggests that the formation mineralogy is heterogeneous, and that neither subsample is necessarily representative of the rock on a large scale.

Upper Mannville Group: The rock sample EN-30 from the Upper Mannville group is relatively quartz poor but similar in many ways to the Lower Mannville group samples. Although the proportions differ, the minerals identified in the core are the same as in sample EN-4, although siderite is also detected in this sample. As with the Lower Mannville samples, the LPNORM and XRD results from sample EN-30 are discordant in that the quartz content calculated with LPNORM (~30%) is considerably lower than that suggested by the XRD results (75%). As there was no good-quality water sample

recovered from the Upper Mannville from within the expanded study area (Figure 3), it was not possible to determine if the mineralogy as determined from LPNORM calculations is compatible with the formation water. The LPNORM results for Upper Mannville are shown in Table 12.

Viking Formation: The core sample representative of the Viking Formation is EN-8, and the water is sample # 5. Although sample EN-32 is also recovered from the Viking Formation, it represents a shaley unit. The bulk of the fluid recovered is thought to originate from the sandy unit (Bachu et al, 2011), so sample En-32 was not considered as representative of the aquifer. XRD results indicate that the dominant minerals in EN-8 are quartz and plagioclase, taken here as albite. Trace amounts of illite, kaolinite and pyrite are also reported, with no evidence of other minerals. Specifically, there is no clear evidence of any particular carbonate minerals, although the CO_2 content is greater than 2%, which indicates that carbonate minerals are present in the rock.

The water analysis suggests that albite is undersaturated in the recovered solution; the saturation of albite listed in Table 7 is -0.28. This value decreases further to -0.58 if chalcedony is used to define the aqueous SiO_2 concentration. Due to uncertainties in the phase solubilities used in these calculations, inaccuracies in the measure water composition, as well as potential contamination of the recovered waters, it is unreasonable to expect that the calculated saturation index of each phase to be 0.0. However, a value of +/- 0.2 is reasonable to expect for the simpler minerals such as albite. This tolerance will be greater for clays due to issues with phase purity and crystallinity. In order to stabilize the albite, the solution composition was defined to be in equilibrium with cristobalite rather than chalcedony. Furthermore, the solution composition was recalculated assuming that calcite is slightly supersaturated; CO_2 was titrated back into solution to achieve a saturation index of 0.1 for calcite. Following this change, the saturation indices of dolomite, albite, and Na montmorillonite increased to 0.98, -0.18, and 0.29 respectively. These values are typical of those for other waters listed in Table 7.

Table 7 also indicates that the aqueous solution is essentially in equilibrium with respect to the montmorillonites of Na and Mg. These considerations lead to the choice of potential minerals within the core of albite, kaolinite, Na and Mg montmorillonite (to represent the illite identified by XRD), K-feldspar, pyrite, and each of the potential carbonate phases (siderite, dolomite, calcite, and rhodochrosite). Again, the phases annite, vivianite, apatite and ilmenite are also included as potential phases in order to host the measured phosphate and titanium. These mineral constraints were applied to obtain the mineralogy for sample EN-8 in Table 12.

Basal Belly River Formation: The core sample EN-9 and water sample # 6 are both recovered from the Basal Belly River Group. XRD results from EN-9 indicate that significant amounts of quartz, plagioclase (albite), kaolinite and an illite-type clay are present. LPNORM generated a mineral norm which is essentially consistent with these

XRD results, although the calculated K-feldspar content (11.3%) was great enough that it would be expected to be detected by XRD. As well, the LPNORM results indicate that there is some 8% of Na-Montmorillonite in the sample; this is assumed to be representive of the illite type mineral in the XRD trace. Finally, LPNORM apportioned a significant amount of iron into an iron oxide phase, represented in Table 12 as hematite. There is no other evidence that this phase is present, and as discussed later, the type of iron-rich minerals present in the rocks can play a major role in determining the interactions between the rock and CO_2.

This mineralogy is compatible with the inferred water composition (Table 2), although with several qualifications. First, at cristobalite saturation, the calculated saturation index of the montmorillonites and albite are highest for this water. This suggests that another phase is controlling the dissolved silica concentration in this water. A second column in Table 7 gives the saturation indices for the same set of minerals for the case when Na montmorillonite is assumed to be an equilibrium phase. Under this assumption, the saturation indices of the silicate phases for this water is more comparable to the waters; however, albite is considerably undersaturated. This albite undersaturation is incompatible with the above mineralogy. For future simulations albite is considered an equilibrium phase. Practically, this means that albite solubility will control the amount of silica in the water as long as albite is present in the rock.

The second chemical anomaly with water sample 6 is the very high saturation indices of the many of the potassium bearing phases (c.f. illite, K-feldspar in Table 7). This is likely an indication of contamination of the produced water by a potassium rich drilling fluid. In subsequent calculations the amount of potassium is reduced to bring K-feldspar into equilibrium with the formation water; this requires a roughly 95% reduction the amount of K in the water. When these corrections are made to the water composition, the mineral/water stability relationships are similar to those associated with the other recovered waters discussed here.

Upper Belly River Group: Core samples EN-33 and EN-34 and water sample # 7 were recovered from the Upper Belly River Group. LPNORM results for EN-33 are given in Table 12. Aside from the dolomite noted in sample EN-33, the XRD and XRF analyses of these rocks are very similar; only sample EN-33 will be discussed here. Many of the same factors that were noted with respect to the Basal Belly River also arose in treating these samples. Specifically, albite was noted in both cores while it was not stable in either of the solution compositions represented in Table 7 in that it is supersaturated in the column labelled 7 and undersaturated in the 7A column. Again this is treated by setting albite as an equilibrium phase which serves the purpose of controlling the aqueous SiO_2 concentration. When this is done, the saturations indices of K-feldspar and Na montmorillonite are 0.4 and 0.74 respectively. These values are greater for this sample than for the other samples; however, again there are a number of factors which can be invoked to explain discrepancies of this order. With this water composition the mineral illite is also close to stability (saturation index -0.23). Halite is reported in both

cores; this is inconsistent with the recovered waters. Halite can form in recovered cores as they dry; this mechanism likely accounts for its presence.

4.2.3 Normative calculations of rock samples from aquitards

The normative calculations to estimate the mineralogical composition of the aquitards (caprocks) are complex. Clay minerals are generally are prevalent in these rocks. It is not possible to unambiguously identify most clay minerals with standard XRD techniques as small clay particles tend to give broad peaks making them difficult to resolve and integrate. Additionally, the chemical compositions of clays are generally poorly defined; these varying compositions also add further complexity to the interpretation of XRD spectra. This compositional variation also affects the thermodynamic properties of clay minerals. Finally, the composition of the water within the aquitards is unknown; this removes the possibility of constraining the mineralogy using equilibrium assumptions as presented in the previous section regarding aquifer minerals. As such these normative estimates are necessarily less well constrained than those presented in the previous section; and any results presented here are necessarily uncertain. The LPNORM derived mineral norms for the aquitard samples are given in Table 13.

Table 13: Mineralogical composition (wgt %) of aquitard samples based on LPNORM analysis.

Mineral	Sample					
	EN-1	EN-2	EN-3	EN-5	EN-6	EN-32
Albite						8.63
Anhydrite	1.80		56.73			
Anatase				0.55	0.48	0.72
Ankerite					2.48	
Annite	2.63	3.00				
K-Beidellite			0.48			
Calcite			2.27		17.20	
Clinochlore				1.30		
Dolomite	62.05	45.77	40.08	8.68	8.56	2.07
Halite	0.24	0.34		0.41	0.39	
Ilmenite	0.53	0.78				
Kaolinite	7.76	12.28	0.14	24.86	8.60	14.14
K-feldspar	8.33	16.06		15.27		
Muscovite					14.80	15.76
Phlogopite	3.17	6.96		3.15		4.13
Pyrite	0.69	0.47	0.14	0.17	1.09	0.51
Quartz	12.80	13.72	0.45	26.88	42.70	38.97
Rhodochrosite	0.03	0.05		0.21	0.13	0.18
Siderite		0.64		15.34		11.47
Vivianite	0.13	0.23		2.69	0.71	0.68

Additionally, some features noted in the XRD spectra could not be replicated with LPNORM. For instance the whole rock composition could not be reproduced unless K-feldspar was included in samples EN-1 and EN-5; however, there was no evidence of

this mineral in the XRD trace. This suggests that clay minerals in these rocks are more potassic than the stoichiometries used in the representation of clay minerals in LPNORM.

4.2.4 Impact of choice of iron minerals

The reactivity of the host rock can be greatly influenced by the reservoir mineralogy; this choice can be especially significant for the mineral hosts of divalent cations such as Ca, Mg, or Fe. With the exception of pyrite, the XRD results (Table 9) show no direct evidence iron-bearing minerals in the in the aquifer or reservoir rocks despite the iron content of the aquifer samples typically being in excess of 2 weight percent (see Table 10). Some indication of the difficulty in assigning iron-hosting minerals is found in the SEM-EDX results given in Bachu et al. (2012). For example a note accompanying the analysis of EN-9 presented by Bachu et al., (2012) states that "The main mineral is iron oxide or siderite ..". Similarly, the description of sample EN-33 includes the statement "The mineral is high in Mg and Fe but was not identified." Additionally, there are no iron analyses in the recovered solutions to test for potential mineral equilibria. Iron, if present in its reduced state in silicate minerals, will increase the potential to trap CO_2 in the mineral siderite (e.g Gunter et al., 1996). A typical reaction between a ferrous-iron rich silicate, represented below by the iron rich mica annite, and CO_2 can be represented by

$$KFe_3AlSi_3O_{10}(OH)_2 + 3CO_2 \rightarrow 3FeCO_3 + KAlSi_3O_8 + H_2O \qquad (2)$$

with the K-feldspar potentially able to react further with CO_2 to produce kaolinite. The trapping reactions involving oxidized-iron bearing minerals are much less effective.

Equally valid mineral norms can be obtained using the methodology described in the previous sections, but with some, or all of the iron partitioned into iron silicates (e.g. annite), iron oxides (e.g. hematite) or hydroxide (e.g. goethite). Such changes will potentially introduce slight differences in the amount of K-feldspar and/or clay phases in the norm, but would otherwise not significantly affect the calculated mineral norms. However, this partitioning may greatly affect the results of reactive simulations such as presented below. The results presented in the following chapter will be conservative compared to those which would be obtained were ferrous silicates included in the rock mineralogy. Further, detailed mineralogical characterisation work could better resolve the mineral hosts and the oxidation state of iron in these rocks, which would clarify their reactivity and CO_2 trapping potential.

In all of the LPNORM runs, the iron was hosted in iron oxide, pyrite, vivianite and/or siderite. When siderite was present in the rock, the Fe^{2+} activity in solution was estimated based on the assumption of siderite equilibrium. (As an aside, since the rocks are also assumed in equilibrium with calcite, the estimated value of Fe^{2+} in solution is determined directly from the measured Ca value). Similarly, the activity of Fe^{3+} is fixed by the in-situ pH, if equilibrium with a specified iron oxide or hydroxide is assumed. From these calculated of activities of Fe^{2+} and Fe^{3+} a redox potential can be directly

calculated; this redox potential can then be used to estimate the sulphide concentration in a solution with a known sulphate content. As these values are derived from unrelated measurements and assumed equilibria (i.e. the values are based solely on three direct measurements, pH, Ca and SO_4, and several assumed equilibria) these values should be subjected to independent checks. Apps et al. (2010) estimated the oxidation state of groundwater systems using a similar set of similar equilibrium assumptions. They used the simultaneous equilibrium of pyrite and the iron hydroxide, goethite, to estimate the redox state; this information was then used to calculate the saturation index of siderite in their solutions.

The LPNORM analysis of EN-9 from the Basal Belly River Formation (Table 12) indicates that the three iron bearing minerals siderite, pyrite, and an iron oxide (or hydroxide) are all present in the rock, although there is no x-ray diffraction evidence of these specific minerals. Water composition calculations using pyrite and siderite as equilibrium mineral phases determined that, with these constraints, the iron hydroxide mineral, goethite was very slightly supersaturated in the resulting water; this result suggests that the mineralogical assignments are sound. However, the resulting waters were highly supersaturated with respect to the iron clay minerals in the nontronite family. A possible interpretation of this result is that the thermodynamic data for the nontronite minerals are incorrect; this will be assumed here. This assumption results in conservative estimated for the amount of CO_2 fixed as mineral phases, as the tendency will be for the iron silicates to breakdown at elevated CO_2 pressures, with much of the released iron subsequently re-precipitating as siderite (Gunter et al., 1996).

To conclude, the results presented above represent an attempt to develop a consistent geochemical description of the reservoirs and aquifers within the Clive study area prior to the onset of CO_2 injection. Such a description ensures that chemical changes predicted with the geochemical model are primarily driven by chemical changes associated with the CO_2 injection, and not initial disequilibria between the host rock and the aquifer solution, which, if even if initially present, are not expected to be induced by the addition of CO_2.

Simulation results of the interactions between injected CO_2, or aqueous solutions which are equilibrated at the elevated CO_2 pressures associated with CO_2 injection, with the minerals within the reservoirs and overlying aquifers are presented in the following chapter.

5. Interactions between CO_2, Water and Rocks in Local Reservoirs and Deep Aquifers

Geochemical reactions induced by CO_2 injected into the subsurface and local water and rocks can be complex. These reactions may be associated with acidification by CO_2 within the injection zone, or induced by vertical leakage of CO_2 away from the injection zone (Apps et al, 2010), and also with the cross-formational flow of water.

Apps et al. (2010) explored issues associated with CO_2 leakage into potable groundwater aquifers and determined that the greatest concern is in regard to the mobilization of the trace elements As and Pb (arsenic and lead) by aquifer acidification under reducing conditions. The restricted geochemical data set available for the work presented here precludes specific conclusions regarding the mobilization of trace elements; however, the conclusions drawn by Apps et al. (2010) will also be relevant here. Specifically, increased acidity can enhance both mineral dissolution, including those containing hazardous trace elements, and desorption of the same trace elements from adsorption sites on mineral surfaces (particularly clays, hydroxides, carbonates and detrital mineral coatings). This emphasis on pH changes associated with CO_2 leakage indicates that the buffer capacity of the rock into which the CO_2 may leak is a critical determinant on, at least, the potential to mobilize trace elements.

Aside from buoyancy-driven mobility of a free CO_2 phase, the increased pressure in the formations targeted for CO_2 injection can initiate cross formational fluid flow (Birkholtzer and Zhou, 2009). This flow may involve reservoir water which is chemically affected by the injected CO_2 (water saturated with CO_2, and also containing elevated TDS resulting from geochemical reactions between injected CO_2 and the reservoir).

Fluids escaping (leaking) into the overlying aquifers may include free CO_2, water, and hydrocarbons (oil). Depending on the proximity to the CO_2 injection well, the composition of migrating water may vary from CO_2-rich reactive water to the original reservoir water. Similarly, the oil may be impacted by CO_2 or not depending on the location within the reservoir from which the oil is sourced.

Oil is considered either to remain in the reservoir or to be produced; only the dense CO_2-rich phase (gaseous CO_2) or CO_2-saturated water will be considered as potentially leaking. Only one mobile phase will be considered in each simulation. These conditions are discussed in more detail in below.

5.1 Representation of the thermodynamic properties of the CO_2-rich phase

Within the oil reservoir, many distinct chemical environments will develop surrounding CO_2 injection wells. Initially, in-situ conditions are expected to be maintained so that CO_2 will be miscible in the oil phase within the reservoir (at/or above the minimum miscibility pressure). As such, the reservoir can be considered as being a two-phase system; an aqueous phase and a hydrocarbon phase which becomes progressively richer in CO_2

with continued injection. The hydrocarbons (and the water) will be mobilized away from the injection zone, resulting in a zone which is sufficiently rich in CO_2 that a third, CO_2-dominated, phase will be present locally. This zone will expand and become increasingly CO_2-rich with time. Specifics of these processes may be modelled using compositional reservoir simulation tools; these have the potential to simulate the spread of CO_2 throughout the oil reservoir, both in terms of total concentration and its distribution between the existing phases.

Lower and upper limits can be placed on the local fugacity of CO_2 within the reservoir based on the CO_2 content of the oil prior to CO_2 flooding (lower limit), and the solubility limit of pure CO_2 in water at in-situ conditions (upper limit). This latter limit is determined by pressure, temperature and water salinity. Since mineral equilibria are determined by water composition, the potential variability of CO_2 fugacity (and hence total dissolved CO_2 in the water phase) means that the potential for diversity in mineral equilibria within the reservoir is great. Here, only the most reactive water are considered. Specifically, these are aqueous solutions that are equilibrated with pure CO_2 at local temperatures and pressures. This represents the hypothetical state that would exist following a complete local sweep of all hydrocarbons from the reservoir. The amount of water present will be limited by the residual water saturation.

Two distinct mechanisms may transport CO_2 into the overlying aquifers, in both cases the resulting state of CO_2 must be defined. Water leaking from the reservoirs into aquifers at lower pressures will exsolve CO_2 when the bubble point of CO_2 in solution is less than the local pressure in the aquifer. Other hydrocarbon gases dissolved in the water will also exsolve, but, due to the comparatively high solubility of CO_2 in water, the gas will be much richer in CO_2 than in the much-less soluble hydrocarbon components (neglecting the potential presence of hydrogen sulfide in the oil phase). Thus, any hydrocarbon components in leaking reservoir water will be neglected and only CO_2-rich reservoir water will be considered. Less well-defined is the case when a CO_2 gas phase is escaping (leaking) upwards from the reservoir. In this case the gas composition cannot be assumed to be pure CO_2 as other hydrocarbon components will be entrained in the gas; however, the maximum reactivity will be realized with pure CO_2 and so this phase composition will be used in the calculations presented here. Therefore, results obtained using the limit of a pure CO_2 phase will represent an upper limit of the possible geochemical reactions in the case of CO_2 leakage.

This free-phase CO_2 will interact with discrete mineral phases primarily by acidifying local waters; this acidification will induce a set of interactions within the aqueous and co-existing mineral phases. These interactions, at least for the case of local equilibrium, can be described using the program PHREEQC.

The PHREEQC database used in this study is constructed with a phase which represents a gaseous CO_2 phase (represented here as **CO2(g)**) referenced to 1 bar pressure. If a user defines this phase as an equilibrium phase the program will maintain

the solution in equilibrium with a gas with a prescribed fugacity. For instance, the PHREEQC input file

SOLUTION 1

temp 25; pH 7; pe 4

EQUILIBRIUM_PHASES 1

CO2(g) -1.0 8.0

END

will simulate an aqueous solution which is pure water with an imposed CO_2 fugacity of 0.1 bars (e.g. $10^{-1.0}$) by reacting up to **8.0** moles of **CO2(g)** with the solution.

The program AQUAlibrium (Carroll, 1996) calculates the fugacity of CO_2, (and density) of the CO_2-rich phase for the two component water/CO_2 system as a function of temperature and pressure. Table 14 presents the calculated fugacity of CO_2 at in-situ temperatures and pressures, using the program AQUAlibrium, within each of the aquifers of interest in the Clive field. This represents the chemical activity of CO_2 at the point when CO_2 will freely evolve (exsolve) from solution within each aquifer. Alternatively, a bubble of CO_2 at the local temperature and pressure will hold the activity of CO_2 at this specific value (ignoring effects related to surface tension) as long as the bubble remains. From the application of Henry's Law, the concentration of CO_2 in the associated water can be determined. The value required for PHREEQC simulations can be obtained by taking the logarithm (base 10) of the calculated fugacity in Table 14 and subtracting 2 (conversion from kPa to bars) from the result.

Table 14: Properties of CO_2 at in-situ temperatures and pressures typical for the aquifers in the Clive area.

No.	Aquifer or Reservoir	Pressure (kPa)	Temperature (ºC)	f_{CO2} (kPa)	CO_2 Density (kg/m^3)
1	Leduc D3-A	17,250	65	8730	630
2	Nisku D2	16,900	60	8279	663
3	Lower Mannville-1	11,500	55	6776	461
4	Lower Mannville-2	11,850	57	6966	461
5	Viking	7,000	50	5058	180
6	Basal Belly River	7,100	35	4775	242
7	Upper Belly River	3,150	30	2649	67

It is important to note here the variation in CO_2 density as CO_2 moves up through the sedimentary succession. In the Leduc D3-A and Nisku D2 reservoirs, and the Lower

Mannville aquifer, in-situ pressures and temperatures are above the critical point for CO_2 (P_c=7,380 kPa and T_c=31.1 ºC), hence CO_2 will be a dense supercritical fluid, with density decreasing as pressure decreases (pressure having a stronger effect on density than temperature, which affects CO_2 density in opposite direction). Because the Viking aquifer is severely underpressured, its pressure is below the critical pressure, similar to the Basal and Upper Belly River aquifers. However, because temperature is above the critical temperature for the Viking and Basal Belly River aquifers, and both temperature and pressure are below the critical point for the Upper Belly River aquifer, CO_2 in these three aquifers will be in a compressed gaseous phase. Carbon dioxide density in the Viking aquifer will be less than that in the overlying and much shallower Basal Belly River aquifer because the temperature in the former is significantly higher than in the latter while pressures are very close (Table 14). This means that CO_2 moving upwards along the sedimentary succession will undergo a complex thermodynamic path of cooling, decompression and recompression between the Viking and Basal Belly River aquifer, followed by decompression as it moves towards the surface.

5.2 CO_2-Induced reactions in reservoirs

The mineralogy of the recovered reservoir samples is very simple (see Table 12, columns 2 and 3); the rocks are dominated by the mineral dolomite, although there are minor amount of silicate minerals, and other carbonates in both samples. As well, the sample from the Nisku D2 reservoir contains an appreciable amount of anhydrite.

At first glance, the expected response to acidification by CO_2 of a carbonate-rich formation will be dominated by the reaction

$$CaMg(CO_3)_2 + 2\,H_2O + 2\,CO_2 = Ca^{2+} + Mg^{2+} + 2\,HCO_3^-, \qquad (3)$$

with the added consideration that there will also be a simultaneous equilibrium with calcite, and possibly anhydrite. The silicate minerals will also react with the injected CO_2.

5.2.1 Simulation results for Leduc D3-A oil reservoir

Mineralogically, the EN-11 sample from the Leduc D3-A reservoir is the simplest considered here. As such the analysis of the model results are also the simplest; this presents an opportunity to give a more detailed analysis of model results; these are much more complicated for the other sites and simulation results will be more briefly presented in those cases.

The PHREEQC input file used to generate results of CO_2 geochemical reactions within this reservoir is given below. Specific text from this file is referred to below using the same font as in the input file (e.g. END). This run consists of four separate, sequential, calculations; each of these is terminated with an END statement. The water composition as presented in Table 2 is described in the input up to the first END statement under the heading “SOLUTION 1”. This segment of the input file will generate the data presented in Table 4. The second, four line section, simulates heating the water introduced

previously to the in-situ temperature of 65°C (results presented in Table 5). The results of this calculation are then saved as "solution 2", for subsequent calculations. The subsequent input section is used to generate the results presented in Tables 6 and 7. Here, the solution generated by the previous calculation, and saved as solution 2, is manipulated by: adding up to 10 moles of CO_2(g) to bring the value of the saturation index of Calcite to 0, adding the components in the phases kaolinite, and quartz, to the solution until it is in equilibrium with kaolinite and supersaturated with quartz (final SI = 0.35), corresponding to chalcedony saturation – see Section 4.2.1, and adding KCl to bring the solution into equilibrium with K-Feldspar.

PHREEQC input file used to calculate the equilibrium response of chemical interactions between the Leduc D3-A oil field mineralogy and injected CO2.

```
SOLUTION 1  Leduc D3-A, water sample 1 in Table 2
temp  23; pe      4
density     1.145; units      mg/l
redox pe; pH      6.7
Na    56522; Ca   20567; Mg   3071; Cl    131464; Br  996
I     21; C 89.70; S    425
SAVE  solution 1; END

USE   solution 1
REACTION_TEMPERATURE 1
      65
SAVE  solution 2; END

USE solution 2
EQUILIBRIUM_PHASES 1
  Calcite   0 CO2(g)  10
  Quartz    0.35   10
  Kaolinite 0 10
  K-Feldspar 0 KCl  10
save solution 3; END

use solution 3
EQUILIBRIUM_PHASES 2
CO2(g)    1.941014    10
Dolomite    0.84  239.94;   Calcite       0     10.284
Quartz      0.35  3.4779;   Kaolinite     0     1.01
Pyrite      0     0.8212;   K-Feldspar    0     0.199
Anhydrite   -0.1 0.000
END
```

The final section of the input file simulates the changes brought about by bringing this solution into equilibrium with both the reservoir mineralogy and a free CO_2 phase at in-situ conditions. The calculation is similar to that in the previous step, although the number of equilibrium constraints is greater. These constrain the solution to be in equilibrium (SI = 0) with the equilibrium phases from the preceding calculation (calcite, K-feldspar, and kaolinite) with a further constraint on pyrite equilibrium added. The number of moles of these phases available for reaction is also listed; these values are

based on the mineralogical composition given in Table 12 following a calculation along the lines described below.

PHREEQC calculations are based on an assumed initial one kg of water. This mass of water will very nearly fill one dm^3 (0.001 m^3) of pore space in a fully saturated rock. The assumed porosity (based on the field scale) of the Leduc D3-A reservoir is 5.9% (Table 3); one dm^3 of pore space corresponds to a total 16.9 dm^3 of volume in the reservoir, or 15.9 dm^3 of rock. Based on the distribution of minerals in the rock, its density is calculated to be 2.77 kg/dm^3; so that each kg of water, in a fully water saturated rock, will be in contact with 46.9 kg of rock. The number of moles of each mineral required for the PHREEQC input file can be calculated from this mass of rock, the weight percentages of each mineral as reported in Table 12, and the molar mass of each mineral. The total mass is immaterial for some minerals, such as quartz, which will remain present in the reservoir irrespective of the extent of the reaction; however, this is not the case for some of the more reactive minerals.

Four other equilibrium constraints are also imposed. The first (CO_2(g) 1.941 10) increases the amount of CO_2 in the modelled system by 10 moles, with the requirement that the resulting solution will be in equilibrium with free CO_2 at in-situ conditions (see Table 14 for the fugacity which defines this equilibrium). The phase Dolomite is present in the reservoir, but rather than constraining the solution (water) to be in equilibrium with dolomite it will maintain a degree of supersaturation (SI = 0.84). This is the same value as was obtained from the previous calculation (see Table 7), and is equivalent to maintaining equilibrium between the water and a Ca-Mg carbonate which is somewhat less stable than dolomite (but more stable than disordered dolomite). Similar logic applies for the remaining two constraints (Quartz and Anhydrite), although, in the case of anhydrite it is not initially present in the reservoir. With this input file, anhydrite precipitation is allowed in waters that are apparently slightly undersaturated (SI = -0.1); this choice is equivalent to assuming that the recovered solution (water) was in equilibrium with anhydrite at the calculated SI = -0.13 (Table 7), and that, by some combination of analytical error and inaccuracy of the thermodynamic description of the system (e.g. the solution activity model), the calculated saturation index is too low by 0.1[3]

The results from this simulation are presented below in two tables. The predicted mineralogical changes, as well as the thermodynamic parameters defining their stability, are listed in Table 15. Table 16 shows corresponding changes in water chemistry.

[3] See also footnote on page 38

Table 15: Calculated equilibrium mineral changes within the Leduc D3-A reservoir. Mineral changes are presented as moles of mineral / kg water (SI, IAP and KT stand for saturation index, ion activity product, and equilibrium product, respectively).

Phase	SI	log IAP	log KT	Moles in assemblage		
				Initial	Final	Change
Anhydrite	-0.1	-4.9	-4.8	0	0.00	1.39×10^{-4}
Calcite	0	1.23	1.23	10.28	10.37	9.01×10^{-2}
CO2(g)	1.94	-6.15	-8.09	10	9.246	-7.54×10^{-1}
Dolomite	0.84	2.00	1.16	239.9	239.9	-4.75×10^{-3}
K-feldspar	-0.27	-1.53	-1.25	0.199	0	-1.99×10^{-1}
Kaolinite	0	2.64	2.64	1.01	1.109	9.94×10^{-2}
Pyrite	0	-22.54	-22.54	0.82	0.82	-2.67×10^{-6}
Quartz	0.35	-2.96	-3.31	3.48	3.88	3.98×10^{-1}

Table 15 demonstrates that the dominant reaction is the breakdown of K-feldspar (0.199 moles) primarily via the reaction

$$2\ KAlSi_3O_8 + 2\ CO_2 + 2\ H_2O \rightarrow Al_2Si_2O_5(OH)_4 + 2\ K^+ + 2\ HCO_3^- + 4SiO_2. \qquad (4)$$

The breakdown of 0.199 moles of K-feldspar via eq. (4) produces 0.0994, 0.398 and 0.0914 moles of kaolinite, SiO_2, and K^+ respectively. These amounts (and proportions) correspond well with the increases in the amount of kaolinite and quartz (column 6 in Table 15) as well as the increase in the amount of K in solution. This is the difference of 0.249 and 0.0496 (row 9 of Table 16). However, the total amount of CO_2 removed from the free CO_2 phase (CO_2(g)) is 0.7029 moles, which is more than 0.61 moles greater than the 0.199 moles expected to be ionically trapped as HCO_3^- via eq. (4). This discrepancy indicates that additional reactions affect the distribution of CO_2 between the phases present. One of these is simply the dissolution of CO_2 into the formation water; this amount is 0.638 moles, which is the difference of the amount of CO_2(aq) prior to, and following, equilibration with the high-pressure CO_2 (last row in Table 16). Smaller amounts of CO_2 are transferred between the aqueous and mineral phases by reactions involving the minerals calcite and dolomite (Table 15). These amounts are small, and of opposite sign; dolomite dissolves and calcite precipitates. The net effect of these reactions is that the total amount of CO_2 mineralized as carbonates will increase by 0.081 moles/kg of water in those portions of the reservoir where the activity of CO_2 is maintained at the in-situ solubility limit. Practically there is no volume change in the solids associated with these predicted geochemical reactions; the resulting porosity is practically 5.9%, the same as the initial porosity of 5.9%.

Table 16: Calculated changes to the water composition within the Leduc D3-A reservoir associated with bringing the solution and mineral assemblage into equilibrium with high pressure CO_2 (fugacity = $10^{1.94}$ bars). Values below the bold line correspond to aqueous species, rather than the elemental concentrations.

Element	Molality	
	Pre-CO_2	Post-CO_2
Al	3.23×10^{-9}	7.10×10^{-7}
C	2.71×10^{-2}	7.03×10^{-1}
Ca	5.51×10^{-1}	4.67×10^{-1}
Cl	4.03×10^{0}	4.05×10^{0}
Fe		2.68×10^{-6}
K	4.96×10^{-2}	2.49×10^{-1}
Mg	1.36×10^{-1}	1.41×10^{-1}
Na	2.64×10^{0}	2.65×10^{0}
S	4.75×10^{-3}	4.63×10^{-3}
Si	5.90×10^{-4}	5.93×10^{-4}
pH	4.728	3.967
CO_2(aq)	0.0189	0.657

An exact mass balance calculation based on differences in solution (water) concentrations is difficult to achieve, since the initial 1 kg mass of water considered in the PHREEQC run may change via hydrolysis reactions. For example, the breakdown of one mole of K-feldspar via eq. (4) consumes one mole of water. Such reactions will change the concentration of components in solution, with the consequence that there is not an exact correspondence between the concentration as reported by PHREEQC, and the total number of moles of each component in solution.

These numbers allow for an estimate on the total amount of CO_2 which will be removed from the free CO_2-rich phase by geochemical processes. The amounts are minor. The assumed rock volume of 16.9 dm^3 will fix some 0.75 moles of CO_2, which corresponds to 31 g of CO_2; equivalently this is about 1.9 kg of CO_2/m^3 rock.

The above calculations are based on three assumptions. The first is that the fugacity of CO_2 locally is $10^{1.94}$ bars; this implies that there is a free high-density CO_2 phase which is uncontaminated by hydrocarbon components. The second is that the volume of water per unit rock is given by the $\phi/(1-\phi)$, where ϕ is rock porosity. This value is based on the premise that the porosity is entirely water filled. This leaves no volume for a free CO_2 rich phase, which means that there will not be a phase capable of maintaining a constant CO_2 fugacity in the system. Practically, some volume must be assigned to this phase; failing to do so, results again in an over-estimate of the capacity of the rock to react with the injected CO_2. The third is that equilibrium is attained between all of the phases present in the system. Achievement of equilibrium may be hindered by a number of factors including: low rate of mineral reactions, preferential formation of meta-stable

minerals, and protection of mineral surfaces from contact with water by hydrocarbons or reaction products.

There is an interesting aspect to the simulation results dealing with the mineral anhydrite ($CaSO_4$). While initially absent from the rock (although the solution is assumed to be equilibrated with anhydrite), a small amount of anhydrite is predicted to form. This is not unremarkable; however, it is occurring under conditions where the calcium content of the water is decreasing. The Ca content drops by close to 10% following the equilibration with CO_2 (Table 16). Despite the decrease in Ca (and SO_4) content in the solution, the product of the activities of Ca^{2+} and SO_4^{2-} must be increasing in order for anhydrite to precipitate. The increase is caused by the changes in the activity coefficient, brought about by, among other factors, the increased bicarbonate concentration following the injection of CO_2. While this result is not implausible, it should be viewed with some degree of scepticism as the activity model is less well parameterized for CO_2-rich systems.

5.2.2 Simulation results for Nisku D2 oil reservoir

The sample EN-10 recovered from the Nisku D2 reservoir, while primarily dolomite, is mineralogically more complex than sample EN-11. Although, both samples are relatively pure dolomite, sample EN-10 also contains significant quantities of anhydrite. The trace minerals in both samples are also similar, although siderite is present in sample EN-10 but absent from sample EN-11.

The structure of the PHREEQC input file used to calculate the equilibrium relationships arising from interactions between the reservoir water and the injected CO_2 is the same as for previous case. The calculated equilibrium-water compositions prior to, and post CO_2 injection are given in Table 17. While the impact of CO_2 injection is similar in both simulations, some differences are evident. The decrease in the pH of water is similar, though slightly greater, than that calculated for the Leduc oil reservoir. As well, the breakdown of the magnesium-bearing clay in the rock (see Table 18) provides a Mg source, which results in dolomite being formed as a reaction product. Calcium is also required for dolomite formation; its source is the dissolution of calcite. This result - dolomite formation and calcite dissolution - is the opposite of the case simulated for the Leduc reservoir.

Results from an additional calculation are also included in Table 18. This calculation is identical to the previous one with a single exception: K-feldspar was omitted as a reactant. As noted in the discussion in the previous section, its breakdown is responsible for much of the ultimate chemically-trapping of CO_2. However, it is a much more slowly reacting mineral than the more dominant carbonates. The results of this simulation may provide a closer approximation to the reservoir waters during the active CO_2-EOR phase. Without neutralization by K-feldspar, the water within the reservoir will be more acidic than when K-feldspar is included as a reactant. The difference between the

equilibrium water composition in which K-feldspar is omitted as a reactant and that where it is included is minor. This is shown in Table 18 where the two compositions are reported. With the exception of the K concentration, the difference in concentration of each component is less than 15%.

Table 17: Calculated changes to the water composition within the Nisku D2 reservoir associated with bringing the solution and mineral assemblage into equilibrium with high pressure CO_2 (fugacity = $10^{1.92}$ bars). Values below the bold line correspond to aqueous species, rather than elemental concentrations.

Element	Molality		
	Pre-CO_2	Post-CO_2	No K-feldspar
Al	5.91×10^{-9}	7.20×10^{-7}	8.15×10^{-7}
C	4.37×10^{-2}	7.69×10^{-1}	7.73×10^{-1}
Ca	4.92×10^{-1}	4.20×10^{-1}	4.86×10^{-1}
Cl	3.66×10^{0}	3.69×10^{0}	3.68×10^{-0}
Fe	1.39×10^{-2}	1.64×10^{-2}	1.88×10^{-2}
K	5.57×10^{-2}	2.36×10^{-1}	5.67×10^{-2}
Mg	1.63×10^{-1}	1.68×10^{-1}	1.87×10^{-1}
Na	2.29×10^{0}	2.31×10^{0}	2.30×10^{0}
S	6.03×10^{-3}	5.30×10^{-3}	4.99×10^{-3}
Si	5.40×10^{-4}	5.38×10^{-4}	5.40×10^{-4}
pH	4.718	4.042	4.004
CO_2(aq)	0.031	0.713	0.716

Table 18: Calculated equilibrium mineral changes within the Nisku D2 reservoir. Mineral changes are presented as moles of mineral / kg water (SI, IAP and KT stand for saturation index, ion activity product, and equilibrium product, respectively).

Phase	SI	log IAP	log KT	Moles in assemblage		
				Initial	Final	Change
Anhydrite	-0.1	-4.83	-4.73	4.04×10^{1}	4.04×10^{1}	5.45×10^{-4}
Calcite	0	1.32	1.32	3.98×10^{0}	3.93×10^{0}	-4.64×10^{-2}
CO_2(g)	1.92	-6.14	-8.06	1.00×10^{1}	9.08×10^{0}	-9.20×10^{-1}
Dolomite	0.96	2.27	1.31	2.61×10^{2}	2.61×10^{2}	1.31×10^{-1}
K-Feldspar	0	-1.14	-1.14	2.19×10^{-1}	4.14×10^{-2}	-1.78×10^{-1}
Kaolinite	0	3	3	2.75×10^{-1}	5.88×10^{-1}	3.13×10^{-1}
Montmo-Mg	-0.71	-0.94	-0.23	2.69×10^{-1}	0	-2.69×10^{-1}
Quartz	0.35	-3.01	-3.36	1.93×10^{0}	2.91×10^{0}	9.81×10^{-1}
Siderite	0	-0.84	-0.84	6.66×10^{-1}	6.49×10^{-1}	-1.63×10^{-2}

The volumetric changes associated with these mineral reactions are positive (i.e., increase in the solid volume, or net precipitation); although the magnitudes are minor. The calculated porosity following these reactions is 5.17%, slightly lower than the initial porosity of 5.2%. The difference is well within the measurement error in the laboratory

and the approximations inherent in the scaling up process, such that, for all practical purposes one may consider that there are no changes in porosity.

5.2.3 Overview of geochemical reactions within the oil reservoirs

The geochemical simulations indicate that the injection of CO_2 in the Leduc D3-A and Nisku D2 oil reservoirs will have a negligible impact on reservoir porosity. This is even more the case since the simulations were performed for the extreme case when there is no oil in the pore space, having been completely displaced by CO_2. The effects on reservoir permeability cannot be quantified and are less certain because these changes depend on where the dissolution or precipitation of mineral assemblages takes place, in the pores themselves or in the pore throats. However, it is expected that the effects on reservoir permeability, hence injectivity, will also be negligible-to-minor and will have no practical effect on the CO_2-EOR operations, particularly when compared with the original reservoir heterogeneity.

Other effects relate to the amount of CO_2 that will be stored (sequestered) in the oil reservoirs. There are relatively small differences between the simulations presented above. In both cases, the calculated uptake is somewhat less than one mole (44 g) of CO_2 per kg of water within the rocks. The actual values are 0.76 moles (Leduc D3-A) and 0.9 moles (Nisku D2). The dominant reaction controlling this uptake is simple CO_2 dissolution in the formation water (solubility trapping). These amounts are 0.64 moles/kg H_2O for the Leduc D3-A reservoir and 0.68 moles/kg H_2O for the Nisku D2 reservoir, respectively. These numbers are derived from the difference in the CO_2(aq) concentrations listed in the second and third columns of Tables 16 and 17.

The relatively greater uptake of CO_2 within the Nisku D2 reservoir is due to an increased amount of ionic, or mineralogical trapping. This is due to the greater abundance of alkali, and alkali-earth bearing silicate minerals in this reservoir. On degradation, these minerals consume hydrogen ions, the source of which is dissolved CO_2. The total amount of CO_2 trapped within mineral structures, which is calculated as twice the change in the amount of dolomite plus the change in the amounts of calcite and siderite, is also greater within the Nisku D2 reservoir (0.2 moles) than within the Leduc D3-A reservoir (0.026 moles). This difference is primarily due to the assumed presence of the Mg-bearing clay mineral, Mg-montmorillonite within the reservoir.

As demonstrated in Section 5.2.1, the amount of chemical trapping is small – on the order of 1.9 kg of CO_2/m^3 of the reservoir Leduc D3-A reservoir. The amount of CO_2 chemically trapped in the Nisku D2 reservoir, while greater (2.1 kg of CO_2/m^3), is comparable. In both cases, the predicted mineralogical transformations are minor; only minor amounts (on the order of parts per thousand) of the carbonate minerals present in the reservoirs are expected to react as a result of CO_2 injection. Since these comprise over 90% of the rocks, the overall impact on the physical rock properties is expected to be minor.

Some of the injected CO_2 will dissolve in and mix with oil. Assuming that the oil and contained CO_2 are completely displaced through the enhanced oil recovery process, the proportion of injected CO_2 which remains as a free phase within the reservoir (i.e., neither mineralized nor dissolved in water) can be estimated if the phase saturations are defined. Bennion and Bachu (2008; 2010) determined the residual brine and CO_2 saturations following CO_2 displacement for various sedimentary rocks from the Alberta basin. For the Nisku Fm., the brine irreducible saturation is on average 0.4, meaning that the maximum CO_2 saturation is 0.6. The average irreducible CO_2 saturation determined by Bennion and Bachu (2008, 2010) is 0.212. This means that, for a porosity of 5.2% and CO_2 density at in-situ conditions of 663 kg/m^3 (Table 14), 7.3 kg CO_2/m^3 will be residually trapped in the reservoir at irreducible saturation, which is greater by a factor of 3 than the amount of chemically trapped CO_2. However, up to 13.4 kg (=7.3·(0.60-0.212) / 0.212) of CO_2/m^3 can remain as a mobile phase within pore space, and this free CO_2 can leak upwards if a pathway is found, driven by buoyancy and pressure gradients.

5.3 Reactions in aquifers overlying the Leduc-D3A and Nisku-D2 oil reservoirs

Results of the equilibration of fluids migrating upwards from the reservoirs undergoing CO_2-EOR with overlying aquifer materials are presented here. The fluids considered here are either a pure CO_2 phase, or waters from the reservoir. Reactions induced in overlying aquifers by the leakage of pure CO_2 are well described in Apps et al. (2010). Those due to the migration of other fluids, such as CO_2-saturated reservoir water, from the pressured reservoir are less well studied. This leakage may be distal to the CO_2 injection well, hence the composition of the leaking fluid will be unaffected by chemical interactions with injected CO_2. This case of potential leakage is not within the scope of this study. Alternatively, if the leakage is proximal to the CO_2 injection wells, any migrating fluid will be acidified by contact with the injected CO_2. Specifically, the composition of the leaking acidified-water is derived from the second case presented in section 5.2.2; that of a water which is in equilibrium with a free CO_2 phase within the reservoir, as well as the clays and carbonate minerals within the reservoir. The equilibrium is determined for the replacement of 0, 1/3, 2/3, and all of the water in the aquifer. This is done to determine potential mineral reactions which may be induced by cross formational leakage. Although it is difficult to relate the closed system simulations presented here directly to specific physical situations, these varying proportions are meant to approximate scenarios of varying fluxes of intra-formational and inter-formational flows.

The extent to which the overlying aquifers will be impacted depends on both the rate of fluid flow from the reservoir and the kinetics of mineral reactions within the aquifer. Potential fluid flow rates from the reservoir may be estimated based on hydraulic head differentials between the hydrocarbon reservoir and overlying aquifers, and the permeability of probable leakage pathways although such analyses are outside the scope of this study. Additionally, there is a lack of data about the possible permeability of potential leakage pathways. Similarly, the extent to which leaked fluids will be diluted

within the aquifers depends on the rate at which local flow within the each aquifer sweeps reaction products away. Low rates of the potential reactions will also limit the extent to which the reaction described here may proceed. Compilations of mineral dissolution rates are available (i.e., Palandri and Kharaka, 2004); however, many of parameters required to transform these experimentally-derived rates into equivalent field properties (such as total available mineral surface area) are not known for the aquifers studied here. Finally, the rates of the mineral transformations (as opposed to dissolution), which play an important role in controlling the equilibrium response in some aquifers, are not well characterized in the geochemical literature.

5.3.1 Simulation results for leakage of free phase CO_2 into overlying aquifers

The PHREEQC runs simulating the impact of leakage of pure CO_2 into various aquifers are constructed following the same structure as the simulations in Section 5.2. Required inputs are the initial water composition and mineral abundances in the aquifer, as well as the fugacity of the CO_2 at in-situ conditions. Results of the simulations consist of the changes to the equilibrium mineralogy and water chemistry. Select results will be presented for all aquifers; these include the equilibrium water composition for each aquifer both prior and after to the introduction of CO_2 (Tables 19 and 20, respectively), as well qualitative indications about changes in mineral masses (Table 21). Table 19 is mostly a reiteration of the data previously presented in Tables 2 and 6; these are repeated here both for ease of comparison, as well as to standardize the reported concentration units. Some of the compositions differ between Tables 6 and 19. This is due to the fact that a different mineral phase was assumed, in a few cases, to control the silica content (see Section 4.2.1). This was done to bring the saturation indices of a few clay minerals to more realistic values.

Table 19: Original water compositions corrected for assumed equilibria. Concentrations are given in moles/kg of water. Values in the last two lines correspond to aqueous species, rather than elemental concentrations.

Aquifer	Lower Mannville	Viking	Basal Belly River	Upper Belly River
Na	1.47×10^{0}	5.59×10^{-1}	2.11×10^{-1}	1.08×10^{-1}
K	1.30×10^{-2}	2.47×10^{-3}	2.45×10^{-4}	3.07×10^{-4}
Mg	4.69×10^{-2}	2.03×10^{-3}	1.40×10^{-3}	6.59×10^{-4}
Ca	1.42×10^{-1}	6.54×10^{-3}	3.01×10^{-3}	1.40×10^{-3}
Fe	1.88×10^{-3}	7.45×10^{-5}	3.17×10^{-5}	1.88×10^{-5}
Al	1.31×10^{-10}	2.04×10^{-11}	2.89×10^{-10}	7.99×10^{-10}
TIC	1.82×10^{-2}	9.90×10^{-2}	4.36×10^{-3}	5.38×10^{-3}
SiO_2	9.28×10^{-4}	1.03×10^{-3}	4.82×10^{-4}	4.08×10^{-4}
H_2S	3.39×10^{-9}	1.03×10^{-8}	1.95×10^{-9}	1.568×10^{-9}
Cl	1.83×10^{0}	5.33×10^{-1}	2.32×10^{-1}	1.07×10^{-1}
SO_4	4.01×10^{-3}	1.57×10^{-4}	2.09×10^{-5}	2.085×10^{-5}
pH	5.46	5.91	7.335	7.525
pCO_2	-0.05	0.49	-2.01	-2.09

The concentration of the solutions following equilibration with a free CO_2 phase at in-situ conditions is reported in Table 20. Clearly, introducing CO_2 at high pressures into the system results in significant changes to the water compositions; the most significant changes are seen in the upper two aquifers (Basal and Upper Belly River). This is to be expected based on the initial (pre-CO_2) low-salinity water composition. The equilibrium CO_2 fugacity estimated in the previous chapter (Tables 6 and 19) is considerably lower for the shallower Basal and Upper Belly River formations than the deeper two formations (Viking and Lower Mannville) – with the initial equilibrium CO_2 fugacity being the greatest in the Viking Fm. The pH shift following equilibration with a free CO_2 phase is greater than 1.0 for the upper two aquifers, but less than 0.3 for the Viking aquifer.

Table 20: The concentration of aquifer waters equilibrated with a free CO_2 phase and the assumed local mineralogy of four aquifers overlying the Clive oil field. The concentrations are given in moles/kg of water, except for pH (last line) which is dimensionless.

Aquifer	Lower Mannville	Viking	Basal Belly River	Upper Belly River
Na	1.82×10^{0}	9.48×10^{-1}	2.91×10^{0}	2.02×10^{0}
K	4.67×10^{-2}	2.49×10^{-3}	4.38×10^{-3}	6.79×10^{-3}
Mg	1.40×10^{-2}	1.02×10^{-3}	4.69×10^{-3}	3.26×10^{-3}
Ca	2.74×10^{-2}	1.89×10^{-3}	1.34×10^{-4}	1.58×10^{-4}
Fe	7.004×10^{-4}	5.51×10^{-5}	3.66×10^{-5}	3.30×10^{-5}
Al	1.11×10^{-8}	3.18×10^{-10}	1.29×10^{-8}	2.89×10^{-9}
C	9.67×10^{-1}	1.27×10^{0}	2.92×10^{0}	2.51×10^{0}
SiO_2	9.81×10^{-4}	1.10×10^{-3}	7.07×10^{-4}	5.42×10^{-4}
H_2S	2.13×10^{-8}	3.83×10^{-8}	0	4.83×10^{-8}
Cl	1.85×10^{0}	5.43×10^{-1}	2.19×10^{-1}	1.36×10^{-1}
SO_4	4.04×10^{-3}	1.60×10^{-4}	2.69×10^{-1}	2.65×10^{-5}
pH	4.82	5.62	6.14	6.25

Figure 10 gives a representation of the relative reactivity of each formation. This is a plot of the ratio of the concentration of many of the components reported in Table 20 to the corresponding value in Table 19. The Viking Formation, as discussed previously, is the least reactive of the four aquifers considered. This is clearly seen in Figure 10 as the ratio of the concentration of most components (with the exception of C) in these two waters (pre- and post-CO_2 exposure) are close to 1.0. The spread in these ratios is somewhat greater for the Lower Mannville and considerably greater for the Basal and Upper Belly River Formations.

Table 21: Predicted mineralogical changes to aquifers overlying the Clive oil field in the event of CO_2 migration into these aquifers.

Aquifer	cal cite	dolomite	K-spar	albite	kaolinite	SiO_2	clays	Magnesite	Pyrite	FeOOH	Siderite
Upper Mannville	+	+	-	-	+	+	x	x	+	x	+
Viking	-	+	x	+	+	+	-	x	x	x	+
Basal Belly River	x	+	+	-	+	+	0	+	0	-	+
Upper Belly River	x	+	+	+	+	+	0	+	-	x	-
key	+: reactions lead to an increase in the amount of mineral in formation -: reactions lead to a decrease in the amount of mineral in formation 0: reactions lead to a exhaustion of the amount of mineral within formation x: mineral absent in formation both initially and finally										

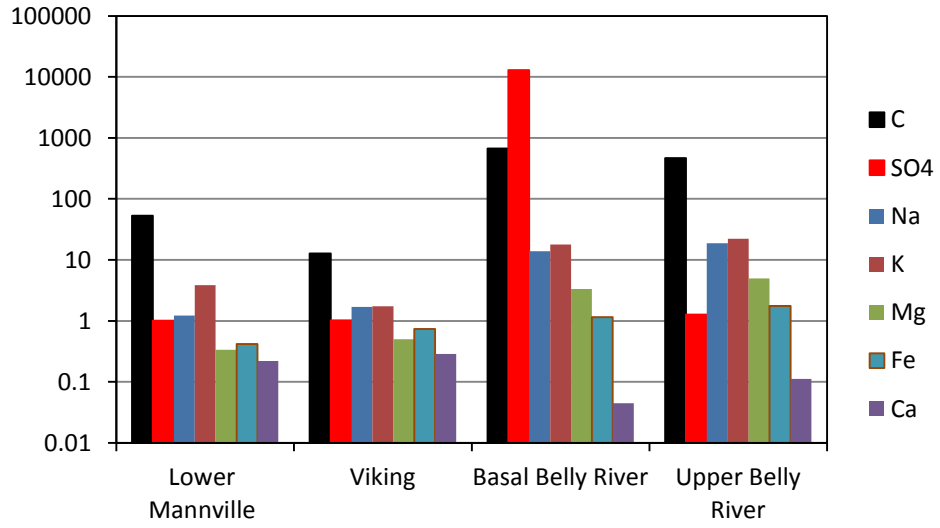

Figure 10: The ratio of the concentration of selected elements in solution following equilibration with a free CO_2 phase at in-situ conditions to pre-CO_2 contamination concentrations.

The geochemical behaviour of the Basal Belly River Formation is particularly sensitive to the addition of CO_2. This is seen in the behaviour of SO_4, the concentration of which increases by more than four orders of magnitude following equilibration with the high pressure CO_2 phase. The reason for this increase lies in the behaviour of the iron-bearing phases within this formation. The LPNORM calculations suggest that both pyrite (FeS_2) and an iron oxide or oxyhydroxide (e.g. goethite – FeOOH) are present. Acidification of the aquifer waters by the addition of CO_2 leads to the dissolution of goethite via:

$$FeOOH + H_2O + CO_2 = Fe^{3+} + HCO_3^- + 2\ OH^- \quad (5)$$

The Fe^{3+} produced through eq. (5) has the capacity to oxidize the bisulphide in pyrite; this reaction can be written as:

$$14\ Fe^{3+} + FeS_2 + 4\ H_2O = 15\ Fe^{2+} + 2SO_4^{2-} + 8\ H^+ . \quad (6)$$

These two equations, combined together with the formation of siderite ($FeCO_3$), give the net reaction:

$$14\ FeOOH + FeS_2 + 15\ CO_2 = 15\ FeCO_3 + 2SO_4^{2-} + 4\ H^+ + 5\ H_2O \quad (7)$$

This reaction produces H^+, further acidifying the water, which then can dissolve more goethite. In the presence of excess CO_2 this reaction, once initiated, will continue until the pyrite or goethite is exhausted. Trace metals present in either the goethite or pyrite will be mobilized by (7). While this is a concern, the pH of the evolved water remains essentially neutral (equilibrium pH = 6.14). This suggests that most of the metals mobilized will re-precipitate locally rather than be transported at levels significantly greater than the background.

Changes in the volume of solids, hence porosity, within the aquifers associated with the reactions described above can be calculated given the molar volume of the minerals involved in the reactions. Again, these porosity changes are calculated based on the equilibrium mineralogy and, as such, are likely overestimates. Calculated changes in porosity, as well as the calculated amount of CO_2 trapped within the aquifers, for each of the four aquifer systems considered are presented in Table 22. In three of the four aquifers the porosity decreases following equilibration with the high pressure CO_2, with very slight decreases in the deeper Lower Mannville and Viking aquifers, and with a significant decrease in the Upper Belly River aquifer. In contrast, porosity in the Basal Belly River aquifer increases significantly. Although these volume changes result from a complex set of coupled reactions, the behaviour of the feldspars seems to be an important indicator of the volume changes on reaction. The largest volume gain (porosity loss) was associated with extensive feldspar production from pre-existing clays (reverse weathering). Conversely, extensive feldspar loss is predicted within the Basal Belly River aquifer; this is associated with a significant increase in porosity. The geochemical simulations show that the changes in aquifer porosity as a result of leakage of CO_2 from the oil reservoirs into overlying aquifers will be negligible-to-minor for the Lower Mannville, Viking and Basal Belly River aquifers. In regard to effects on aquifer permeability, these cannot be quantified and they will depend mainly where on the solid grains mineral precipitation or dissolution will take place, in the pores or in the pore throats. The reduction in porosity in the Upper Belly River aquifer is more significant (a decrease of 22%), which likely will lead to a local decrease in permeability, with corresponding effects on the flow of free-phase CO_2.

Table 22: Calculated impact of leaked CO_2 on aquifers overlying the Leduc D3-A and Nisku D2 oil reservoirs. Values reported in this table include the mass of CO_2 which may be trapped in various forms within the aquifers (see text), as well as aquifer porosity prior to and following equilibration with CO_2 at in-situ conditions.

Aquifer	Trapping CO_2 by Mechanism (kg CO_2/m^3 rock)					Porosity (%)	
	Mineral	Solution	Ionic	Residual Gas	Maximum Gas	Initial	Final
Mannville	6.65	3.73	0.38	11.63	21.46	9.70	9.66
Viking	1.93	3.64	1.76	7.35	8.26	10.20	10.00
Basal Belly River	15.10	2.99	10.09	10.39	11.68	12.20	13.77
Upper Belly River	21.48	3.38	10.46	2.18	4.02	12.50	10.12

Note that, although porosity in these aquifers increases with decreasing depth (Table 3), the amount of CO_2 in free phase per m^3/rock in each aquifer, expressed in mass units (kg) in Table 22, decreases with decreasing depth (i.e., as aquifers become shallower) because of the decrease in CO_2 density with decreasing depth (Table 14). This effect particularly stands out in the case of the Viking aquifer, where, because of severe underpressuring (i.e., very low pressure), CO_2 density is much lower than in the case of the Basal Belly River Aquifer.

Table 22 also reports the amounts of CO_2, which are estimated to be fixed (trapped) in various phases during the evolution of the CO_2 within each aquifer. There are two types of mechanisms responsible for trapping CO_2; it may either be in a free phase at immobile residual gas saturation, or it can be chemically trapped within the water or mineral phases through dissolution and mineral precipitation. Free CO_2 above the residual saturation is mobile and it will flow up-dip and upwards unless trapped in a stratigraphic or structural trap. Values reported in Table 22 require a brief explanation. During an active leakage of CO_2, the gas will displace water in the aquifer (drainage cycle) up to the point that the brine saturation within the aquifer reaches the irreducible brine saturation (this is the maximum gas saturation in Table 22). On cessation of CO_2 leakage, the CO_2 will migrate within the aquifer and the aquifer water will imbibe back (imbibition cycle), decreasing the local CO_2 saturation until the CO_2 saturation reaches the irreducible gas saturation (residual gas saturation in Table 22). Bennion and Bachu (2008) and Bachu (2012) have published irreducible brine and CO_2 saturation values for rock samples from various sandstone strata in the Alberta basin, including five samples from the aquifers studied here (two from the Ellerslie Fm. of the Lower Mannville Group, and three from the Viking Fm.). Average values representative for these two aquifers were used to calculate the mass of CO_2 which would be present in a cubic meter of rock at in-situ conditions at both residual brine saturation (maximum gas saturation) and residual gas saturation (minimum gas saturation). For the Basal and Upper Belly River aquifers, the values for the Viking Fm. and Ellerslie Fm., which are mineralogically and depositionally similar to these, were used, respectively. The variables required to

calculate the mass of CO_2 at these saturation limits depend on both rock properties (porosity, irreducible brine and CO_2 saturations) and in-situ CO_2 phase density.

Both during and subsequent to CO_2 leakage, the CO_2 will react with the local rocks and water. It can dissolve into the water (solution trapping), hydrolyze to bicarbonate (ionic trapping), or precipitate as a mineral phase (mineral trapping). These chemical trapping mechanisms operate essentially independently of the processes responsible for the emplacement and displacement of the free CO_2 phase; however, at any given time the amount of CO_2 available for reaction will be less than the amount reported in Table 22 as Maximum Gas, with the Residual Gas value being typical. In the presence of free CO_2 phase, an amount of CO_2 will dissolve into the local water until it is saturated with this phase (on the order of 0.6-0.8 moles of CO_2/kg water (kgw) for the aquifers and conditions considered here). This concentration corresponds to some 26-35 g of CO_2/kgw. This is normalized in terms of rock volume in Table 22; comparison of these values to the amounts physically trapped requires that this amount must be converted to rock volume units. A typical porosity of the aquifer rocks considered here is 10%. This means that the pore volume in a cubic meter of rock is on the order of 0.1 m^3; if this pore space is fully water saturated, it will contain about 100 kg of water. If saturated with CO_2 at in-situ conditions, 100 kg of water will contain 2.6 to 3.5 kg of dissolved CO_2. These values are reported in the third column of Table 22. Note, however, that the scenarios described above are predicated on having a free CO_2 phase also within the pore space, so that the volume of water in the total pore space will be, loosely speaking, closer to one half of the total pore space.

It is clear that the amount of gas dissolved into the aquifer water in the lower three aquifers (Lower Mannville, Viking and Basal Belly River) is much less than the amount which can be trapped as a free phase in the pore space. In the Upper Belly River aquifer, these amounts are comparable, meaning that there is capacity to trap most of the leaked CO_2 through simple dissolution. The other two columns (Mineral and Ionic trapping) represent the hypothetical maximum amount of CO_2 that could react with the leaked CO_2 in a relatively stagnant system (i.e. any flow transporting fresh reactive water is restricted, or is extremely slow, as is usually the case in deep saline aquifers).

There are two components of ionic trapping; there is formation of bicarbonate by simple hydrolysis of dissolved CO_2 ($H_2O + CO_2 = HCO_3^- + H^+$), and bicarbonate production which is coupled to the mineral reactions (e.g. $CaCO_3 + CO_2 + H_2O = Ca_{2+} + 2HCO_3^-$). The first of these operates on the same time scale as solution trapping, which is decades to centuries (IPCC, 2005). However, the amount due to this reaction is minor, usually a few percent of the amount trapped as dissolved CO_2 (the amount reported as Solution Trapping). The second reaction occurs on time scales similar to mineral trapping (centuries to millennia; IPCC, 2005), and its rate depends on the mineral reactions involved. As such, it is dependent on aquifer properties. For the Lower Mannville and Viking aquifers the total amount of CO_2 trapped through chemical trapping processes (solubility, ionic and mineral) is comparable with the amount of CO_2 that will

be trapped through residual gas saturation, indicating that any free CO_2 phase within these aquifers will be persistent over long periods, and mobile CO_2 (above the residual saturation) will still be able to migrate and/or leak. In the case of the Basal and Upper Belly River aquifers, the amount of CO_2 that will be trapped at irreducible saturation (residual gas) is much smaller than the amount of CO_2 that may be trapped through solubility, ionic and mineral trapping. Since the time-scales of these processes are vastly different this means that, although all the CO_2 that will reach these aquifers may ultimately be trapped through chemical trapping processes, in the early times of CO_2 leakage, free-phase CO_2 will still be able to migrate and possibly leak upwards if a leakage pathway, such as a defective or uncemented well, is encountered. As well, when considering the leakage of CO_2 towards even shallower strata and the surface, the coal beds present in the Belly River Group and overlying strata (Figure 4) will adsorb free-phase CO_2, reducing the flux of CO_2, therefore lessening the risk of leakage into shallow potable groundwater and to the surface.

5.3.2 Simulation results for leakage of CO_2-rich water into overlying aquifers

Carbon dioxide-charged waters leaking into an aquifer overlying the oil reservoirs will, in general, not be in equilibrium with the aquifer. PHREEQC simulations were set up to simulate the mixing of aquifer waters with CO_2-charged water leaking from the oil reservoirs, whose composition is given in the rightmost column of Table 17. This mixing process is undertaken while maintaining the resulting water composition in equilibrium with the aquifer mineralogy.

A single simulation consists of a number of steps that are required to define the equilibrium water compositions and the mineralogical constraints within the aquifer and the reservoir that is the source of the leaking CO_2-rich water; these are based on input files used in the previous sections run sequentially. A further three sets of commands are required to simulate the mixing of the reservoir and aquifer waters while maintaining equilibrium with the aquifer mineralogy. A complete PHREEQC input file required for a single simulation is reproduced in Appendix B.

Some results generated by this type of simulation, undertaken for the Lower Mannville aquifer (the basic data used in this simulation is water sample #3 and rock sample EN-4) are shown in Figure 11.

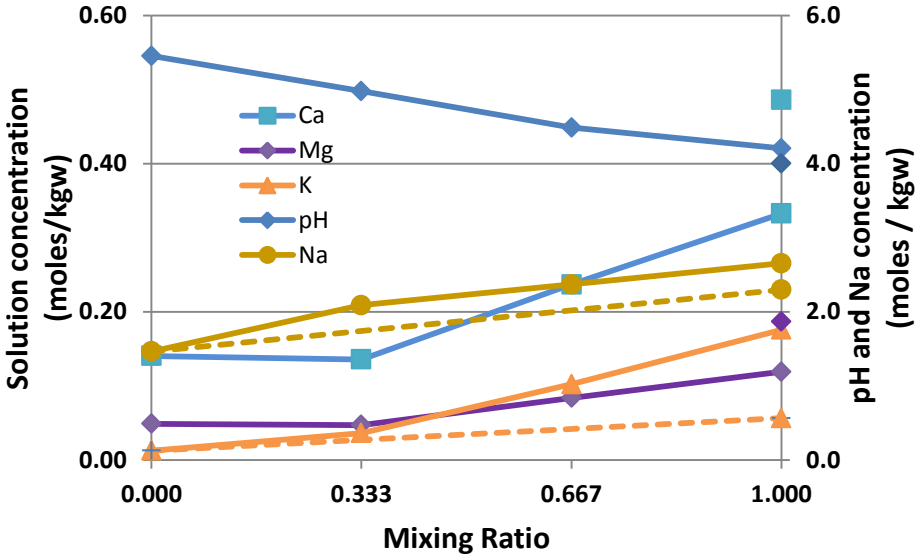

Figure 11: Calculated concentration of several components and pH of evolved water obtained by mixing original water from the Lower Mannville aquifer and CO_2-rich water from the Nisku reservoir while maintaining equilibrium with the aquifer mineralogy. The values of the pH and Na concentration are given on the right hand axis. The concentrations in the reservoir water are shown as isolated points on right-most side of the plot using the same symbols as for the respective connected lines.

Figure 11 is a plot of the equilibrium water composition calculated when different mixtures of the equilibrated aquifer water and a CO_2-enriched water derived from the Nisku reservoir are mixed. In this, and following figures, the relative proportion of the Nisku D2 CO_2-rich water defines the x-axis, which is plotted as the mixing ratio between the water leaked from the Nisku D2 reservoir and the resident aquifer water. A mixing ratio of zero indicates that only aquifer water is present, and a mixing ratio of one indicates water derived from the Nisku D2 reservoir only.

Several aspects of the mixing process are evident. Firstly, none of the components plotted conserve in this system; none falls directly on a straight mixing line (shown as dashed lines) from the initial concentration of that element in the Lower Mannville aquifer (the value at a mixing ratio of 0) to the points representing the assumed concentration of the upward-leaking reservoir water (mixing ratio of 1). Secondly, following equilibration of the reservoir-derived water with the aquifer rocks at a mixing ratio of 1, the resulting water is only marginally less acidic (pH = 4.2) than the CO_2-charged water leaked from the Nisku D2 reservoir (pH = 4.0) but much more acidic than the original water in the Lower Mannville aquifer (pH = 5.4). Aside from this consumption of acid, mineral interactions within the aquifer are predicted to remove significant amounts of Ca from solution through precipitation; this is evident as the calculated Ca value at a mixing ratio of 1.0 (0.33 mols/kgw) is significantly less than the value corresponding to the water from the carbonate Nisku D2 reservoir (0.48 mols/kgw). The equilibrated water contains more than twice as much Ca as there was originally in the Lower Mannville waters.

Lesser amounts of Mg are also predicted to be fixed in mineral phases through precipitation as indicated by a resulting value of 0.12 mols/kgw compared with an initial value of 0.19 mols/kgw. The small slope of the line segment associated with the lowest mixing ratios indicates that that the reactions which fix these components are most effective for dilute mixtures of the reservoir water into the aquifer. The release (dissolution) of Na and K is also evident in Figure 11. A steady increase over the conservative mixing line (dashed orange-brown line) is seen in the K concentration; however, following an initially relatively steep increase, the Na concentration roughly parallels the conservative mixing trend (dashed yellow-brown line) indicating that there are no other reactions significantly affecting Na concentration. At lower mixing ratios between Nisku D2 and Lower Mannville waters, these effects are also present, but less drastic.

Figure 12 shows the changes in the amount of many of the phases present in the equilibrium assemblage in a manner similar to Figure 11. Calcite and dolomite are the phases responsible for removing Ca and Mg from the water mixtures through precipitation; the amounts of these phases are seen to increase with the proportion of CO_2-enriched reservoir water in the mixed water. Other mineralogical aspects that are evident in Figure 12 are the relative instability of albite; a minor influx of CO_2-charged water from the Nisku D2 reservoir has the capacity to strip all of the albite from the impacted volume of the Lower Mannville aquifer. The degradation of albite results in the production of kaolinite (Figure 12), as well as serving to reduce the acidity of the water, which leads to the precipitation of the carbonate minerals noted previously. While less reactive than albite, degradation of K-feldspar to kaolinite is also apparent in Figure 12.

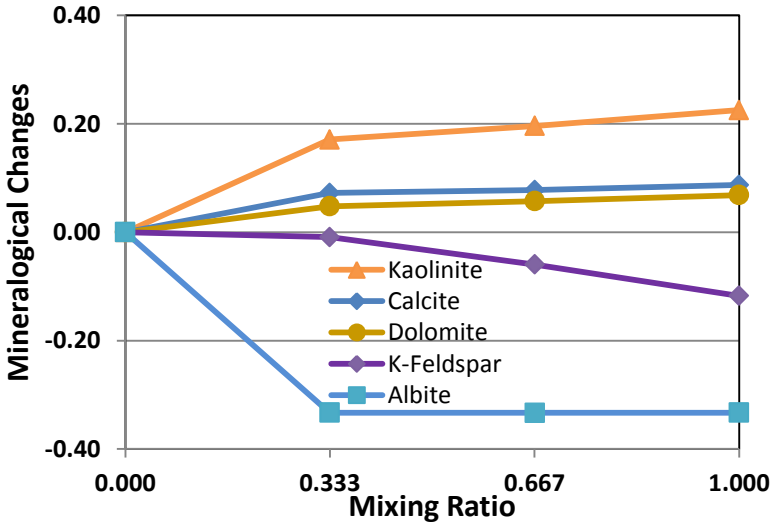

Figure 12: Calculated changes in the equilibrium mineralogy associated with the reactions induced by mixing CO_2-charged waters from the Nisku D2 reservoir with minerals from the Lower Mannville aquifer.

Overall, the dominant reactions expected within the Lower Mannville aquifer are the formation of carbonates (calcite, siderite - not shown, and dolomite) and kaolinite. The source of the components incorporated into the carbonate minerals is primarily the water leaked from the carbonate Nisku reservoir, and the kaolinite being derived from the breakdown of feldspars. These reactions lead to a slight decrease in porosity, with the total volume of solids increasing by 0.07% which is equivalent to about 0.7% of the total initial porosity of 9.7%. This change is also within the laboratory measurement error and scaling up for porosity, such that, for all practical purposes porosity can be considered as remaining unchanged. Generally the weathering of feldspars to kaolinite and quartz results in a decrease in the volume of mineral solids; however, in the case considered here the weathering of feldspar also induces carbonate precipitation, leading to a net increase in the volume of solids.

Similar calculations were performed for the Viking and the Basal and Upper Belly River aquifers. Results for the Viking aquifer are, in many ways, comparable to those presented for the Lower Mannville aquifer. However, within the Viking aquifer, the concentration of the feldspars in general, and albite in particular, is significantly greater than in the Lower Mannville aquifer (see Table 12). This difference means that the capacity to neutralize the incoming acidic reservoir water is greater in the Viking aquifer than in the Lower Mannville aquifer, and that albite will remain present even at a mixing ratio of one. Additionally, the presence of the complex clay, Na-montmorillonite (represented here as $Na_{0.33}Al_{1.67}Mg_{0.33}\ Si_4O_{10}(OH)_2$) in the formation provides an additional source of Mg; its degradation will result in the stabilization of dolomite over calcite in the overall reaction between the formation and waters. Similarly, the introduction of a silicate, which is more reactive than K-feldspar, stabilizes this phase, such that, at equilibrium, the overall effective impact of introducing CO_2-charged water from the Nisku D2 reservoir into the Viking aquifer is to break down very nearly equal (on a molar basis) amounts of albite and Na-montmorillonite, while producing kaolinite and dolomite, with virtually no change in the amount of K-feldspar or calcite in the aquifer. These results are shown in Figure 13. Again, the net result of these reactions is to increase the volume of solids within the aquifer; the net effect being as great as 0.23% of the total sample volume, or slightly more than 2% of the total pore space. This change in porosity is negligible compared with all the measurement error and scaling-up approximations. Again, the net result of these reactions on the final pH of the equilibrium solution is minor, with the equilibrium pH being only 0.17 units greater than that of the original value calculated for the CO_2-rich water derived from the Nisku D2 reservoir.

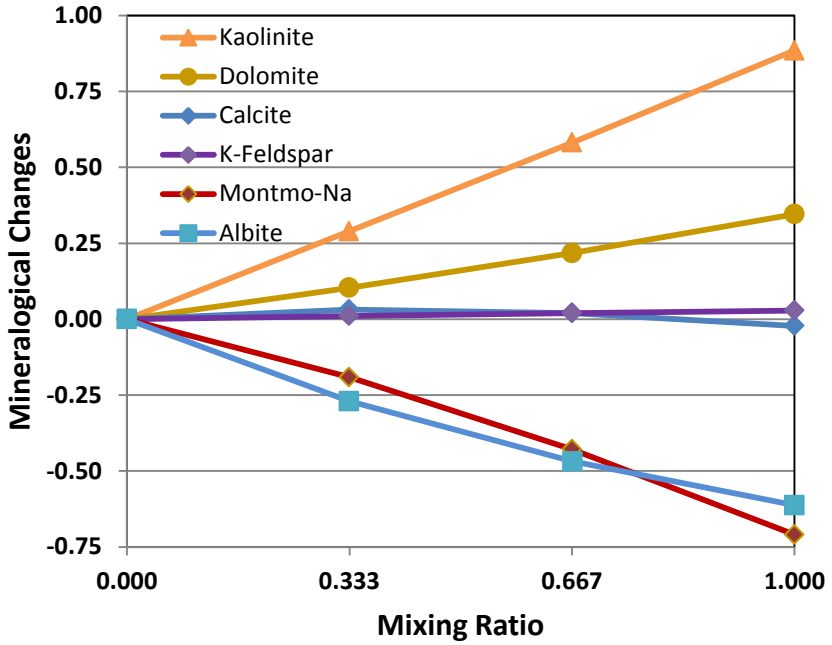

Figure 13: Calculated changes in the equilibrium mineralogy associated with the reactions induced by mixing CO_2-charged waters from the Nisku D2 reservoir with minerals in the Viking aquifer.

The calculated impact of leakage of CO_2-charged water from the Nisku D2 reservoir on the rocks and less saline waters of the more recent Basal and Upper Belly River aquifers is more dramatic, as shown in Figures 14 and 15, respectively. These demonstrate that reactions may occur in the clay fractions within these formations. As with the previous two cases, adding the saline, acidic water derived from the Nisku D2 reservoir is predicted, at least at low mixing ratios, to lead to the formation of kaolinite (and a silica polymorph which is not shown) from albite, with this reaction driving up the pH to allow dolomite to precipitate. However, with an increase in the mixing ratio, the net reaction changes noticeably. For the case of the Basal Belly River aquifer (Figure 14), illite and albite form at the expense of K-feldspar and kaolinite at the highest mixing ratio. The impact of these reactions on porosity is negligible; there is an increase of up to 2% of the total porosity at the lower mixing ratios, and porosity increase of less than 1% at the highest mixing ratio. In contrast, in the reactions in the Upper Belly River aquifer (Figure 15), illite is consumed while K-feldspar is formed at higher mixing ratios. The trends in albite and kaolinite are similar in both formations. At low mixing ratios of waters in the Upper Belly River aquifer with CO_2-rich water from the Nisku D2 reservoir, the complex clay K-montmorillonite degrades to illite, which subsequently degrades to kaolinite. The calculated volume of minerals within the Upper Belly River aquifer increases with the mixing ratio, with total porosity decreasing from an initial value of 12.5% to about 11.9%.

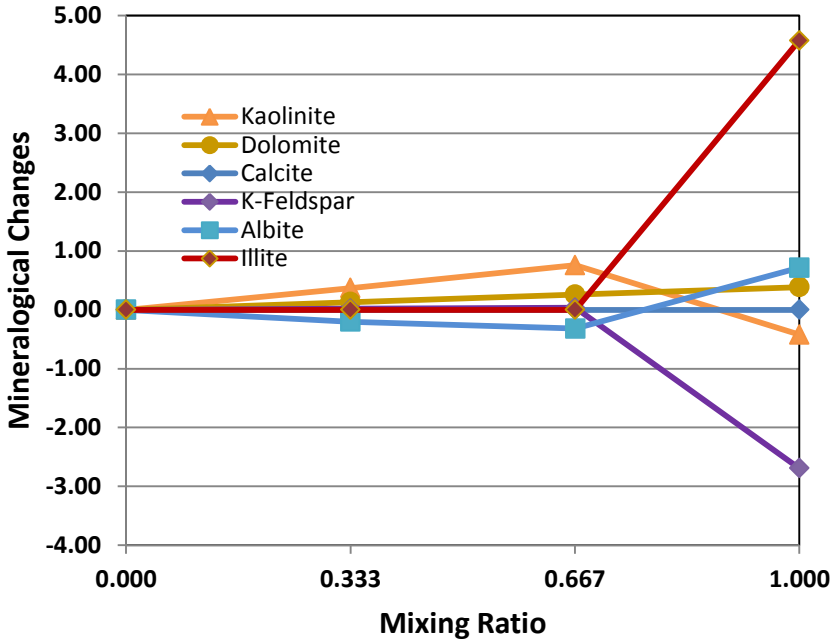

Figure 14: Calculated changes in the equilibrium mineralogy associated with the reactions induced by mixing CO_2-charged waters from the Nisku D2 reservoir with minerals from the Basal Belly River aquifer.

Water in both aquifers is locally considerably more acidic following the leakage of water from the Nisku D2 reservoir. The equilibrium pH in Basal Belly River has a value of 6.0 at a mixing ratio of 1; this value is down from an initial pH of 7.3. While more acidic than the initial water, it is considerably less acidic than the calculated pH of 4 that the Nisku D2 CO_2-rich water would have been were there no mineral reactions in the aquifer. These values are quite similar to those calculated for the Upper Belly River (the pH of the equilibrated mixture is 5.9 compared to the initial pH of 7.6).

As in the case of the oil reservoirs, the geochemical simulations show that the changes in aquifer porosity as a result of leakage of CO_2-rich water from the Nisku D2 reservoir into overlying aquifers will be negligible-to-minor. In regard to effects on aquifer permeability, these cannot be quantified and they will depend mainly where on the solid grains mineral precipitation or dissolution will take place, in the pores or in the pore throats. However, one should take into account that these geochemical simulations represent extreme cases that assume that CO_2-rich water will leak from the Nisku D2 reservoir unaltered up to the respective aquifer (Lower Mannville, Viking, Basal Belly River or Upper Belly River), where then it will mix with aquifer water and react with aquifer solids. Such a scenario may happen only if the leakage occurs inside a well casing up to the respective aquifer, and then through a casing hole into the aquifer. Otherwise, if leakage would occur through an open hole or outside casing, the CO_2-rich water originating from the Nisku D2 reservoir will be increasingly diluted by mixing with the water in the aquifers in the overlying sedimentary succession, with the net effect of lessening geochemical effects as this water moves upwards through the succession. This more realistic scenario allows for any number of possible permutations in mixing of

CO_2-rich water originating from the Nisku D2 reservoir and the water in the four aquifers considered here; investigating these is beyond the scope and ability of this study. By studying the most extreme cases, even if unrealistic, the results indicate that the effects of leaking CO_2-rich water on the porosity and permeability of the overlying aquifers will be local and minimal.

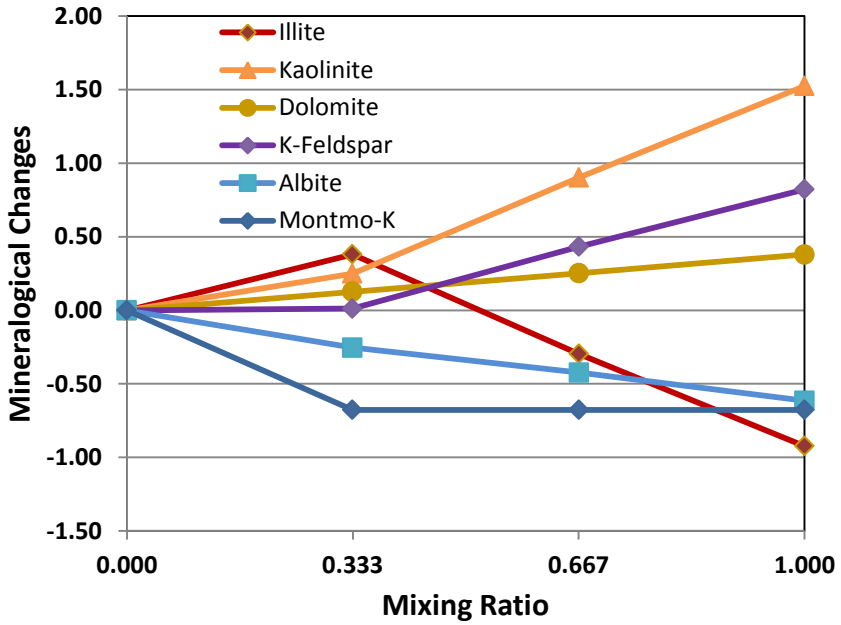

Figure 15: Calculated changes in the equilibrium mineralogy associated with the reactions induced by mixing CO_2-charged waters from the Nisku D2 reservoir with minerals from the Upper Belly River aquifer.

Leakage of either CO_2 or CO_2-rich waters from the oil reservoirs will induce mineralogical transformations within the overlying aquifers through which these fluids will pass. In the case of CO_2 gas leaking, the aquifers will become more acidic; this acidification will destabilize some minerals which will dissolve, releasing base cations from the mineral phases and transforming CO_2 to bicarbonate ions. The case of flow of CO_2-charged waters from the reservoir is more complex. This is because, as well as being an acidic water, it is also charged with high concentrations of base cations transported from the reservoir. These can stabilize a different suite of minerals, with some of the mineral forming reactions generating acid. For example, the precipitation of dolomite, which is predicted to form in all of the aquifers studied, produces acid via the reaction

$$Mg^{2+} + Ca^{2+} + 2\ CO_2 + 2\ H_2O = MgCa(CO_3)_2 + 4\ H^+ \quad . \qquad (8)$$

In other words, in contrast to the case of free CO_2 leakage in which all reactions will act to neutralize (albeit not always extensively) the acidic components transported into the aquifer, the influx of waters from the reservoir may initiate mineral precipitation reactions which act as a further acid source depending on the cation loading of the incoming waters.

This can be seen in Table 23, which presents the equilibrium pH calculated for the cases of free CO_2 leakage and CO_2-charged brine leakage into the four aquifers. In the case of the Lower Mannville aquifer, the equilibrium water in the case of a CO_2 leak will be more acidic than that which would result from the leak of CO_2-rich water; however, the opposite will happen in the other three overlying aquifers.

Table 23: Calculated pH resulting from equilibration at in-situ conditions of aquifer formation water and minerals with free CO_2 (second column) and with CO_2-rich reservoir water leaking from the oil reservoirs.

Aquifer	CO_2	CO_2-charged water
Lower Mannville	4.79	5.06
Viking	5.62	4.88
Upper Belly River	6.15	6.00
Basal Belly River	6.25	6.05

The resulting equilibrium pH has important implications for the mobility of trace elements, particularly heavy metals; the solubility of trace metals commonly increases exponentially with the hydrogen ion activity in slightly-to-moderately acidic solutions. A more detailed discussion of trace metal mobilization is not given here for the following reasons. As noted, trace element mobility is highly dependent on pH, but also on the oxidation state of within the aquifers, on the concentration of ligands which form stable aqueous complexes with the trace metals, and on the concentration of components which co-precipitate with the trace metals. Much of these data are lacking for the aquifers discussed here. With the exception a few analyses of Fe, there are no metal analyses for recovered formation waters; this limitation prevents the determination of potential mineralogical controls of the trace element concentrations. As well, even with measured concentrations, thermodynamic data for Pb (lead) and As (arsenic), the two elements of greatest interest as shown in the study by Apps et al. (2010) are absent from the PHREEQC thermodynamic data base incorporating the Pitzer activity model which was used in the geochemical simulations presented here. These limitations alone preclude analysis of the effects of aquifer acidification on trace metals. That said, the total As and Pb contents of the aquifer and caprocks given in Bachu et al. (2012) are fairly typical of sedimentary rocks (c.f. Hitchon et al., 1999). Evaluating the mobility of trace elements contained in the mineral assemblage, particularly Pb and As, would require collection of additional data, laboratory experiments and supplementary modelling. However, the available data suggest that the results of similar studies (e.g. Frio pilot study: Kharaka et al, 2006; Weyburn CO_2-EOR monitoring project: Wilson and Monea, 2004) could be used as a first proxy for evaluating the mobilization of trace elements at this site.

In regard to the effects of CO_2 and/or CO_2-rech water leaking from the oil reservoirs on the aquitards in the sedimentary succession: Wabamun, Upper Mannville, Joli Fou, Colorado and Lea Park, although some mineralogical samples were collected and analyzed (see Table 13), no evaluation of the geochemical effects of CO_2 on these rocks

can be performed in the absence of information about the composition of the water filling the pore space in these aquitards. The high variability between waters in the oil reservoirs and overlying aquifers indicates that the water saturating the pore space in the aquitards will have a different composition than any of the waters analyzed and presented here, and no reasonable assumptions can be made about their composition. On the other hand, geochemical modelling of the effects of CO_2 and/or CO_2-rich water on aquitard rocks is not important in this case because, given the very low permeability of these aquitards and their significant combined thickness when more than one aquitard separates two aquifers (e.g., Wabamun, Upper Mannville and Joli Fou, and Colorado and Lea Park), CO_2 will migrate into these aquitards only through diffusion, which is an extremely slow process that can be practically neglected. As mentioned previously, the only potential leakage pathways in the area are existing wells, with leakage being possible only in the aquifers in the sedimentary succession overlying the Leduc D3-A and Nisku D2 oil reservoirs.

6. Conclusions

The objective of the Alberta Carbon Trunk Line project being implemented by Enhance Energy Inc. is to collect CO_2 from large-scale industrial CO_2 emitters in and around Alberta's Industrial Heartland for use in CO_2-assisted enhanced oil recovery in aging oil reservoirs in central Alberta. Specifically, CO_2 injection into the Leduc D3-A and Nisku D2 oil reservoirs of the Clive oil field is targeted; however, other oil fields will be successively included as the project progresses. Alberta Innovates – Technology Futures has performed several studies to assess the effects of injecting CO_2 in the Leduc D3-A and Nisku D2 oil reservoirs in the Clive oil field. The objective of the study reported here is to assess the likely geochemical interactions between the injected CO_2 and the rocks and water contained in these two oil reservoirs. In addition, given the possibility of leakage of CO_2 and/or CO_2-rich water from the oil reservoirs through defective wells, the geochemical effects of this hypothetical leakage on the overlying Lower Mannville, Viking, Basal Belly River and Upper Belly River aquifers were also examined. Only interactions with a phase containing pure CO_2 (free CO_2 or CO_2-rich water) at in-situ conditions were considered; dilution of this phase with volatile hydrocarbons and other light gases dissolved in the reservoir oil will decrease the impact of CO_2 reactions within the reservoir and overlying aquifers. Aspects of the interactions between caprocks (aquitards) with free CO_2 and brines enriched with CO_2 are also briefly discussed; however, a lack of analytical data precludes quantitative modelling of the effects of these fluids on the intervening aquitards. Nevertheless, CO_2 leakage into the aquitards, accompanied by associated geochemical reactions, is less of a concern because the only transport mechanism of CO_2 in the aquitards is diffusion, which is an extremely slow process. If leakage of CO_2 or CO_2-rich brine will occur through defective wells, it is the aquifers, not the aquitards, that will be affected.

Interactions induced by fluids associated with CO_2-EOR and rocks (reservoirs and aquifers) and formation water in aquifers were modelled using the geochemical code PHREEQC. The relatively high salinity of the waters within the oil reservoirs and the lower aquifers (lower Mannville and Viking) demands that an ion-interaction (Pitzer) model be used to describe the thermodynamic properties of waters modelled here. This model is less comprehensive than models available for dilute solutions, which limits the number of elements that can be modelled. PHREEQC can calculate the equilibrium conditions which arise when fluids mix, as well as the time evolution of compositions associated with reactions with known reaction rates. The results presented here are restricted to equilibrium calculations; these results represent upper limits on the extent of geochemical reactions. As a result, in general, the extent of chemical trapping and acid neutralization are overestimated in the results presented in this report.

Results indicate that within the oil reservoirs, in both of which the host rock is relatively pure dolomite, the interaction between the injected CO_2 and reservoir minerals will lead to the breakdown of feldspars, present in minor amounts, to form clays. There is also some transformation of the carbonate minerals within the reservoir, however, this will be minor. The extent of the carbonate reactions is limited by the relatively high partial

pressure of CO_2 which apparently is currently present within the reservoirs; adding pure CO_2 will drive up the already high partial pressure of CO_2, but the impact is less dramatic than it would in environments with a lower inherent content of CO_2. The current CO_2 partial pressure was estimated based on the recovered water composition and an assumed equilibrium with the mineral calcite. Overall, the predicted geochemical reactions will lead to a trivial decrease in porosity in the oil reservoirs; although the short term trend is likely to involve a modest increase in porosity first, followed by a decrease back to almost the initial state. In any event, there is no reason to believe that reservoir characteristics, particularly permeability, and hence oil recovery, will be adversely affected by geochemical reactions associated with CO_2 flooding.

Available geological, hydrogeological and mineralogical evidence indicates that the Leduc D3-A and Nisku D2 oil reservoirs in the Clive oil field are capped by a strong and thick primary seal (caprock), the Calmar-Wabamun Aquitard. This primary seal constitutes a barrier to upward migration and leakage of CO_2 from the oil reservoirs targeted for CO_2 enhanced oil recovery in the area. The greatest risk of leakage of fluids (CO_2 or acidified brines) from the oil reservoirs will be associated well bores that penetrate these reservoirs. Leaking fluids will interact with formation water and minerals in a succession of saline aquifers. This leakage will acidify the formation water, initiating reactions with the rock minerals and, potentially, the formation of new minerals. The analysis of the predicted reactions involved defining the equilibrium relationships which currently exist within each aquifer, based on recovered water compositions and core samples. Incomplete water analyses were supplemented by assuming equilibrium with minerals which are either identified within each specific aquifer (preferable) or commonly present in similar rocks. Mineral proportions within each formation were estimated refining X-ray diffraction data with whole rock analyses using the mineral norm software, LPNORM.

Two types of fluid interactions were considered within the overlying aquifers: interactions with pure CO_2 and with CO_2-enriched brines derived from the Nisku D2 reservoir. The overlying aquifers, being of siliciclastic nature, are mineralogical more complex than the carbonate oil reservoirs; hence the resultant geochemical reactions will be accordingly more complex. In the case of pure CO_2 leakage into these aquifers, the general tendency will be for the pre-existing feldspars and complex clays to breakdown, forming the simpler, more acidic clay mineral kaolinite and a pure silica phase (modelled here as chalcedony). Significant quantities of the magnesium carbonate, magnesite, are predicted to form within the Basal and Upper Belly River aquifers. As with the oil reservoirs, the predicted changes in the porosity of the lower two aquifers (Lower Mannville and Viking) are inconsequential; however, this is not the case for the upper two aquifers; an increase in porosity is expected within the Basal Belly River aquifer, while a significant porosity reduction is expected within the Upper Belly River aquifer. Permeability changes are difficult to predict, and such a prediction was not attempted here because changes in permeability depend not only on the total amount of dissolved or precipitated solid phase, as in the case of porosity, but also on the place of dissolution

or precipitation: in the pore body or in the pore throats. However, permeability is not expected to change appreciably in the two lower aquifers (Lower Mannville and Viking), and maybe only locally in the two upper ones (Basal and Upper Belly River).

The capacity of the aquifers overlying the oil reservoirs to trap CO_2 either within mineral phases or as bicarbonate in the water is also greater in the upper two aquifers (Basal and Upper Belly River) than in the lower ones (Lower Mannville and Viking), one reason being their markedly lower salinity in the former than in the latter. Calculations suggest that it is likely that a free-phase CO_2 will exist within the Mannville and Viking aquifers following equilibration with the aquifer mineralogy, but that this is not the case in the Basal and Upper Belly River aquifers. In addition to the reactions considered here, leakage through any of these aquifers will also result in some dispersion and dilution of any vertical flux of CO_2 into each of these aquifers.

As with the case of pure CO_2, leakage of acidified brines into these aquifers will also induce a complex set of reactions. However, in contrast to the former case, where the rock acts to buffer pH changes associated with the acidification of aquifer water, the flow of cation-laden brines can induce acid forming reactions. As such, the pH of waters resulting from the mixing of CO_2-enriched reservoir-derived water with that from the overlying aquifers will generally be lower (more acidic solution) than in the case of pure CO_2 flow. This has implications when considering trace metal mobility within affected aquifers – generally the mobility of trace elements, such as lead and arsenic, increases as pH decreases.

The results presented here represent the state towards which reservoir and aquifer mineralogy and water chemistry will ultimately tend when interacting with fluids in and leaking from the oil-reservoirs into which CO_2 is injected. Limitations on quantification of important parameters, such as mineral reaction rates in brines, detailed understanding of small scale concentration profiles which develop around reacting mineral grains, and mineral surface areas exposed to the reactive fluids, preclude accurate assessments of the time required to reach equilibrium. Conservative, in the sense of maximizing risk assessments, short term simulations of flow within the oil reservoirs and leakage into protected aquifers containing potable water and to the surface may be performed neglecting these geochemical considerations; however, these geochemical calculations provide insights into mechanisms which may be responsible for reducing leakage rates and effects, and also provide an insight into potential compositional changes induced by leakage which may influence future monitoring approaches.

7. References

Appelo, A., Postma, D., 1993. *Geochemistry, Groundwater and Pollution*. Balkema., Amsterdam, The Netherlands.

Apps, J.A., Zheng, I., Zhang Y., Xu T., Birkholtzer, J.A., 2010,.Evaluation of potential changes in groundwater quality in response to CO_2 leakage from deep geological storage. *Transport in Porous Media*, v. 82, p. 215-246.

Bachu, S., 2012. Drainage and imbibition CO_2/brine relative permeability curves at in-situ conditions for sandstone formations in western Canada. In: *Proceedings of the 11th International Conference on Greenhouse Gas Technologies*, Kyoto, Japan, November 18-22, 2012, Energy Procedia, In press.

Bachu, S., Hauck, T., Peterson, J., Melnik, A., Main, C., Perkins, E., 2011. *Geological, Hydrogeological and Mineralogical Characterization of the Sedimentary Succession Overlying the Leduc D3-A and Nisku D2 Oil Reservoirs in the Clive Oil Field in Alberta*. Client report to Enhance Energy Inc.

Benbow, S.J., Metcalfe, R., Wilson, J.C., 2008. *Pitzer Database for Use in Thermodynamic Modelling*. Quintessa QRS-3021A-TM, 69p.

Bennion, D.B., Bachu, S., 2008. Drainage and imbibition relative permeability relationships for supercritical CO_2 and H_2S/brine systems in intergranular sandstone, carbonate, shale and anhydrite formations. *SPE Reservoir Evaluation and Engineering*, v. 11, no. 3, p. 487-496, doi: 19.2118/99326PA, 2008.

Bennion, D.B., Bachu, S., 2010. Drainage and imbibition CO_2/brine relative permeability curves at reservoir conditions for carbonate formations. *SPE Paper 134028*, 18 p., SPE Annual Technical Conference and Exhibition, Florence, Italy, September 19-22, 2010.

Birkholzer, J.T., Zhou, Q., 2009. Basin-scale hydrogeologic impacts of CO_2 storage: Capacity and regulatory implications. *International Journal of Greenhouse Gas Control*, v. 3, no. 6, p. 745-756.

Carroll, J.J., 1996, AQUAnews: The newsletter for AQUAlibrium users, vol. 1, available at http://www.telusplanet.net/public/jcarroll/NEWSL12.PDF

Chebotarev, I.I., 1955. Metamorphism of natural waters in the crust of weathering, 1. *Geochemica et Cosmochimica Acta*, v. 8, p. 22-48.

de Caritat, P., Bloch, J., Hutcheon, I. 1994. LPNORM: a linear programming normative analysis code. *Computers & Geoscience*. v. 20, no. 3, p. 313-347. doi: 10.1016/0098-3004(94)90045-0.

Doughty, C., Freifeld, B., 2012. Modeling CO_2 injection at Cranfield, Mississippi: Investigation of methane and temperature effects. In: *Proceedings of the TOUGH2 Symposium 2012,* Lawrence Berkeley National Laboratory, Berkeley, California, September 17-19, 2012

Faltinson , J., Jafari., A., Hauck, T., and Bachu, S., 2011. *Characterization of the Wells that Penetrate the Leduc D3-A and Nisku D2 Oil Reservoirs in the Clive Oil Field in Alberta*. Client report to Enhance Energy Inc.

Garrels, R.M., 1984. Montmorillonite/Illite Stability Diagrams. *Clays and Clay Minerals*, v. 32, no. 3, p. 161-166.

Ghaderi, S.M., Keith, D.W., Lavoie, R., Leonenko, Y., 2011. Evolution of hydrogen sulfide in sour saline aquifers during carbon dioxide sequestration. *International Journal of Greenhouse Gas Control*, v. 5, p. 347-355.

Gunter, W.D., Wiwchar, B., Perkins, E.H.1996. Autoclave experiments and geochemical modelling. in: B. Hitchon (ed.) *Aquifer disposal of carbon dioxide – Hydrodynamic and mineral trapping – Proof of concept*. Geoscience Publishing Ltd., Sherwood Park, AB, p. 115-141.

Hanor, J.S., 1994. Origin of saline fluids in sedimentary basins. In: *Geofluids: Origin, Migration and Evolution of Fluids in Sedimentary* Basins. (J. Parnell, ed.). The Geological Society, London, UK, London Geological Society Special Publication No. 78, p. 151-174.

Harvie, C. E., Møller, N., Weare, J. H., 1984. The prediction of mineral solubilities in natural waters: The Na-K-Mg-Ca-H-Cl-SO4-OH-HCO3-CO3-CO_2-H2O system to high ionic strengths at 25 °C. *Geochimica et Cosmochimica Acta*, v. 48, no. 4, p. 723-751.

Hitchon B., Perkins, E., Gunter, W., 1999, Introduction to Ground Water Geochemistry. Geoscience Publishing. Sherwood Park, Ab., 310 p.

Hutcheon, I., 1999. Controls on the distribution of non-hydrocarbon gases in the Alberta Basin. *Bulletin of Canadian Petroleum Geologists*, v. 47, p. 573-593.

IPCC (Intergovernmental Panel on Climate Change), 2005. *Special Report on Carbon Dioxide Capture and Storage*. Cambridge University Press, Cambridge, UK, and New York, NY, USA.

IPCC (Intergovernmental Panel on Climate Change), 2007. Climate Change 2007: *The Physical Science Basis. Fourth Assessment Report*, IPCC Secretariat, Geneva, Switzerland.

Kharaka, Y., W.D. Gunter, P.K. Aggarwal, E.H. Perkins, and J.D. DeBraal. 1988. *SOLMINEQ.88: A Computer Program for Geochemical Modelling of Water-Rock Interactions*, U.S. Geological Survey Water-Resources Investigations Report 88-4227.

Kharaka Y.K, Cole, D.R., Hovorka, S.D., Gunter, W.D., Knauss K.G., Freifeld, B.M., 2006. Gas-water-rock interactions in Frio Formation following CO_2 injection: Implications for the storage of greenhouse gases in sedimentary basins. *Geology* v. 34 no. 7 p. 577-580

Monnin, C., 1990. The influence of pressure on the activity coefficients of the solutes and on the solubility of minerals in the system Na-Ca-Cl- SO4-H2O to 200°C and 1 kbar and to high NaCl concentration. *Geochimica et Cosmochimica Acta,* v. 54 no. 12, p. 3265-3282.

Nesbitt, H.W., 1977, Estimation of the thermodynamic properties of Na- Ca- and Mg-beidellites, *Canadian Mineralogist*, v. 15, p. 22-30.

Nesbitt, H.W., 1982. The Stokes and Robinson hydration theory: A modification with application to concentrated electrolyte solutions. *Journal of Solution Chemistry*, v. 11, no. 6, p. 415-422.

Oar, T., Hawkes, C.D., Soltanzadeh, H., 2011. *Geomechanical Analysis of the Clive Oil Field for CO_2 Injection: Phase 1 – Mechanical Earth Model*. Client report to Enhance Energy Inc.

Paktunc, A. D., 1998. MODAN: An interactive computer program for estimating mineral quantities based on bulk composition. *Computers & Geoscience*, v. 24, no. 5, p. 425-431, doi:10.1016/S0098-3004(98)00018-1.

Palandri, J.L. Kharaka, Y.K. 2004. *A Compilation of Rate Parameters of Water- Mineral Interaction Kinetics for Application to Geochemical Modelling*. U.S. Geological Survey Open File Report 2004-1068. 70 p.

Parkhurst, D.L., Appelo, C.A.J., 1999. User's guide to PHREEQC (Version 2) — A computer program for speciation, batch-reaction, one-dimensional transport, and inverse geochemical calculations. USGS Water Resources Investigation Report, v. 99, no. 4259, p. 312.

Pitzer K.S., 1991. Ion interaction approach: Theory and data correlation. In: *Activity Coefficients in Electrolyte Solutions*, 2nd edition. (K.S. Pitzer, ed.). CRC Press, Boca Raton, FL, USA, p. 75-153.

Plummer, L. N., Parkhurst, D. L., Fleming, G. W., Dunkle, S. A., 1988. *A Computer Program Incorporating Pitzer's Equations for Calculation of Geochemical Reactions in Brines*. U.S. Geological Survey Water-Resources Investigations Report, 88-4153.

Rimstidt, J.D. 1997, Quartz solubility at low temperatures. *Geochimica et Cosmochimica Acta*, v. 61, no. 13, p. 2553-2558.

Sandia National Laboratories, 2007. Qualification of thermodynamic data for geochemical modeling of mineral-water interactions in dilute systems. U.S. Department of Energy, ANL-WIS-GS-000003 REV 01. U.S. Department of Energy, Office of Civilian Radioactive Waste Management. Las Vegas, Nevada, 2007.

Slaughter, M., 1989. Quantitative determination of clays and other minerals in rocks. In: *CMS Workshop Lectures*, Vol. 1, Quantitative Mineral Analysis of Clays (Pevear, D.R., and Mumpton, F.A., eds.). The Clay Minerals Society, Boulder Colodardo p.120-151.

Soltanzadeh, H., Jafari, A., and Hauck, T., 2012. *Geomechanical Analysis of the Effects of CO_2 Injection in the Leduc D3-A and Nisku D2 Reservoirs in the Clive Field*. Cient report to Enhance Energy Inc.

Warren, J., 2000, Dolomite: occurrence, evolution and economically important Associations, *Earth-Science Reviews*, v. 52, p. 1–81.

Wigston, A., Ryan, D., 2011. *Characterization of CO_2 Emissions from Large Stationary Sources in the Canadian Portion of the Basal Cambrian Aquifer of the Northern Plains-Prairie Region of North America*. CanmetENERGY, 89 p.

Wilson, M., Monea, M., 2004, *IEA GHG Weyburn CO_2 Monitoring and Storage Project Summary Report*, 2000-2004. PTRC, Regina, SK, Canada, 268 p.

8. Appendix A

Important mineral phases, and idealized formulae, which are used in the PHREEQC modelling presented herein.

Mineral	Formulae as cited in the YPF database[1]
Albite	$NaAlSi_3O_8$
Alunite	$KAl_3(SO_4)_2(OH)_6$
Anatase	TiO_2
Anhydrite	$CaSO_4$
Annite (mica)	$KFe_3(AlSi_3)O_{10}(OH)_2$
Apatite	$Ca_5(PO_4)_3OH$
Calcite	$CaCO_3$
Dolomite	$CaMg(CO_3)_2$
Gibbsite	$Al(OH)_3$
Goethite	$Fe(OH)_3$
Gypsum	$CaSO_4{\cdot}2H_2O$
Halite	NaCl
Illite	$K0.{}_6Mg0.{}_{25}Al_{1.8}Al0.{}_5Si_{3.5}O_{10}(OH)_2$
Kaolinite	$Al_2Si_2O_5(OH)_4$
K-Feldspar	$KAlSi_3O_8$
K-mica	$KAl_3Si_3O_{10}(OH)_2$
Montmorillonite-X	$X_{0.33}Mg_{0.33}Al_{1.67}Si_4O_{10}(OH)_2$
Muscovite (mica)	$KAl_3Si_3O_{10}(OH)_2$
Nontronite-X	$X_{0.33}Al_{0.33}Fe_2Si_{3.67}O_{10}(OH)_2$
Pyrite	FeS_2
Quartz	SiO_2
Siderite	$FeCO_3$
Vivianite	$Fe_3(PO_4)_2{\bullet}8(H_2O)$

[1] X in any of these above formulae can represent H, Na, K, ½ Mg, or ½ Ca

9. Appendix B

A sample PHREEQC input file used for Aquifer simulations of interactions between reservoir fluids (CO_2 charged brines and pure CO_2) and aquifers.

```
SOLUTION 1  Mannville, Porosity = 9.7
temp  23
pe    4
density     1.145
units mg/l
redox pe
pH    6.4
Na    50065; K    ;  Ca  19139; Mg  3815;
Ba    ; Sr  ; B       ;  Cl   121400; Br  ;
C     143.607     ;  S     530;

SELECTED_OUTPUT
-file       Cases_1_2_and_3_Mannville_1_try2_more_output.sel
-activities SiO2 HCO3-
-si Gibbsite Kaolinite Illite K-feldspar CO2(g) Nontronite-Na
Nontronite-K Nontronite-Mg Nontronite-Ca
-si Albite Gypsum Anhydrite Halite Dolomite Talc Montmo-Mg Montmo-Na
Montmo-K     Muscovite Quartz Goethite
-tot Mg Ca Na K Al C Si S(-2) Cl S(6)
-mol CO2 HCO3- Ca+2
-temperature
-equilibrium_phases   Calcite Dolomite Albite K-Feldspar Siderite
Quartz
-equilibrium_phases   Kaolinite CO2(g) Montmo-Mg Montmo-Na Montmo-K
Muscovite Illite Goethite Cristobalite(alpha)
-ionic_strength
user_punch
 -start
10   punch "Mannville - Define Nisku water @ surface conditions"
-end
SAVE  solution 1
END

USE   solution 1
user_punch
 -start
20   punch "'Mannville - Define Nisku water @ 60 C"
-end
REACTION_TEMPERATURE 1
60
SAVE  solution 2
END

USE solution 2
user_punch
EQUILIBRIUM_PHASES 1
    Calcite   0 CO2(g)    10
```

```
    Cristobalite(alpha)    -0.138575315 10
    Kaolinite 0 10
    K-Feldspar 0 KCl  10
    Pyrite 0 0.377584148
 -start
30   punch "Mannville - Define Nisku water @ 60 C, K-spar, calcite etc,
equilibrium"
-end
save solution 3
END

EQUILIBRIUM_PHASES 1
CO2(g)             1.9175      10
Dolomite    0.96   261.1669564
Anhydrite   -0.1   40.41447571
Calcite     0      3.978248403
Quartz      0.35   1.927828185
Siderite    0      0.665556422
Kaolinite   0      0.274860834
Montmo-Mg   -0.06  0.268749
K-Feldspar  0      0.218975757
Albite             0.0000      0.0000
Goethite           0.0000      0.0000
Halite             0.0000      0.0000
Illite             0.0000      0.0000
Montmo-K           0.0000      0.0000
Montmo-Na          0.0000      0.0000
Muscovite          0.0000      0.0000
user_punch
 -start
35   punch "Mannville simulation - Define Nisku water @ 60 C, High pCO2
equilibrium "
-end
END

use solution 3
EQUILIBRIUM_PHASES 1
CO2(g)             1.9175      10
Dolomite    0.96   261.1669564
Anhydrite   -0.1   40.41447571
Calcite     0      3.978248403
Quartz      0.35   1.927828185
Siderite    0      0.665556422
Kaolinite   0      0.274860834
Montmo-Mg   -0.06  0.268749
# K-Feldspar      0     0.218975757
Albite             0.0000      0.0000
Goethite           0.0000      0.0000
Halite             0.0000      0.0000
Illite             0.0000      0.0000
Montmo-K           0.0000      0.0000
Montmo-Na          0.0000      0.0000
Muscovite          0.0000      0.0000
user_punch
 -start
```

```
40   punch "Mannville simulation - Define Nisku water @ 60 C, High pCO2
equilibrium - K-spar not in equilibrium"
-end
save solution 4
END

#  next steps define local mineralogy and solubility limits (i.e. local
SiO2 solubility limit, and dolomite
#  stuff - should be in table 7)
SOLUTION 6  Mannville-1  - Sample 3 in Table 2
temp  23
pe    4
density     1.074
units mg/l
redox pe
pH    6.5
Na    32724   ; K 493   ; Ca  5542
Mg    1107    ; Ba            ; Sr
B           ; Cl  63000 ; Br
C     96    ; S   374
user_punch
 -start
50   punch "'Mannville 1 (sample 3) water at 23 as analyzed:    "
-end

REACTION_TEMPERATURE 1
      55
user_punch
 -start
60   punch "'Mannville 1 water as analyzed heated to 55:    "
-end
SAVE solution 6
END

USE solution 6
EQUILIBRIUM_PHASES 1
    Calcite   0 CO2(g)    10
    Cristobalite(alpha)    0 10
    Kaolinite 0 10
user_punch
 -start
70   punch "'mannville 1 water at 55 C modified for equilibria:
Cristobalite saturation    "
-end
Save solution 7
END

USE solution 7
EQUILIBRIUM_PHASES 2                # alright to here
    Calcite   0 CO2(g)    10
    Cristobalite(alpha)    0 10
    Kaolinite 0 10
    Pyrite   0   H2S 1
    Siderite 0  FeCl2  1
save solution 7
user_punch
```

```
 -start
80   punch "'Mannville (Conc) water at 55 modified for iron equilibria:
"
-end
END

Use solution 4    - Cool CO2 charged reservoir water to aquifer
conditions
#  define temperature in overlying aquifer
Reaction_temperature 2        # temperature in Mannville 1 (see water 3
rock en-4)
55
save solution 4
user_punch
 -start
90   punch "'Reservoir water high CO2 no K-spar equilibrium cooled to
55:    "
-end
End

Use solution 3    -  Cool original reservoir water to aquifer
conditions
#  define temperature in overlying aquifer
Reaction_temperature 2        # temperature in Mannville 1 (see water 3
rock en-4)
55
save solution 5
user_punch
 -start
100   punch "'Reservoir water, no added CO2 equilibrium water cooled to
50:    "
-end
End

Use solution 5    -  Cool original reservoir water to aquifer
conditions
#  define temperature in overlying aquifer
Reaction_temperature 2        # temperature in Mannville 1 (see water 3
rock en-4)
55
save solution 5
user_punch
 -start
110   punch "should be identical to above:    "
-end
End

USE solution 7
EQUILIBRIUM_PHASES 3

      Cristobalite(alpha) 0.0 3.77955E+02
      Pyrite              0.0000    3.16880E+00
      Kaolinite   0.0000      2.44478E+00
      Calcite     0.0000      2.30851E+00
      Dolomite    0.9300      1.85406E+00
      K-Feldspar  0.2800      1.47627E+00
```

```
      Siderite    0.0000      7.97414E-01
      Albite      -0.1800     3.32865E-01
      Montmo-Na   0.51  0.0000
      Montmo-Mg   0.45  0.0000
      Montmo-K    0.07  0.0000
      Montmo-Ca   0.42  0.0000
 CO2(g)  1.830589  0.0 # log (69.6) no CO2 present, will exsolve
                           #  if pCO2 gets too high
user_punch
 -start
120   punch "'mannville (Conc) water, low CO2  "
-end
Save solution 7
End

use solution 7
EQUILIBRIUM_PHASES 3
      Cristobalite(alpha) 0.0 3.77955E+02
      Pyrite              0.0000    3.16880E+00
      Kaolinite   0.0000      2.44478E+00
      Calcite     0.0000      2.30851E+00
      Dolomite    0.9300      1.85406E+00
      K-Feldspar  0.2800      1.47627E+00
      Siderite    0.0000      7.97414E-01
      Albite      -0.1800     3.32865E-01
      Montmo-Na   0.51  0.0000
      Montmo-Mg   0.45  0.0000
      Montmo-K    0.07  0.0000
      Montmo-Ca   0.42  0.0000
 CO2(g)  1.830589  0.0 # log (69.6)- will exsolve if pCO2 gets too high
user_punch
 -start
130   punch "'Should be same as before - needed to define the
equilibrium phases for further work:   "
-end
save equilibrium_phases 4
End

use equilibrium_phases 4
Mix 1            # 0.33  CO2 reacted reservoir water
   4   0.3333
   7   0.6667
user_punch
 -start
140   punch "'Mix of 1/3 CO2 reservoir water, 2/3 Mannville:    "
-end
end

use equilibrium_phases 4
Mix 1           # 0.67  CO2 reacted reservoir water
   4   0.6667
   7   0.3333
user_punch
 -start
150   punch "'Mix of 2/3 CO2 reservoir water, 1/3 Mannville:    "
-end
```

```
End



use equilibrium_phases 4
Mix 1           #   0.99  CO2 reacted reservoir water
   4   0.9999
   7   0.0001
user_punch
 -start
160   punch "'Mix of 2.999/3 CO2 reservoir water, 0.001/3 Mannville:
"
-end
End

use equilibrium_phases 4
Mix 1            # 0.33  original reservoir water
   5   0.3333
   7   0.6667
user_punch
 -start
170   punch "'Mix of 1/3 pristine reservoir water, 2/3 Mannville::    "
-end
End

use equilibrium_phases 4
Mix 1           # 0.67  original reservoir water
   5   0.6667
   7   0.3333
user_punch
 -start
180   punch "'Mix of 2/3 CO2 pristine water, 1/3 Mannville:    "
-end
End

use equilibrium_phases 4
Mix 1           #   0.99  original reservoir water
   5   0.9999
   7   0.0001
user_punch
 -start
190   punch "'Mix of 2.999/3 pristine reservoir water, 0.001/3
Mannville:    "
-end
End

USE solution 7
EQUILIBRIUM_PHASES 3
      Cristobalite(alpha) 0.0 3.77955E+02
      Pyrite              0.0000    3.16880E+00
      Kaolinite   0.0000      2.44478E+00
      Calcite     0.0000      2.30851E+00
      Dolomite    0.9300      1.85406E+00
      K-Feldspar  0.2800      1.47627E+00
      Siderite    0.0000      7.97414E-01
      Albite      -0.1800     3.32865E-01
```

```
      Montmo-Na    0.51  0.0000
      Montmo-Mg    0.45  0.0000
      Montmo-K     0.07  0.0000
      Montmo-Ca    0.42  0.0000
      CO2(g) 1.830589  10.0 # log (69.6)- excess of free CO2 present
user_punch
 -start
200   punch "'CO2 phase into the Mannville:    "
-end
End
```